Fleet-wide transit bus energy consumption modelling and techno-economic analysis of stationary energy storage systems for high-power electric bus charging

by

Graham Wilson
B.Sc., University of Saskatchewan, 2019

A Thesis Submitted in Partial Fulfillment of the Requirements for the Degree of

MASTER OF APPLIED SCIENCE

in the Department of Mechanical Engineering

Fleet-wide transit bus energy consumption modelling and techno-economic analysis of stationary energy storage systems for high-power electric bus charging

by

Graham Wilson
B.Sc., University of Saskatchewan, 2019

Supervisory Committee

Dr. Curran Crawford, Supervisor
(Department of Mechanical Engineering)

Dr. Nedjib Djilali, Departmental Member
(Department of Mechanical Engineering)

ABSTRACT

Electric buses offer a range of benefits, including a drastic reduction of greenhouse gas emissions compared to personal transit, or to conventional diesel buses. Unfortunately, electric buses also require additional planning to ensure affordable and reliable operation. This thesis proposes two contributions that help to model and plan electric bus deployments, and generally examines how system-focused thinking is required for this application.

First, a novel data driven method for estimating the energy consumption of a bus is presented and validated against 1 Hz driving data. Rather than requiring ad hoc data collection, or entire theoretical drivecycle patterns, this new method leverages existing low fidelity driving data from public transit feeds. This data driven method can be used to quickly and accurately model the driving patterns and energy consumption of a whole fleet of buses, as is demonstrated for a case study in Victoria, BC, Canada.

Second, using the energy estimating methods previously mentioned, the electricity demand profile for a high-power electric bus charging hub is modelled for various locations and charging systems. Using this modelled demand profile, the potential for using a stationary energy storage system to reduce the peak power demand is investigated. The advantages of three different energy storage technologies (lithium ion, redox flow, and flywheel energy storage systems) are explored. Energy storage was found to be optimal for most charging scenarios modelled, with lithium ion providing the most economical solution for 65% of cases considered.

Both the data drive energy estimation modelling, and the energy storage feasibility study constitute novel contributions to the literature. These contributions help to advance the knowledge surrounding electric bus planning and modelling, and help to underpin the systems level thinking required for electric bus deployments.

Contents

List of Tables

List of Algorithms

List of Figures

ACKNOWLEDGEMENTS

First, I'd like to thank my supervisor Dr. Curran Crawford for guiding me during my project, and for welcoming me into the world of sustainable systems. I've appreciated your trust and support, and have thoroughly enjoyed my time with the Sustainable Systems Design Lab. I also need to acknowledge and thank the help of all the friends I've made within the SSDL and IESVIC. You've made me feel truly welcome here, and I hope I've done the same for you. There are too many names to mention, but I hope you all know how much you've helped me just by being there for me to laugh with, and talk (and sometimes complain) to.

To the Pacific Institute for Climate Solutions, Mitacs, and the Canadian Urban Transit Research and Innovation Consortium, thank you for providing financial support over the course of my project, and allowing me to spend the time I have on this work.

I also need to thank my family. To my parents, thank you for always believing in me and proving me unconditional love and support. Although I might not always show it, your support means the world to me, and I'm genuinely thankful that I'm lucky enough to be your son. To my sister, thank you for being a role model in life, even to this day.

To my close friends in Saskatchewan and B.C., thank you as well. Whenever I question or doubt myself in any capacity, I've always been reassured that I must be doing O.K. in life to have people like you choose to call me a friend.

Finally, to my partner Gillian, thank you for just being there when I needed you, without questioning or ever complaining. I hope I can eventually return the favor.

Chapter 1

Introduction and Background

1.1 Canadian Greenhouse Gas Emissions and Electric Transport

As the consequences of continued Greenhouse Gas (GHG) emissions become better understood, national governments have begun to take measures and set goals to reduce emissions [4]. The Government of Canada has announced their goals of reducing emissions by 40% compared to 2005 levels [5], and then becoming net-zero by 2050. As seen in Figure 1.1, the Canadian transportation sector accounts for 25% of all of the GHG emissions produced.

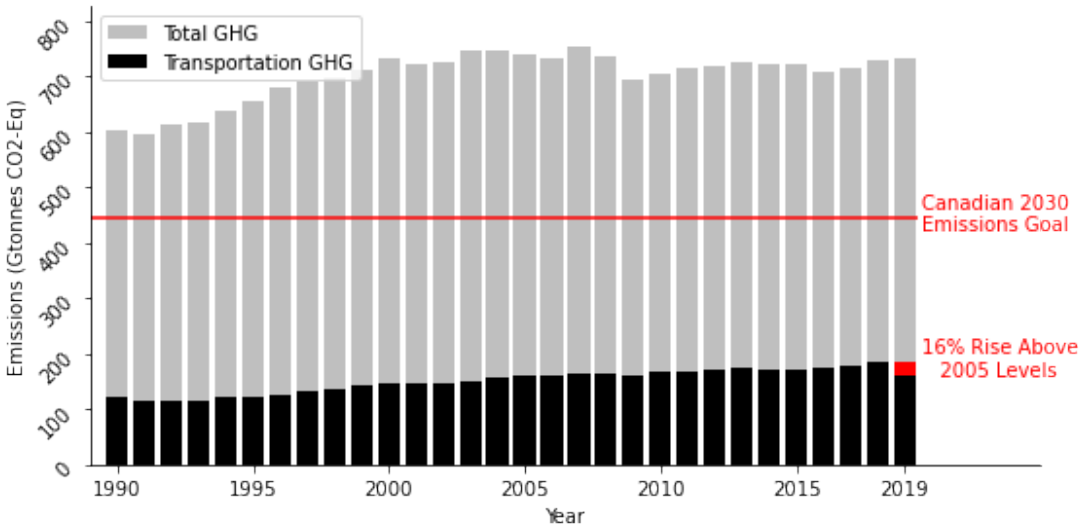

Figure 1.1: Canadian GHG emissions from transportation [1]

In discordance with the 2030 emissions goal, transportation emissions have risen by 16% rather than decreased. As seen in Figure 1.2, the transportation sector is one of the only sectors to see emissions rise consistently since the 1990s. Based on these trends, it becomes clear that action must be taken to address transportation sector emissions if Canadian emissions goals are to be met.

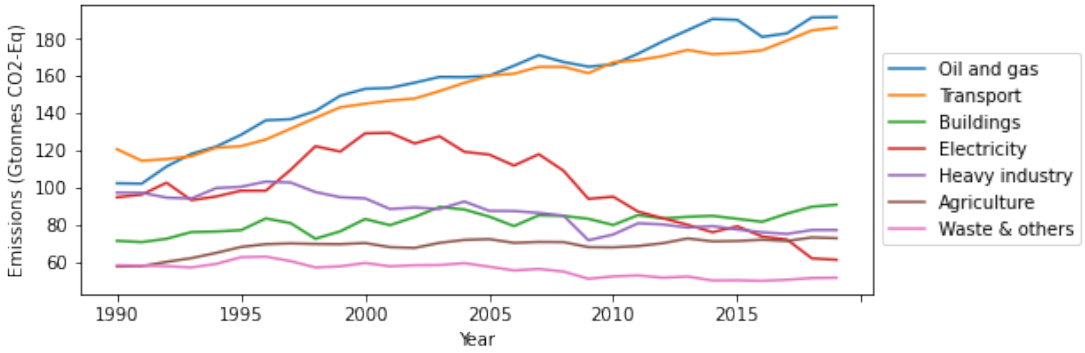

Figure 1.2: Canadian GHG emissions by sector [1]

While transport GHG are large and growing, several opportunities to decarbonize exist. On their own, personal Electric Vehicles (EV) and public transit present viable pathways to reduce GHG emissions, but each has its own concerns and barriers to adoption. Personal EVs eliminate tailpipe GHG emissions, and have been found to result in lower lifetime ownership costs in comparison to personal Internal Combustion Engine (ICE) vehicles [6] [7]. Unfortunately, despite the overall reduction in operating costs, the high purchase price and concerns about charging infrastructure mean that EVs remain out of reach to many consumers [8]. Additionally, despite their direct emissions reductions, some have questioned whether a transition from personal ICE vehicles to personal EV is a long term solution when accounting for embodied emissions and contribution to road congestion [9].

Conversely, public transit offers a lower energy intensity per passenger-kilometer travelled when compared to passenger vehicles. Across Canada, public transit buses offer an energy intensity of 0.81 MJ/Passenger-km compared to 1.75 MJ/Passenger-km for a typical personal vehicle [10] while also leading to potential reduction in overall road congestion and travel time [11]. Additionally, public transit achieves these benefits without requiring the user to purchase a new vehicle, making it a more equitable pathway to decarbonization. Electrified public transit in the form of Battery Electric Buses (BEB) provide the inherent advantages of public transit combined with the further benefits of EVs, resulting in an especially attractive and

sustainable solution to passenger transportation emissions in Canada.

1.2 Review of Electric Bus Systems

Bus services can be separated into coach services and transit services. Coach bus services typically operate longer distance routes on highways between population centers, and transit buses typically operate within population centers. Although the some of the same BEB concepts apply to both systems, this work focuses on transit bus services operating on set routes and schedules.

As shown in Figure 1.3 successful BEB deployment consists of three main components: the electric bus, the charging system, and some sort of energy provider. For the purposes of this work, the only energy provider considered is the local electrical utility, although obtaining energy from on-site generation would also be possible. Within each aspect of the deployment, system choices and constraints exist that impact the operation of the other parts. While BEB deployments offer many solutions, proper system level planning must take place to ensure that the operations are kept reliable and economical.

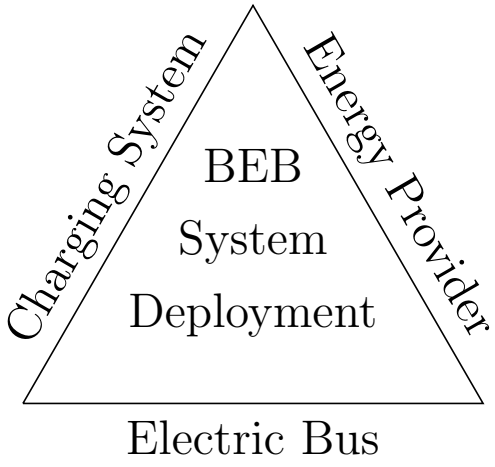

Figure 1.3: Core aspects of a battery electric bus system deployment

Within the electric bus component, bus range is the aspect that most impacts system planning. Heavy duty ICE transit buses usually have 400-500 L [2] fuel tanks that allow them to drive for 1000 km or more without refueling [12], and can be refueled in a matter of minutes. BEB range is considerably less than an ICE bus, and must be recharged at a much slower rate. BEB are generally separated into

"long range" and "short range" buses. A short range bus may only be able to travel 100-200 km with a battery capacity of 100-200kWh, while the longest range buses currently available offer ranges up to 500 km range with battery capacities of up to 675 kWh [13]. While long range buses offer advantages for route planning and flexibility during operation, they come at a higher purchase cost, and with lower operating efficiency due to the extra weight of the battery. BEB battery size will also impact when, and for how long buses need to be charged.

Charging systems can be classified as "in-depot" or "on-route" [14]. In-depot charging systems are located at the bus depot and is typically performed at lower powers ($\leq$ 150 kW) for a longer duration of time while the bus is not operating (ex. overnight). On-route charging, also referred to as "opportunity charging" is characterized by higher power charging events taking place at a charging location away from the depot, and during the operating hours of the bus. Since on-route chargers can operate at power of up to 600 kW, a short charging event of only 5 minutes will deliver a substantial amount of energy to the bus, allowing it to complete its daily driving tasks with a smaller on-board battery. Reduction in on-board battery size not only reduces the weight of the vehicle and increases energy efficiency, but also translates to major capital savings due to the reduction in battery pack costs. While in-depot charging is commonly performed with chargers that need to be physically plugged in, on-route charging is performed with overhead pantograph chargers that allow for automatic connections and charging without any physical action taken by the bus operator [15]. Wireless inductive charging systems have also seen some deployments for BEB charging, although these systems are still under development [15].

While the BEB and the charging system are often considered alone, the energy provider is a third aspect required for system planning. The structure of utility costs can have a large impact on the charging costs, and therefore when and how it is economical to operate a BEB. Utility rate structures can take different forms, but typically consists of some sort of energy cost, and some sort of power costs. Energy costs are analogous to the cost of diesel fuel for an ICE bus, but demand charges are a new cost that can have unexpected impacts on transit operations. Demand charges can vary widely between utility operators. Typically, demand charges are calculated based on the peak 15 minute power demand used of a customer over a monthly billing period, but other systems such as Time Of Use (TOU) pricing that vary the cost of energy based on typical or real-time demand can be considered a type of indirect demand charge [14]. Demand charges can become the dominant BEB fueling cost

[16] [17], which warrants investigation into power management and optimized BEB charging strategies.

One interesting form for energy management to take is that of Stationary Energy Storage Systems (SESS)[1]. In general, an can SESS provide value in several ways:

1. **Peak Shaving:** An SESS can be used to reduce demand charges by discharging during high demand times to reduce peak power demand.

2. **Load Shifting:** An SESS has the potential to avoid energy use during high TOU hours by charging during low cost hours and discharging during high costs hours.

3. **Infrastructure Upgrade Deferral:** Since electrical substation infrastructure is sized based on peak power consumption, an SESS can be used to avoid or defer a required upgrade by reducing the peak power consumption.

While infrastructure upgrade deferral can provide benefit to a transit agency, it generally requires a more specific approach with knowledge about the location, power, and pricing for existing utility connections [18]. This work focuses more on the operational savings possible to a transit agency, rather than the capital expenditure savings, so the main pathways to savings considered in this work are peak shaving, and load shifting.

1.3 Thesis Objective and Contributions

The overarching objective of this thesis is to model energy consumption of electric buses and their charging infrastructure in order to investigate the potential for an SESS to help reduce costs. Under this objective, this thesis has resulted in two main contributions:

1. A novel data driven method for estimating the energy consumption of a fleet of buses was created. While other energy consumption models exist in the literature, the new method presented transforms low-fidelity but widely available data into a higher fidelity form that can be accurately used for energy estimation purposes and to determine the charging system requirements.

[1]The term "stationary" is used throughout this work to differentiate this type of energy storage system from the traction batteries that are on-board an electric bus

2. An investigation of the techno-economic advantages provided by different charging system deployments with an integrated SESS. This was done by modelling SESS costs, creating a framework to model the charging load for a given BEB deployment scenario, and then performing an optimization to find which SESS resulted in the lowest lifetime cost. An array of charging scenarios and price projections are considered.

1.4 Thesis Outline

This thesis has been separated into 4 chapters. Chapters 2 and 3 take the form of co-authored manuscripts that have been/will be submission to academic journals for publication. A short preface is added to these chapters to give the manuscripts context within the thesis, and to attribute credit between the co-authors. These chapters contain their own background, methods, results, and conclusions.

Following this introduction chapter, the remaining thesis is organized as follows:

Chapter 2 - Fleet-wide bus drivecycle modelling and energy estimation using real-time transit feed data

This chapter explains the novel methods used to model the drivecycles and energy consumption of an entire transit fleet using publicly available real-time transit feed information. These methods are then used to determine the amount and timing of energy use resulting from a 100% electric bus fleet operated in Victoria, BC.

Chapter 3 - Techno-economic optimization of Stationary Energy Storage System technologies for Ebus charging

Using the results from the work presented in Chapter 2, this chapter models the utility demand profile for a given on-route charging system deployment and explores the potential for different types of SESS to reduce the total lifetime cost by optimizing their capacity and operation. This chapter also investigates the reduction in required on-board energy storage capacity resulting from the on-route charging deployment.

Chapter 4 - Conclusion

This chapter summarizes the key findings and implications of the previous two

chapters and reviews the potential future work that could be performed in this field.

Chapter 2

Fleet-wide bus drivecycle modelling and energy estimation using real-time transit feed data

This chapter is based on a publication submitted in December 2021 to the *Journal of Transportation Research Part D: Transportation and the Environment* with the same title as this chapter, authored by G. Wilson and Dr. C. Crawford. G. Wilson, the author of this thesis, was responsible for the research methodology, data collection, data analysis, validation, and manuscript preparation. C. Crawford was responsible for supervision of all work and for review and editing of the manuscript.

2.1 Introduction

Electric buses offer a low-carbon alternative to conventional diesel buses, but some challenges remain for transit agencies to begin or ramp-up electrification. More specifically, electric buses require additional infrastructure and planning in order to ensure economical and reliable operation. Ineffective planning can lead to issues with inadequate driving range, unnecessarily high charging costs paid by the transit agency, and issues with insufficient utility infrastructure in areas with a constrained electrical grid [18, 19, 16]. To avoid these issues, it is desirable to have an accurate yet convenient method to estimate the energy used across a fleet of transit buses on each specific route. A critical input to energy estimation models is the speed and acceleration of the transit bus. High fidelity GPS data ($\leq$1 Hz) collected directly from a bus oper-

ating on the specific route(s) being studied is the most desirable form of drive cycle data, and has been used extensively to calculate the energy consumption of buses in previous studies [20] [21].

1 Hz drive cycle data can be difficult to obtain for both system planners and for researchers. Collecting and transmitting real time 1 Hz GPS data for even a small number of vehicles can become costly, and when data is available, it may not be made public due to privacy issues. Several alternative methods can be used to help estimate the energy use of a bus when high quality data is unavailable. The simplest option is to assume the bus consumes a set amount of energy per distance. While this method is fast and easy, it is generally too simple for research or system planning purposes.

An improved alternative is to apply a published standard drive cycle profile to the energy consumption model. Standard drive cycles are speed profiles created from characteristic routes intended to broadly represent different driving scenarios [22]. Different drive cycles may be developed from buses operated in urban or rural areas, and vary in terms of acceleration, velocity, number of stops, and route duration. Different approaches can be used in situations where the transit route being modelled does not match the available standard drivecycles. Lajunen and Lipman [23] performed simulations using a variety of different standard drive cycles to represent a range in operating conditions. De Filippo et al. [24] applied two different drive cycles, one representing the urban portion of their route and the other the rural portion, in order to better match the driving data to their applications. While the shortcomings can be addressed for some applications, the static nature of standard drive cycles makes it difficult to apply them to entire fleets of buses where operating conditions vary substantially due to factors such as differing traffic conditions, bus stop frequency, and driver behaviour.

To better approximate the varied characteristics of the route being studied, a synthetic drive cycle can be created based on the characteristics of the bus route such as speed limits, stop signs, traffic lights, and bus stops. Synthetic drive cycles vary in complexity, but they generally created by defining where and for how long a bus stops (either due to traffic impediments or for passenger service) and then populating the distance between the bus stops with a given acceleration and speed profile based on the traffic system [25]. Synthetic drive cycles are widely applied in the modelling of transit buses. Many research efforts have used manually extracted routes from digital mapping programs, such as Sinhuber et al. [25] who simulated the energy demand for a fleet of buses to determine the proper sizing of on-board electric

bus batteries, or Rogge et al. [26], who simulated the energy use for a transit system to investigate the impacts on the electrical grid. Gallet et al. [27] used information about bus arrival and departure times to create synthetic drive cycles for the entire Singapore public bus network, and used it to investigate the impacts of different levels of transit bus electrification. Synthetic drive cycles can be made increasingly complex as well. Kivekäs et al. [28] incorporated stochastic variables for aspects such as average and peak acceleration, speed, or number of passenger and traffic stops based on distributions from measured data. Kivekäs et al. combined this stochastic synthetic drive cycle construction method with a Monte Carlo analysis to investigate the advantages of different drive train types and configurations.

Stochastic synthetic drive cycles offer improvement over standardized drive cycles, but they still have limitations, specifically for fleet wide use. The parameters required to set up such a model may vary within a transit system, or within a route, making it difficult to ensure that the system accurately reflects the real world characteristics of a system without already being in possession of data describing the drive cycle characteristics. Without operating data, it can be difficult to match the wide range of operating conditions within even a single transit route. While more complex synthetic drive cycle construction methods have been created and applied, the increased human and computational effort required to create and apply these techniques to an entire transit system becomes unwieldy. This is especially true for transit agencies early on their path to electrification who may have limited budgets, data, and analytical capabilities to dedicate towards drivecycle estimation.

This work presents and validates an alternative method for creating drive cycles utilizing publicly available General Transit Feed Specification (GTFS) gtf data that is both accurate and convenient. The GTFS format is a widely used and published by transit agencies around the world [30]. GTFS data comes in two forms; static GTFS data, which relates to the route and scheduling of a transit system, and real time GTFS data, which provides periodic updates for the live position and status of buses in a transit system. Static GTFS data is typically updated on a seasonal or annual basis, or as changes are made to the transit system/routes. Real-time GTFS data contains data from an on-board Automatic Vehicle Location (AVL) system, and is typically published every 15-60 seconds, depending on the transit agency. The main intention of GTFS data is to more easily allow 3rd party developers a standardized source of data to be used to integrate transit scheduling and mapping into their platforms [29]. Not all transit agencies publish both types of GTFS data,

but it is a widely used standard in North America and quickly growing across the world. Additionally, when the GTFS format is not used, an equivalent method for publishing similar transit system information including AVL data is often used, such as the Standard Interface for Real-time Information (SIRI) protocol [31].

This work presents another use for GTFS data; a method for using the low frequency speed and position data from a GTFS real-time feed to easily create a set of high fidelity, fleet-wide, realistic drive cycles for a given transit agency. Public real time transit feeds have been used by researchers in the past in a variety of research fields [32], but only to a limited extent in energy estimation. Addo and Hatzopoulou [33] used AVL data to estimate the power consumption and GHG emissions for transit buses, and He et al. [34] used a SIRI feed to create drivecycle data for transit modelling, but the exact nature of data collected (amount, frequency, etc.) was not presented or discussed at depth in either work.

The primary goal of this work was to rigorously explain the methods used to create higher resolution drive cycles from GTFS data and discuss their accuracy for the purpose of energy estimation. To achieve this goal, a GTFS derived drive cycle has been compared to a synthetic drive cycle, as well as to 1 Hz GPS data collected along the route being modelled. The drive cycles for an entire fleet of buses were created and used to model the energy consumption across the entire transit system. Finally, a sensitivity analysis was performed to investigate which inputs aside from the drive cycle data are of the greatest interest.

For this work, GTFS data was collected from the public transit feed for all active transit buses in the Victoria Regional Transit System (VRTS), in Victoria, British Columbia, Canada for approximately 2 weeks [35]. The VRTS is operated by BC Transit, and consists of 355 transit buses servicing 56 different routes across 13 different municipalities. The VRTS fleet currently consists of a mix of diesel and compressed natural gas buses, but BCTransit, like many other transit operators, has committed to transitioning the fleet to zero carbon vehicles within the next 20 years [36]. Because of these plans, and because the transit system is large and already collecting and publishing GTFS data from their buses, the VRTS is a good candidate for GTFS drive cycle construction and energy estimation. Installing loggers to collect and process 1 Hz GPS data for each bus could become expensive and difficult, while utilizing GTFS data requires no new infrastructure or data collection since it uses tools and telemetry systems already installed in many transit systems.

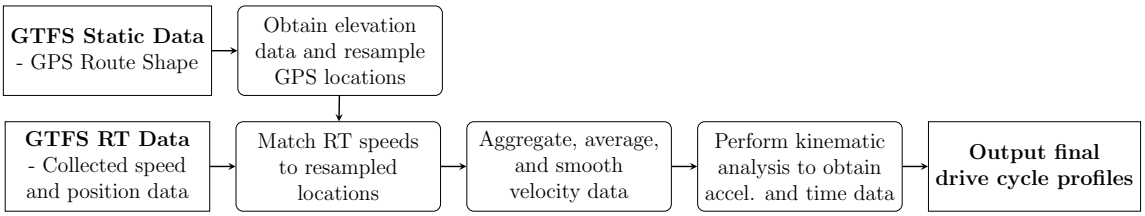

Figure 2.1: Drive cycle creation overview

2.2 Methods

To create and evaluate the drive cycle from the GTFS data, three modelling tasks were performed. The first model processes the static and real-time GTFS data and constructs drive cycle profiles. Second, a synthetic drive cycle model was created as a comparison for the GTFS construction method. Finally, a physics based energy estimation model is created to evaluate the energy consumed by a bus operating on a given drive cycle. The energy estimation model can be used to compare the energy predictions between the GTFS constructed drive cycle, the synthetic drive cycle, and a 1 Hz measured GPS drive cycle to evaluate the performance of the drive cycle construction methods.

2.2.1 GTFS Drive Cycle Construction

An overview of the processes used to construct the GTFS drive cycle is shown in Figure 2.1. Data is collected from both the GTFS static, and real time feeds and processed in several steps to create the final drive cycle profiles.

The first step in constructing the GTFS drive cycle data is to identify the bus route of interest within the GTFS static data. The static data contains a collection of geospatial points describing the path of travel that a bus takes on a given route. The frequency of locations contained in the GTFS static files varies depending on the path taken by the bus, generally containing points at all turns, bus stops, or other locations relevant to the bus drivers path. While the paths defined by these points are well defined, the distance between each point is variable and not required to be provided in the data feed. The Haversine formula, shown in Equations 2.1 and 2.2, is used to calculate the distance d between two locations, accounting for the Earth's curvature.

$$d = 2 \cdot r_e \cdot \sin^{-1}\left(\sqrt{a}\right) \tag{2.1}$$

$$a = \sin^2\left(\frac{\varphi_{i+1} - \varphi_i}{2}\right) + \cos(\varphi_i)\cos(\varphi_{i+1})\sin^2\left(\frac{\lambda_{i+1} - \lambda_i}{2}\right) \tag{2.2}$$

In Equations 2.1 and 2.2, φ_i is the latitude at location i, and λ_i is the longitude at location i, r_e is the radius of the Earth taken to be 6,371 kilometers [37].

Because the locations contained in the original GTFS route data are based on the route features, the sampling frequency is irregular, making it difficult to work with. Once the total length is known for a chosen route, the route locations can be resampled at a regular interval of d_i by interpolating along a path created from the original static route locations. Different choices of sampling distance between 5 and 20 meters are investigated in this work. These values were chosen as they roughly match the distance between data points if 1 Hz data was collected for a vehicle traveling at roughly 20 km/hr and 75 km/hr respectively, which represent the approximate range of average speeds observed by buses operating in transit systems [38]. The resampled route locations form the structure to be populated with drive cycle data.

Elevation data must also be obtained in order to determine the energy consumption of a vehicle. Elevation data was obtained for each of the resampled route locations using the Google Elevations API. The Elevations API uses a digital elevation model maintained by Google. Use of the Google digital elevation model to extract road elevation and grade data has been previously studied and found to be of sufficient accuracy for modelling transportation applications [39].

Road slope is calculated directly from the elevation data using Equation 2.3, where m_i is the road slope and h_i is the elevation at a point.

$$m_i = \frac{h_{i+1} - h_i}{d_i} \tag{2.3}$$

To populate the drive cycle with speed data, several days of GTFS real time data is collected. The amount of time over which data should be collected for a single route depends on the update frequency of the GTFS real time data, the frequency of service along a route, and the length of time that a single route takes to be completed. For this work, data was collected for approximately 2 weeks, amounting to a total of over 2 million data points across 56 transit routes. Although many data fields are published in a typically GTFS feed, the only data collected and used for this work

was the route being serviced, the latitude and longitude of the bus, and the recorded bus speed.

Once all data is collected, the bus real time geospatial locations are each matched to the nearest location from the static route path and the speeds are aggregated. Where more than one real-time bus location is matched to a single static route position, the median velocity from that location is used as the data point. The median velocity is chosen over the mean to help mitigate the influence of outlier data points. Any remaining gaps in the speed data are linearly interpolated and filled before the resulting speed profile is filtered using a second degree Savitzky-Golay filter [40]. The Savitzky-Golay filter smooths data by fitting a least squared error quadratic curve over a window of W data points centered around point i, which is then used to obtain the filtered value for point i before fitting a new quadratic curve for point around $i+1$. The filter is intended to ensure that the data is smooth and continuous. Practically, a value of 1 for W would result in no smoothing, and if W were equal to the number of total data points along the route, the filtered data would create a smooth second degree polynomial speed profile across the entire event. The impact of different filtering values is explored in order to create a model that best matches the real transit data collected along the same routes.

Once the velocities are sorted, aggregated, and filtered, kinematic analysis can be performed to obtain the velocity and time data for each route location. The acceleration is found using Equation 2.4, while the time span between data points is found using Equation 2.5.

$$a_i = \frac{v_{i+1}^2 - v_i^2}{2 \cdot d_i} \tag{2.4}$$

$$t_i = \frac{2 \cdot d_i}{v_{i+1} - v_i} \tag{2.5}$$

It is possible that two or more consecutive data points will have a recorded velocity of zero, making Equation 2.5 undefined. This may, for example occur near a passenger bus stop, since the space that the bus may become stopped at can span more than d_i meters in length. When such an event occurs, the time span is replaced with an arbitrary choice of a 10 second time gap and the acceleration taken to be 0. Since the velocity is zero for these instances, this choice has little impact on the final results of the process in terms of overall energy consumption.

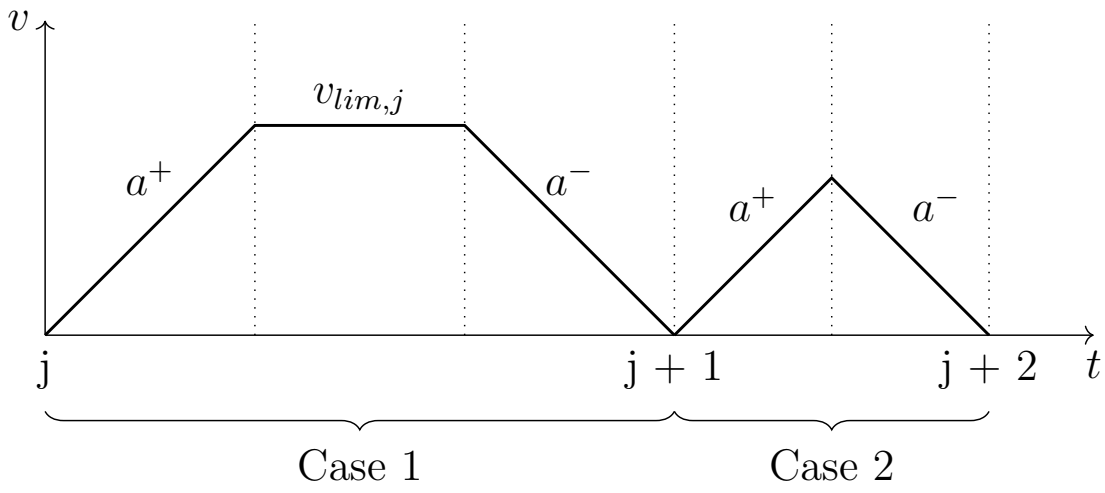

Figure 2.2: Synthetic Drive Cycle Construction Example

2.2.2 Synthetic Drive Cycle Construction

A simple synthetic drive cycle model is used as a comparison for the GTFS drive cycle creation methods explained above. A simple synthetic drive cycle with a uniform acceleration and deceleration values and a uniform target speed was chosen. As discussed above, synthetic drive cycles can vary in complexity, but because the context of this work is fleet wide energy consumption modelling where high fidelity data is unavailable, it is assumed that the model has no route specific speed and acceleration data other than the traffic impediment locations and types. The acceleration and deceleration values were obtained from the National Renewable Energy Laboratory Fleet DNA Project Data, which contains data from 19 buses operating over a total of 472 days [41]. The acceleration value used was 0.407 m/s^2, and the deceleration value used was -0.416 m/s^2.

To create the synthetic drive cycle, traffic impediments, transit stops, and posted speed limit signs were identified along the route. To represent different traffic scenarios, "light duty", "medium duty", and "heavy duty" scenarios were created by varying the probability that a bus would stop at any given traffic impediment or transit stop was varied from 25%, 50%, and 90% respectively.

For a given scenario, moments when the bus is stopped are designated by j, as seen in Figure 2.2. The spaces between stops are filled based on whether or not the bus can reach $v_{lim,j}$, the posted speed limit for the roadway in question, within the space between j and $j+1$. Figure 2.2 shows Case 1, where the bus is able to reach

v_{lim}, and Case 2, where the bus begins to decelerate before reaching $v_{lim,j}$.

2.2.3 Energy Estimation and Comparison Metrics

To investigate the validity of the drive cycle construction methods discussed above, a method to estimate the energy consumption based on the drive cycle is required. To do this, a physics based model describing the forces on a transit bus is applied [42]. The forces accounted for are the aerodynamic force, the gravitational force, the force from the rolling resistance of the tire, and the inertial force due to acceleration. The instantaneous forces are found at each location i along the roadway.

The aerodynamic forces F_{aero} are found with Equation 2.6, where ρ is the density of the air, A_f is the frontal area of the bus, and c_d is the drag coefficient for the bus.

$$F_{aero,i} = \frac{\rho \cdot A_f \cdot c_d \cdot v_i^2}{2} \tag{2.6}$$

The gravitational forces f_{grav} are found with Equation 2.7, where M is the mass of the bus, g is the gravitational acceleration constant, and θ_i is the angle of the road.

$$F_{grav,i} = M \cdot g \cdot \sin(\theta_i) \tag{2.7}$$

The forces due to rolling resistance are found using Equation 2.8, where c_{r0} is the fixed rolling resistance and c_{r2} is the variable rolling resistance for the bus tires.

$$F_{roll,i} = (c_{r0} + c_{r2} \cdot v_i^2) \cdot M \cdot g \tag{2.8}$$

The inertial forces are calculated with Equation 2.9:

$$F_{accel,i} = M \cdot a_i \tag{2.9}$$

The sum of these forces is balanced against the propulsion force $F_{prop,i}$ created by the bus wheels during operation:

$$F_{prop,i} = F_{aero,i} + F_{grav,i} + F_{roll,i} + F_{acc,i} \tag{2.10}$$

The parameters pertaining to the physical bus modelled in this work represent an standard transit bus, and are shown in Table 2.1. The auxiliary load was chosen to represent a scenario where a heating or cooling load is required by the bus, along with the other auxiliary loads such as lighting.

Table 2.1: Bus Parameters Used

Parameter	**Symbol**	**Value**	**Ref.**
Bus Mass	M	14535 kg	[42]
Frontal Area	a_f	8.68 m^2	[2]
Air Density	ρ	1.2041 kg/m^3	-
Drag Coefficient	c_d	0.65	[42]
Fixed Roll. Res.	c_{r0}	0.006	[43]
Variable Roll. Res.	c_{r2}	4.5 x $10^{-7} s^2/m^2$	[43]
Wheel Radius	r_w	0.5 m	[42]
Transmission Eff.	η_t	0.95	[42]
Trans. Gear Ratio	GR	5.67	[42]
Converter Eff.	η_c	0.97	[42]
Auxiliary Load	P_{aux}	5,000 W	-

The energy estimation model used in this work is adapted from literature, and also accounts for inefficiencies within the electric drivetrain of the transit bus, as well as energy saved due to regenerative braking [42]. Figure 2.3 shows the flow of energy within the drivetrain. The propulsion forces found using Equation 2.10 can be translated through the drivetrain to calculate the amount of electrical energy drawn from the bus battery system for a particular mission. Due to regenerative braking, energy flows both directions through the drivetrain, and into and out of the battery system.

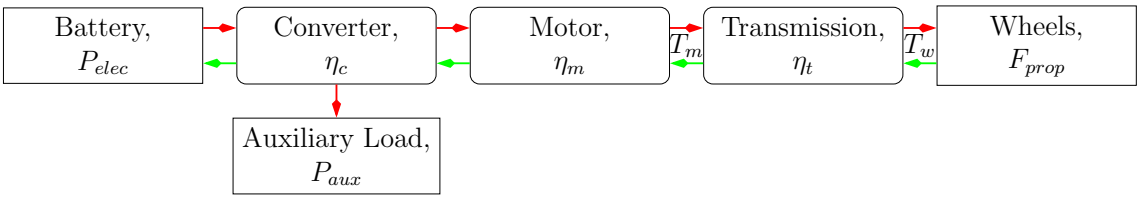

Figure 2.3: Energy Flow in the Drivetrain

The transmission and power converter efficiency are assumed to be constant under all conditions, but the motor efficiency is calculated based on the rotational speed and torque during operated. A motor efficiency plot, shown in Figure 2.4, created from data provided by an electric bus manufacturer, is used to find the motor efficiency for each location [42].

The rotational speed of the motor, $\omega_{m,i}$, can be found using the linear velocity of

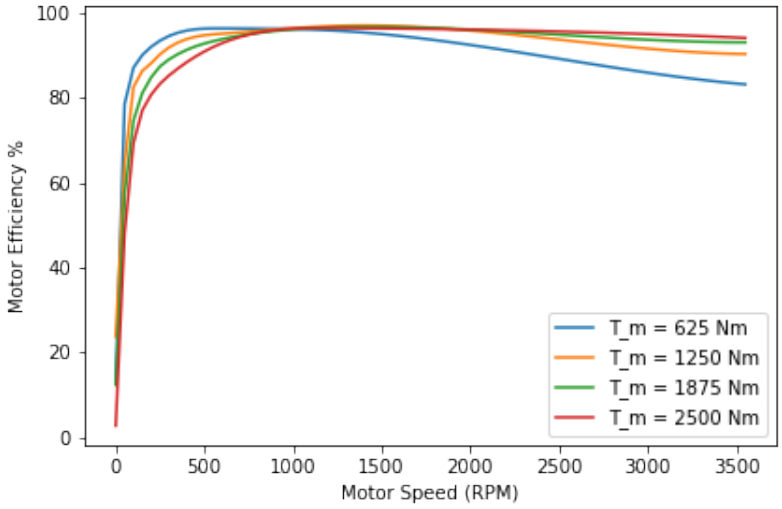

Figure 2.4: Transit Bus Electric Motor Efficiency Map

the bus, as well as GR, the gear ratio of the transmission, and r_w, the radius of the wheel.

$$\omega_{m,i} = \frac{v_i \cdot GR}{r_w} \tag{2.11}$$

The torque required at the wheels is calculated from the propulsion force and the wheel radius.

$$T_{w,i} = F_{prop,i} \cdot r_w \tag{2.12}$$

The motor torque T_m is found using the wheel torque, transmission efficiency η_t, and the gear ratio of the transmission. Once motor torque is known, the motor efficiency can be determined using the motor speed and torque along with the motor efficiency plot.

$$T_{m,i} = \frac{T_{w,i}}{GR \cdot \eta_t} \tag{2.13}$$

The electrical power draw used when the bus draws energy from the battery can be calculated for each position using equation 2.14. S is the portion of energy recovered through regenerative braking (assumed to be 40%), and is applied when the propulsion forces are negative (when the bus is braking) to calculate the energy returned to the battery system.

$$P_{elec,i} = \begin{cases} \dfrac{T_{m,i} \cdot \omega_{m,i}}{\eta_{m,i} \cdot \eta_c} + \dfrac{P_{aux}}{\eta_c} & \forall F_{prop,i} \geq 0 \\ \\ \left(T_{m,i} \cdot S \cdot \omega_{m,i}\right) \cdot \left(\eta_{m,i} \cdot \eta_c\right) + \dfrac{P_{aux}}{\eta_c} & \forall F_{prop,i} < 0 \end{cases} \tag{2.14}$$

The energy consumption over the entire route can be calculated with the instantaneous power draw, and the length of time for each step.

$$E_{route} = \sum_{i=0}^{I} P_{elec,i} \cdot t_i \tag{2.15}$$

The energy consumption can also be communicated in terms of energy intensity, which allows for easier comparison of energy metrics between different routes.

$$\dot{E}_{route} = \frac{E_{route}}{D_{tot}} \tag{2.16}$$

Five additional metrics were also used to compare the constructed drive cycles to the 1 Hz measured drive cycles. These metrics were chosen as they represent the general patterns in the driving behaviour better than some form of time series analysis. Time series analysis would be influenced by the exact number and location of bus stops/traffic impediments experienced on an individual trip, whereas these statistics are intended to be agnostic to the exact drive cycle and instead represent the general patterns. Simple statistics like the average and maximum speeds are compared, as well as the computed metrics of aerodynamic velocity and characteristic acceleration. The characteristic acceleration and aerodynamic velocity are statistics commonly used to compare the energy/fuel consumption characteristics for a given route and are discussed in-depth by O'Keefe et al. and Prohaska et al. [44, 22].

The aerodynamic velocity measures the ratio of the average cubic speed to the average speed. Note that the aerodynamic speed for a drive cycle with a constant velocity would simply be equal to the velocity, while the aerodynamic speed of a drive cycle with variable speed will be higher than the average speed. The aerodynamic speed can be computed with Equation 2.17. The square of the aerodynamic velocity is used as a metric in this work, as it is typically used in the literature.

$$v_{aero}^2 = \frac{\sum_{i=0}^{I} \left(\overline{v_i^3} \cdot t_i\right)}{D_{tot}} \tag{2.17}$$

$$\overline{v_i^3} = \frac{v_{i+1}^3 + v_{i+1}^2 \cdot v_i + v_i^2 \cdot v_{i+1} + v_i^3}{4} \tag{2.18}$$

The characteristic acceleration represents the inertial work performed during acceleration over a drive cycle, and can be computed with Equations 2.19 and 2.20. Characteristic acceleration is only a measure of acceleration profiles for a route, not the deceleration. For a vehicle accelerating at a uniform rate on flat ground, the characteristic acceleration would simply be equal to the given uniform acceleration.

$$a_{char} = \frac{\sum_{i=0}^{I} \overline{a}}{D_{tot}} \quad \forall \overline{a} > 0 \tag{2.19}$$

$$\overline{a} = \left(\frac{1}{2} \cdot (v_{i+1}^2 - v_i^2) + g \cdot (h_{i+1} - h_i) \right) \tag{2.20}$$

Number of stops was also compared between the drive cycles to see how the different filtering parameters affect the stop and go patterns of the bus. While all metrics are important and of interest, the intended purpose for this drive cycle modelling method is to estimate the energy consumption of a transit route, so the energy intensity metric is considered the most important value to be matched.

2.3 Results and Discussion

The results and discussion are presented in four parts. First, in Section 2.3.1 the GTFS drive cycle construction methods are tuned using the 1 Hz measured GPS data, and compared to a synthetic drive cycle created for a similar route. Section 2.3.2 contains analysis of the resulting drive cycles, and the implications of the construction method are discussed. In Section 2.3.3, the drive cycles are used to estimate the energy consumption for an entire fleet of buses, and the results are reviewed. Finally, in Section 2.3.4 a sensitivity analysis is performed for the energy estimation model to investigate the importance of various other input parameters aside from the drive cycle profile.

2.3.1 Parameter Tuning and Accuracy of the GTFS Construction Method

The 1 Hz measured data was collected from two routes in Victoria; Eastbound Route 14 and Northbound Route 27. These routes travel across several municipalities, and through residential and commercial areas. To ensure that individual traffic events did not influence the results, six trips on Route 14, and seven trips on Route 27 were measured on different days and times, and the results presented show the mean statistics over all trips. Parameter tuning is completed with the data for Route 14, and then confirmed using the data from Route 27. For reference, Eastbound Route 14 is shown represented within the modelling framework in Figure 2.5 and by the transit operator in Figure 2.6.

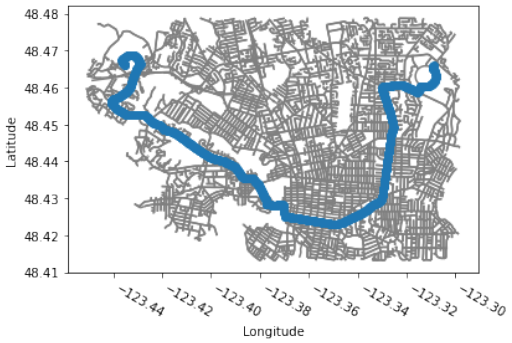

Figure 2.5: Constructed Route 14 Map

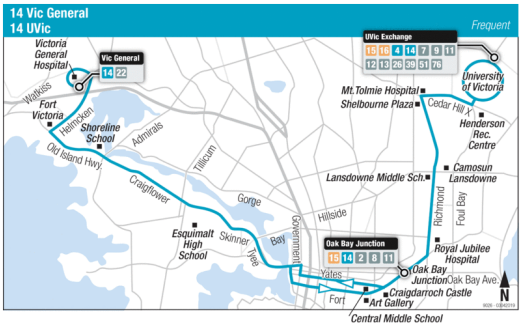

Figure 2.6: Published Route 14 Map [2]

As previously stated, the interval distances d_i and filtering window W impact the characteristics of the drive cycle constructed. Different interval distances d_i of 5 meters, 10 meters, and 20 meters were used along with different filtering window lengths W of 7, 9, and 11 data points for the second degree Savitzky-Golay filter. For each of the 16 possible parameter combinations, the metrics discussed in Section 2.2.3 were computed for both the constructed and measured Route 14 drive cycles. These statistics are shown in Table 2.2.

The different filtering parameters influence the results greatly, with the least filtered drive cycles generally overestimating the speed, acceleration, and energy consumption metrics. Filtering parameters have a much greater impact on the acceleration metrics than the speed metrics. This can be observed in the values for the characteristic acceleration. The high characteristic acceleration is caused by artificial fluctuations in the constructed drive cycles that would not appear in the real drive

Table 2.2: Summary Statistics for Route 14 Constructed Drive Cycles

d_i (m)	w	$\dot{E}$ (kWh/km)	a_{char} m/s^2	v^2_{aero} (m^2/s^2)	Stops	v_{mean} $(m/2)$	v_{max} $(m/2)$
5	7	2.24	0.799	93.8	113	32.2	59.0
5	9	1.97	0.799	93.8	113	32.2	59.0
5	11	1.78	0.799	93.9	113	32.2	59.0
10	7	1.72	0.450	93.6	84	32.0	57.0
10	9	1.57	0.450	93.7	84	32.0	57.0
10	11	1.44	0.450	93.9	84	32.0	57.0
20	7	1.39	0.299	93.9	44	31.8	56.5
20	9	1.23	0.299	94.1	44	31.8	56.5
20	11	1.14	0.299	94.5	44	31.8	56.5
GPS	GPS	1.30	0.227	108.5	46	28.9	63.7

cycle. Figure 2.7 shows this by comparing a subset of the velocity data for the most and least filtered constructed drive cycles along with the 1Hz GPS data. The variability in 1 Hz speed data when the bus is travelling at a constant speed (as seen between 5 km and 5.25 km in Figure 2.7) lies somewhere between the most and least filtered constructed drive cycles.

A value of 20 for d_i creates a drive cycle that best matches the characteristic acceleration of the 1 Hz measured GPS data. Since the aerodynamic velocity values are not greatly influence by the filtering, and since it also resulted in the closest number of stops to the 1 Hz data, a value of 20 for d_i was selected as most appropriate for this application. Although the precise location of each stop in the GTFS drive cycle does not line up with the single measured drive cycle shown in Figure 2.7, the agreement between the number of stops predicted by the constructed drive cycle shows very good agreement with the measured data, which in itself is a useful outcome. Aside from use in energy estimation, the GTFS data could also be of great value in assisting transit operators better plan/predict bus stop probabilities along a route in order to provide better service.

Of the three drive cycles using a d_i of 20, the filtering window of 9 best matches the energy intensity value of the real GPS data. Based on these conditions, the filtering parameters of $d_i = 20$ and $W = 9$ were selected to be used for the remainder of this work.

To evaluate whether these tuned parameters generalize across the rest of the data set, a second transit route was used as a validation test. Route 27 was used for the

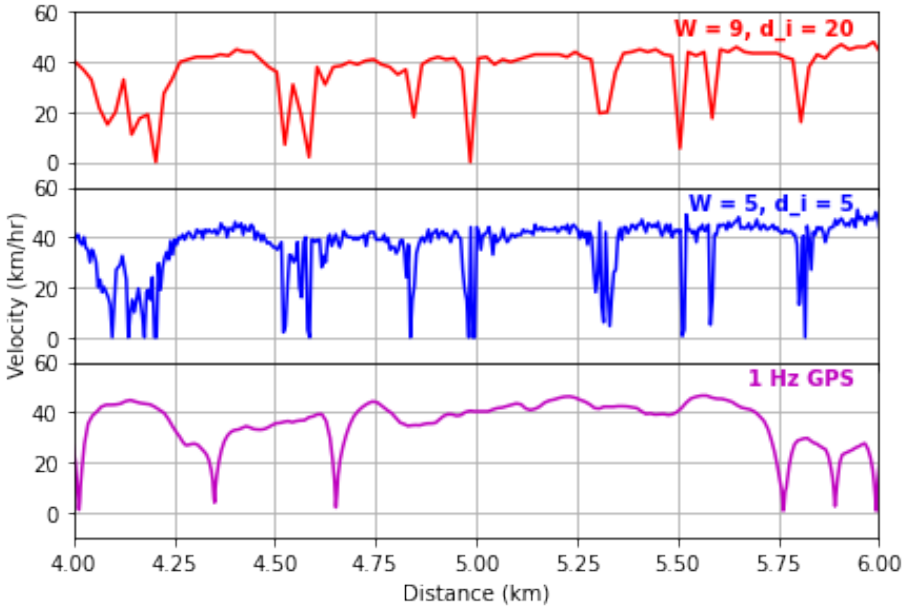

Figure 2.7: Impact of filtering on velocity fluctuations

validation route. The statistics from Route 27 for the 1 Hz data (denoted as "1 Hz GPS (All)") and constructed drive cycles (denoted as "GTFS Derived") are shown in Table 2.3.

Table 2.3: Summary Statistics Route 27

Case	$\dot{E}$	a_{char}	v^2_{aero}	Stops	v_{mean}	v_{max}
GTFS Derived	1.29	0.303	84.0	38	29.5	48.5
1 Hz GPS (All)	1.42	0.276	96.2	49	25.2	60.1
1 Hz GPS (Removed)	1.39	0.257	95.6	46	25.6	58.0

The characteristic acceleration and aerodynamic velocity for Route 27 show a similar margin of error as found for Route 14, with the characteristic acceleration estimation being higher than the measured data, and the aerodynamic velocity being lower. Compared to Route 14, the GTFS derived energy efficiency estimate for Route 27 is less accurate (5.4% vs 9.2% difference from the GPS data). It is noted that the difference in energy estimation between the measured data for this route was much larger than on Route 14. While the standard deviation between the seven 1 Hz GPS measured trips on Route 14 was 0.058 kWh/km, the standard deviation for the eight 1 Hz GPS measured trips on Route 27 was 0.119 kWh/km. This larger standard deviation makes it more difficult to draw insight, but also helps to explain the error.

Table 2.4: Summary Statistics for Synthetic Drive Cycles

case	$\dot{E}$	a_{char}	v^2_{aero}	Stops	v_{mean}	v_{max}
Light	0.99	0.047	134.5	12	40.4	50.0
Medium	1.16	0.124	97.4	42	32.6	50.0
Heavy	1.27	0.176	66.8	75	25.7	50.0
GTFS Derived	1.23	0.299	94.1	44	31.8	56.5
1 Hz GPS	1.30	0.227	108.5	46	28.9	63.7

One of trip on Route 27 showed an abnormally high amount of acceleration (characteristic acceleration of 0.381 m/s^2) and max speed (73.0 km/hr). Removing this single data point results in the mean statistics denoted in Table 2.3 as "1 Hz GPS (removed)". Having removed the outlier, the energy efficiency estimate is 1.39 kWh/km, which results in a difference of 7.2%. The existence of this outlier shows a limitation of this drive cycle construction method, but it also highlights some of its advantages. The GTFS construction methods are unable to predict the variance in energy consumption on a route, but they are able to collect hundreds of hours of data across all traffic conditions and driver behaviours to represent the "typical" driving and traffic patterns for a route.

The tuned GTFS drive cycle can also be compared to a set of synthetic drive cycles created for eastbound Route 14 to demonstrate how the GTFS drive cycles compares to a simple method found in literature. Summary statistics for the synthetic drive cycles as well as the tuned GTFS constructed drive cycle and the 1Hz GPS drive cycle are shown in Table 2.4. Since the synthetic drive cycles involve a random chance of the bus stopping, each synthetic drive cycle was created 10 times and the statistics shown are the mean values for each scenario.

It can be seen that the synthetic drive cycles tend to underestimate the energy consumed even under the "heavy duty" scenario. While the "heavy duty" scenario most closely matches the energy consumption of the measured route, it is important to remember that the measured data is the average of many trips, intended to represent the "typical" bus trip, not a particularly heavy use scenario. For this reason, the measured data, and the constructed drive cycle is more fairly compared to the "medium duty" scenario, which further underestimates the energy consumed.

The characteristic acceleration and aerodynamic speed also show poor agreement with the measured data in all cases. The acceleration is greatly underestimated in the "light duty" and "medium duty" scenarios, while the aerodynamic speed is greatly

underestimated in the "heavy duty" scenario. Overall, this shows how the synthetic drive cycles have a difficult time representing the varied and dynamic nature of transit bus driving.

The similarity between the 1 Hz drive cycle, the GTFS drive cycle, and the "heavy duty" synthetic drive cycle can be seen in Figure 2.8. To allow for better comparison of the number of stops, periods where the bus speed falls below 5 km/h are indicated with a red line. The visual representation of the speed profiles further reinforces the conclusion that the GTFS method has a better ability to represent the varied and dynamic acceleration and speed profiles when compared to a synthetic drive cycle. Comparing these methods also highlights how they could be combined. Using data driven methods to extract the average acceleration profiles, typical speeds, and number of stops from the GTFS data could allow for enhanced synthetic drive cycle creation in future work.

2.3.2 Drive Cycle Analysis and Discussion

This section gives a more in depth look at the data and methods used to construct the drive cycles for each route. First, it is noted that the number of data points collected from the GTFS real-time feed influences the results. For this work, 66,342 raw data points were collected along the eastbound section of Route 14, along with a total of 2,047,338 data points for the rest of the transit system. This amount of still data resulted in some consecutive intervals with missing data. These data points were interpolated in order to obtain a complete speed profile. The completeness of the data for the chosen d_i value of 20 meters is shown in Figure 2.9. Across the entire transit system, more than 95% of the data is present with no interpolation, and more than 98% of the data was present when interpolating across only two interval length, suggesting that the data is well populated. Only two data points were missing from the 961 possible locations on eastbound Route 14, and data was present for all 691 of the 691 possible locations on Route 27.

It is also interesting to look at the distribution of data points within a single location. Across the data for Route 14, the mean of the standard deviation of the raw speed data is 2.46 m/s (8.84 km/hr). The methods presented here are an attempt to quantify a "typical" transit route. Because of this, the GTFS derived drive cycles present stops when the bus is usually stopped, and show steady speeds when the bus is typically at steady speed. Of interest is the behaviour in locations where the bus

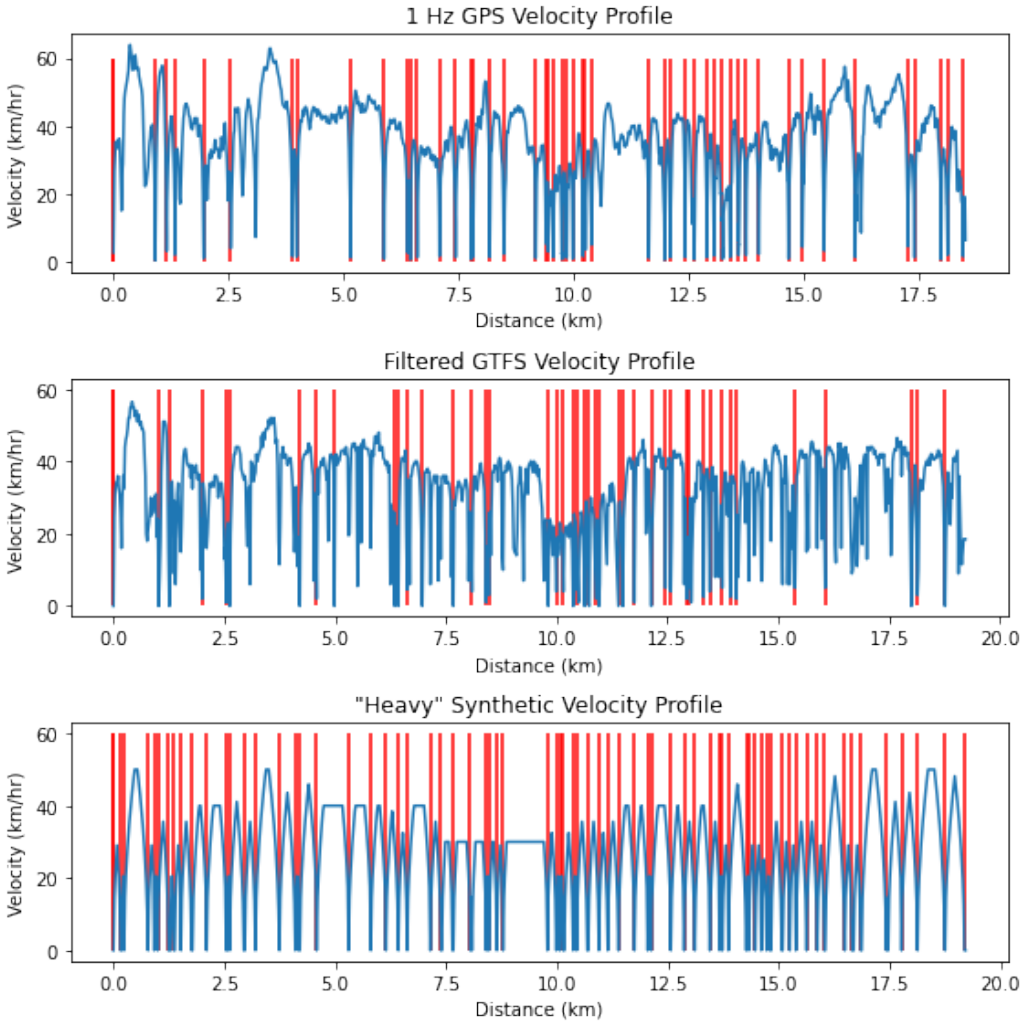

Figure 2.8: Visual comparison of velocity profiles and number of stops

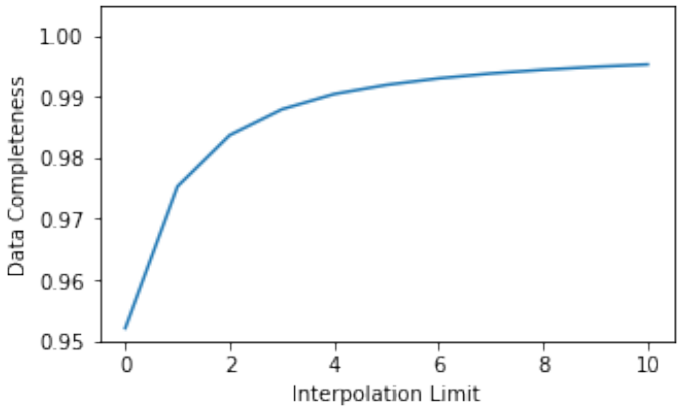

Figure 2.9: Interpolation and average speed profile completeness across all routes

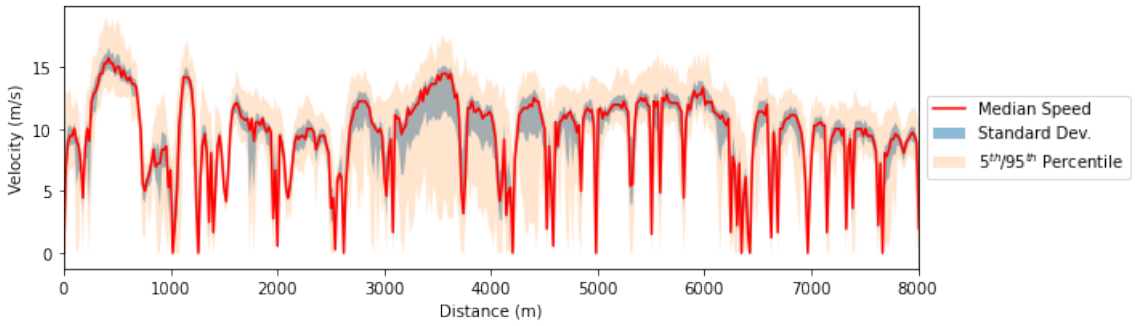

Figure 2.10: Distribution of GTFS real-time speed data for Route 14 by location

is sometimes moving, and sometimes stopped, such as traffic lights, or less frequently serviced bus stops. To investigate this, a subsection of the drive cycle on Route 14 is shown along with the standard deviation, and 95^{th} and 5^{th} percentile limits.

While the method proposed in this work currently only produces a single "typical" drive cycle for the purposes of energy estimation, the underlying data could be used to investigate a range of operating conditions to help model the range of real world driving conditions that a single route may encounter. Looking for periods with high variance in raw speed data could assist with these tasks. Locations with a sudden rise in the variance may suggest the presence of a bus stop that is only serviced during high traffic times, and sections of the routes with consistently high variance may suggest a portion of the road that is frequently slowed down due to traffic at busy hours.

2.3.3 Fleet Wide Energy Consumption Results

Once the proper filtering and interval parameters were selected, the constructed drive cycles for the entire VRTS can be input into the energy efficiency model. While the previous sections discussed the model performance on specific routes, this section analyses the results across all transit blocks, which represent the sequential set of trips that a transit bus performs in a day. The VRTS currently services 131 transit blocks on a regular weekday. The energy efficiency for each of these blocks is shown in Figure 2.11

The energy efficiency ranges from 0.96 kWh/km to 1.27 kWh/km with an average value of 1.11 kwh/km. The energy requirements for each block range 31.2 kWh to 492.7 kWh, and an average of 233.0 kWh. The lower end of this range could easily be serviced with overnight charging of medium or short range buses, while the higher

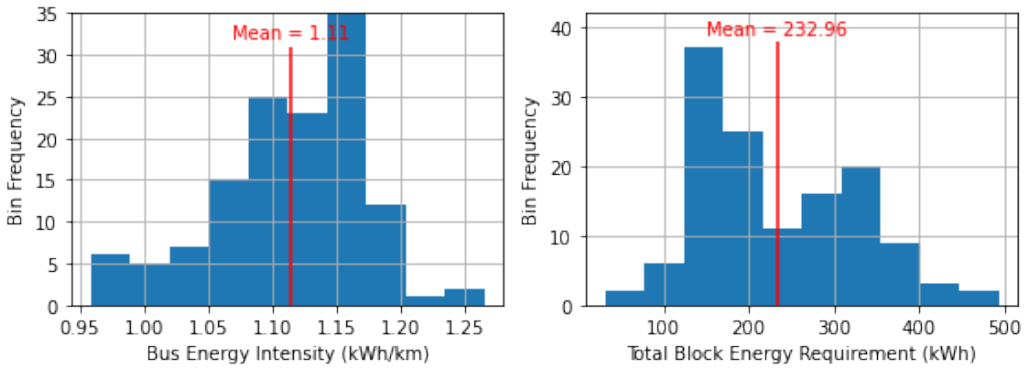

Figure 2.11: Energy Intensity of All VRTS Transit Blocks

end begin to approach the limit of battery capacity available on current electric buses, especially when an allowance for battery degradation is included.

To further investigate the energy use in the VRTS, the fraction of energy used for each specific load was computed and shown in Figure 2.12. For both the constructed drive cycles, as well as the 1 Hz data, almost half of the energy lost was due to acceleration forces. The forces used to overcome the road grade were the next largest, with the rolling resistance forces, aerodynamic forces, and auxiliary load creating the balance. Overall, the energy consumed by each load was fairly consistent between the measured GPS data and modelled GTFS drive cycles.

The portion of energy recovered across the constructed, synthetic, and measured data was also computed and shown in Figure 2.13. The measured GPS drive cycles for Route 14 recovered an average of 23.3% of the energy, compared to 12.0% and 12.3% for the GTFS derived and heavy synthetic drivecycles. This discrepancy is caused by differences in the measured and modelled deceleration characteristics. Regenerative braking occurs when deceleration forces exceed the sum of the aerodynamic, gravitational, and rolling resistance forces, which implies that the measured Route 14 drivecycle exhibits more aggressive deceleration than the GTFS derived or synthetic drivecycle for Route 14. The GTFS derived drivecycle underestimates the amount of regenerative braking taking place, but it performs similarly to existing methods while still offering advantages in other areas.

2.3.4 Energy Estimation Sensitivity Analysis

To explore the sensitivities of the energy efficiency model, several input parameters were chosen to be varied. Table 2.5 shows a list of all parameters varied, along with

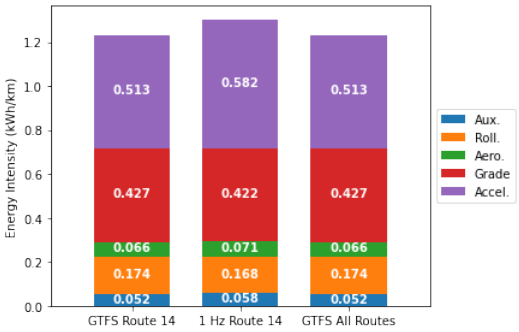

Figure 2.12: Energy Consumption by Source

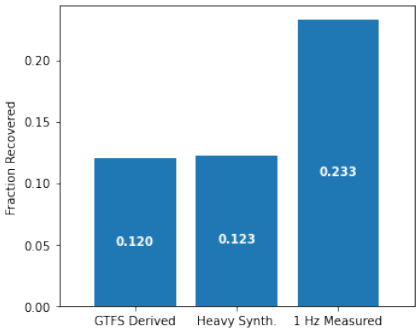

Figure 2.13: Fraction of Energy recovered on Route 14

the maximum and minimum value used in the sensitivity analysis.

Table 2.5: Sensitivity analysis parameter ranges

Parameter	**Symbol**	**Base**	**Min**	**Max**	**Units**	**Refs**
Bus Mass	M	14535	14535	19575	kg	[42] [2]
Auxiliary Load	P_{aux}	5,000	0	10,000	W	[42] [43] [45] [46]
Fixed Roll. Res.	c_{r0}	0.006	0.005	0.008	-	[42] [43]
Transmission Eff.	η_t	0.95	0.80	1.0	-	[42]
Aero. Coeff.	$c_d \cdot A_f$	5.304	4.243	6.365	-	[42] [2] [47]
Regen. Split	S	0.4	0.2	0.6	-	

These values are meant to represent the reasonable range that these parameters could differ during regular operation of a heavy duty transit bus. The original bus mass was assumed to be equal to the weight of the bus, plus a 70 kg driver. The base case represents the lower bound of the bus mass, but for the sensitivity analysis, the impact of adding the weight of 72 passengers weighing 70 kg each was explored. The auxiliary load for the base case was assumed to be 5,000 W, which was intended to represent a moderate heating/cooling load within the bus. Literature published describing the upper bound of auxiliary load varies, but for this analysis, a max auxiliary load of 10,000 W was chosen, which represents a cooling or heating load that would be experienced in extreme weather. The fixed rolling resistance was also varied from 0.005 to 0.008 to represent changes in road quality effecting rolling resistance. Rather than change each efficiency in the drive train individually, the transmission efficiency was varied from 0.8 to 1.0 to explore the uncertainty across

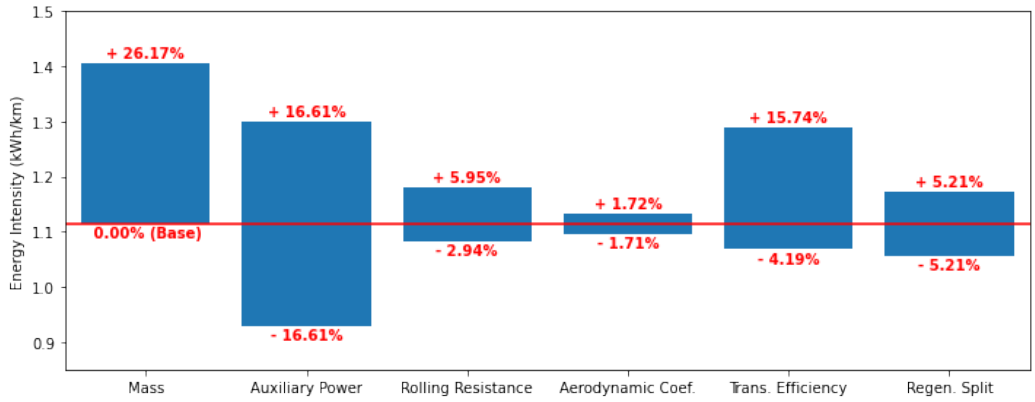

Figure 2.14: Impacts of varying chosen parameters on average energy intensity

the whole drive train system. The product of the drag coefficient and the frontal area was from +20% to -20% to investigate the impact of bus aerodynamics on the energy consumption. Finally, the regenerative braking split was varied from 0.2 to 0.6 to represent different drivers, drive trains, or routes that may achieve different amounts of regenerative braking.

The average energy use across all routes for each case in the sensitivity analysis is shown in Figure 2.14. The factors with the largest influence are the mass of the bus, and the auxiliary load. The impact of the aerodynamic and rolling resistance was small. Inertial forces are the dominant force acting on a transit bus, so these results are as expected. The mass of the bus and the auxiliary power load are also the most difficult of the listed parameters to accurately account for in fleet wide modelling. Weather and passenger count can vary across different times and dates, and the thermal properties and climate control method (heat pump, electric heating, dedicated diesel heating, air conditioning) can vary based on bus manufacturer. The impacts of drive train efficiency assumptions show that little can be gained by improved efficiency, however much can be lost. While transmission efficiency in particular was varied in this study, a degradation of the battery system, converter, or motor system could all also cause the energy requirements to be raised. Finally, we can see that a change to the assumed regenerative braking split (resulting from different driving habits or drive train systems) can result in a modest change to the overall energy intensity.

2.4 Conclusion

A method to construct fleet wide drive cycles for electric buses using public transit data has been presented. With the optimal filtering parameters, the GTFS drive cycle was shown to represent the real driving characteristics of a transit route better than a synthetic drive cycle. Furthermore, the GTFS constructed drive cycles were found to generalize across different routes. The resulting GTFS construction method was used to create drive cycles for an entire fleet of transit buses and thereby to model the energy consumption of the entire transit system.

The average energy intensity for the VRTS transit blocks was found to be 1.11 kWh/km, and the average energy requirements were 230.0 kWh per transit block. A sensitivity analysis was performed which found that variation in passenger load and auxiliary load resulted in the largest changes to the energy estimates. Further work may be warranted to investigate the possibility of incorporating data from automatic passenger counting systems into this modelling effort to create an even more accurate energy estimation model for a transit system, if such data could be obtained.

Overall, the GTFS drive cycle construction method represented the "typical" drive cycle for a given transit bus route by incorporating a data driven modelling approach. The proposed methods allow for a transit operator or researcher to quickly and easily create a set of drive cycles that reflect the real operating characteristics of an entire transit fleet. Where real time transit systems such as GTFS feeds are already in place, this method is proposed as an accurate, and convenient alternative to synthetic drive cycles, or other standard drive cycle estimation methods. This method can be used to model the energy consumption of electric transit buses and assist researchers, transit agencies, and other stakeholders to accelerate the electrification of their transit systems.

Funding

This project was funded by the Pacific Institute for Climate Solutions (PICS) Transportation Futures Project.

Dataset

The GTFS static and real-time data, as well as the 1 Hz GPS data used for this work has been made available for other researchers to access at `https://data.mendeley.com/datasets/cbswzc22bv/1` [48].

Chapter 3

Techno-economic optimization of Stationary Energy Storage System technologies for Ebus charging

This chapter is based on a manuscript prepared for submission to an academic journal. The manuscript was authored by G. Wilson and C. Crawford. G. Wilson, the author of this thesis, was responsible for the research methodology, data collection, data analysis, validation, and manuscript preparation. C. Crawford was responsible for supervision of all work and for review and editing of the manuscript.

In addition to the case study analysis presented in this chapter, Appendix A presents a full parametric sweep performed for the same charging locations, as well as complete results from three additional possible charging locations in the Victoria Regional Transit System.

The List of Symbols provided in this chapter relates only to the symbols used in this chapter.

List of Symbols

H	The charging hub location
B	The total number of transit blocks
J	Total number of event-based timesteps
D_j	The length of timestep j in minutes
E_r	The bus energy consumption for route r
$E^+_{b,j}$	The energy consumption of block b at timestep j
N	The number of chargers located at H
P	The power for each charger located at H
$R_{b,j}$	The charging priority ranking for bus b at timestep j
$E^-_{b,j}$	The charging power delivered to block b at timestep j
$A_{b,j}$	A flagging variable to record if bus b is charging at timestep j
$\eta_{charger}$	The efficiency of the charger
L_k	The event-based charging load for timestep k
E^{req}_b	The energy required for a bus to complete block b
L_m	The minute-based charging load for minute k
NPV	The net present value of the system
k	The minute of the day
$\dot{C}_{cap}$	The capital cost of the SESS
$\dot{C}_{op}$	The yearly operational costs for the system
Y	The assumed system lifetime in years
i	The assumed interest rate
$\dot{C}_{bat,e}$	The SESS energy capacity cost in \$/kWh
$\dot{C}_{bat,p}$	The SESS power capacity cost in \$/kW
S_e	The optimal SESS energy capacity in kWh
S_p	The optimal SESS power capacity in kW
C_U	The fees paid to the utility for energy and power
$C_{O\&M,fix}$	Cost of operation and maintenance for the SESS in \$/kW-year

$C_{O\&M,var}$ Cost of operation and maintenance for the SESS in $/MWh
M_{month} The monthly energy drawn from the grid
$\dot{C}_e$ The electrical energy cost per kWh
$\dot{C}_p$ The electrical power cost per kW
P_{max} The peak monthly power draw averaged over a 15 minute period
$\dot{C}_{e,m}$ The TOU energy cost for period m
M The number of TOU billing periods
$\dot{C}_{e,m}$ The TOU energy cost in period m
θ_k The energy discharged from the SESS at minute k
U_k The utility demand for minute k
X_k The amount of energy stored in the SESS at minute k
η_{RT} The round trip efficiency of the SESS
Y_{real} The real system lifetime in years
N_{cycles} The rated cycles of the SESS at the given DoD
EAA The equivalent annual annuity of the system

3.1 Introduction

Many transit agencies have begun to transition their fleets away from conventional diesel buses towards low carbon alternatives in order to reduce or eliminate their direct GHG emissions. While some transit agencies plan to use renewable fuels such as renewable natural gas during their transition, most agencies such as BCTransit in British Columbia, or Translink in Vancouver plan to replace the majority of their existing fleet with battery electric buses [36] [49]. While electric buses provide a low-carbon alternative to diesel transit buses, their deployments require additional planning to ensure reliable and affordable operation. Well planned electric bus deployments have the potential to reduce total lifetime ownership costs [50], but poor planning can lead to the opposite outcome. More specifically, proper planning must be taken to ensure that the charging systems and strategies do not create utility loads that could result in unnecessarily high utility fees or overloaded electrical infrastructure. To avoid these issues, some sort of energy management is required.

3.1.1 Electric Bus Charging Strategies

A transit agency's choices in charging strategy influences the shape of the electrical demand curve and the charging costs [14]. Charging strategies/systems can be broadly separated into in-depot charging and on-route charging. In-depot charging occurs at the bus depot before or after the bus has completed its daily driving and is typically performed at a lower power ($\leq$ 150 kW). On-route charging, also called opportunity charging, involves charging buses during their operation at a location on the route. On-route charging is typically performed at a high power (up to 600 kW) to compensate for the shorter time that the bus is able to charge at a single time.

While it is useful to differentiate between the two charging strategies, it is most likely that a fully electrified fleet may use aspects from both strategies within their operation. For example, a fleet of buses may charge overnight at low power, but an on-route location may be used to provide a top up charge to key routes that require additional energy. What is important to note is that whatever the charging strategy, the utility fees can quickly become unwieldy. While the cost to operate an electric vehicle is typically much less than a Internal Combustion Engine (ICE) vehicle when considering only the energy inputs, demand charges and other utility fees have been known to yield the opposite result. Reduced operating costs are relied upon to justify the substantially higher capital cost of purchasing an electric bus over a comparable ICE bus, so monitoring demand charges is of special concern for electric bus operators.

In many cases, the demand charges become the dominant fees paid to the utility operator, such as the Denver Regional Transit District in 2019 which found 82% of its charging costs made up of demand charges [16], or the City of Tallahassee Transit Agency in 2014 which paid 75% of its charging costs as demand charges [17]. Both of these cases demonstrate the need for some type of energy management to reduce operating costs.

3.1.2 Energy Management and Utility Markets

Depending on the electrical utility pricing scheme, energy management may be performed in different ways. For the purposes of this work, two different utility markets are considered: energy based markets and power based markets. An energy based market is defined as a market where the charges paid to a utility operator are based only on the energy use. Energy based markets often employ Time-of-Use (TOU) pricing where the cost of electrical energy varies based on the time of day. TOU markets

may employ real-time pricing where the prices are based on the current electrical supply and demand balance, or have set hourly prices based on historic demand.

Power based markets are defined by a utility demand charge which is usually calculated based on the consumer's power demand. Demand charges are usually based on the peak 15 minute power draw during each monthly billing period. A 2017 survey of utility pricing options in the United States found that the mean demand charge in markets where they were present was \$10.43/kWh, with a standard deviation of \$6.94/kWh [51]. Energy costs may be fixed or variable in demand markets.

This work considers scenarios with fixed energy costs or TOU pricing, but does not consider markets where demand charges are completely eliminated as this type of market is uncommon [14]. In a power based market, energy management usually takes the form of "peak shaving", where the goal is to lower the monthly peak 15 minute power draw. In energy based markets, energy management is typically performed using "load shifting" where the goal is to shift utility energy consumption from high cost times to low cost times. In either cases, energy management can be performed using Behind The Meter (BTM) energy storage. To distinguish this type of energy storage from the traction batteries found on-board an electric bus, the term Stationary Energy Storage System (SESS) is used. Figure 3.1 shows an example of an SESS used for energy management. The SESS is charged during off peak hours and discharged during peak hours. The result is a much flatter utility demand profile with additional energy consumed during off peak hours.

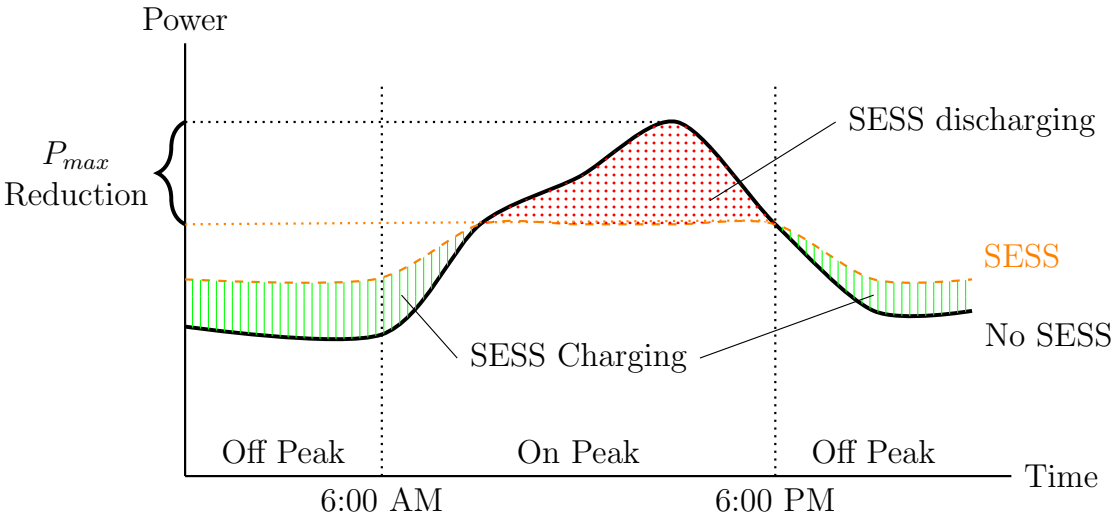

Figure 3.1: Impacts of SESS Energy Management on Net Utility Demand Profile

3.1.3 Storage Technologies

Energy storage systems come in many different forms. For this study, candidate storage technologies were selected primarily using the Levelized Cost of Storage (LCOS) in different operating conditions. The LCOS represents the net present cost of storage over the lifetime of the SESS normalized by the amount of energy discharged by the system. The LCOS simplifies a complex technology down to a single metric to be used for initial comparison before specific modelling takes place.

However, the LCOS for a technology depends not only on the technology, but also the application. Schmidt et al. provides a framework for analysing LCOS for different energy storage technologies and applications based on the discharge duration and discharge frequency of the proposed application [3]. Using this framework, three candidate technologies were selected for further modelling: Lithium Ion Batteries (LIB), Redox Flow Batteries (RFB), and Flywheel Energy Storage Systems (FESS).

LIB are often treated as the default option for BTM energy storage. Their popularity is reflected in the amount of published literature that considers only LIB in their modelling [52], [53], [54], [55], [56]. LIB have been shown to have the lowest LCOS for a range of applications, so this choice is often justified. However, the degradation that LIB are susceptible to means that under certain duty cycles, alternative options like RFB or FESS with better cycle lifetimes may be more economical.

RFB and FESS also offer a notable technical advantage over LIB in that their power and energy capacity are entirely decoupled. Although the Power Conversion System (PCS) components can be sized according to the actual power demand, both the energy and power capacity of a LIB system are determined by the number of cells used in the system. In a RFB system, the electrolyte tanks that determine the energy capacity can be sized independently of the cell stack which determines the power capacity [57]. Similarly, the maximum power of a flywheel is determined by the motor unit whereas the energy capacity is determined by the rotor inertial characteristics [58]. Independent sizing of power and energy storage components can lead to greater flexibility in system design, which is reflected in the system costs.

While LIB [52, 53, 54, 55, 56] and RFB [59, 60] are well studied options that are competitive over a large range of charging duty cycles, FESS are well suited for only a niche application. FESS provide high power capacity and very high cycle life, but very low energy capacity. This means that they are typically used in high frequency, low duration discharge applications. Because bus schedules are tightly scheduled

with buses often arriving and leaving a location with only a short layover window, the FESS may be able to provide an advantage in infrequently visited charging hubs with high power charging where they can help to smooth frequent and predictable peak power draws. While the literature is sparse, some research has already been completed investigating the integration of flywheel energy storage into fast charging systems [61].

All storage technologies considered are also expected to see substantial cost reductions in the future [3, 62]. Figure 3.2 shows the expected decrease in cost for each technology until 2050 based on 2015 costs, as projected by Schmidt et al. [3]. These cost projections were obtained by reviewing real project costs between 1995 and 2017 and using the data to estimating future learning rates [3].

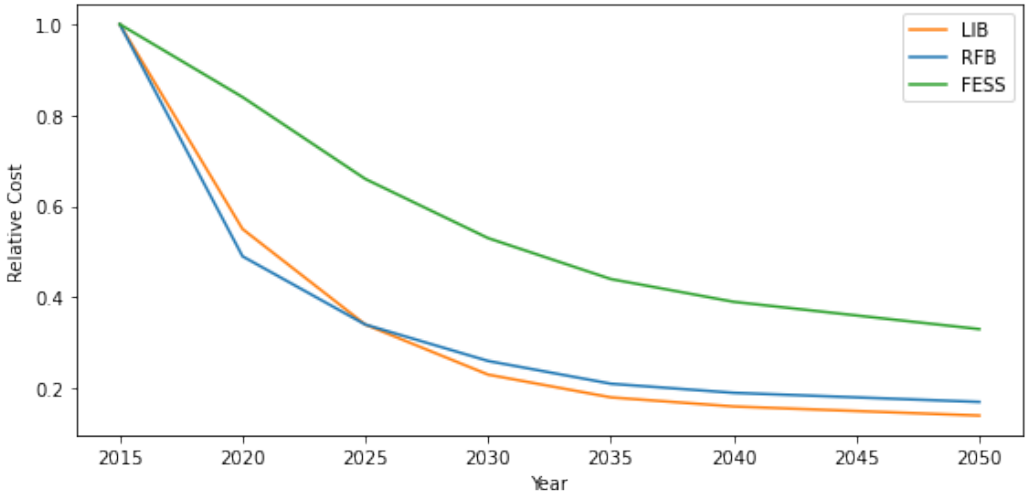

Figure 3.2: Predicted Cost Reduction for SESS Technologies [3]

3.1.4 SESS Application

Overall, these three storage technologies cover the range of duty cycles that may result from electric bus charging systems. Between peak shaving and load shifting, an SESS can provide several avenues for savings in both capital and operational costs. Since the potential savings rely greatly on the system in question, modelling tools that can be flexibly applied to different scenarios are desirable.

This work presents a framework for modelling the utility demand created from different charging scenarios and optimizing the load with SESS integration. This work optimizes the power and energy capacity of the SESS system, and also accounts

for the cycle lifetime of the technology under the given application. The optimal SESS deployment for each technology is compared to investigate which offers the most economical operation in different charging configurations and power market scenarios.

Section 3.2 outlines the methods used in this paper, while Section 3.3 presents and discusses the results of the analysis. The results section presents several contributions to the body of literature surrounding this subject. In particular, this work investigates:

1. The impacts of different charger unit number and power on the electric bus energy requirements,

2. The optimal SESS sizing and technology for different charger deployment scenarios.

3. The impact of different utility market structures on the optimal SESS technology and size.

3.2 Methods

The modelling performed in this work has been separated into two sections, as shown in Figure 3.3. Section 3.2.1 explains the methods used to obtain the utility demand profile from the bus operating data, and Section 3.2.2 explains the methods used to optimize the SESS capacity based on the modelled utility demand profile.

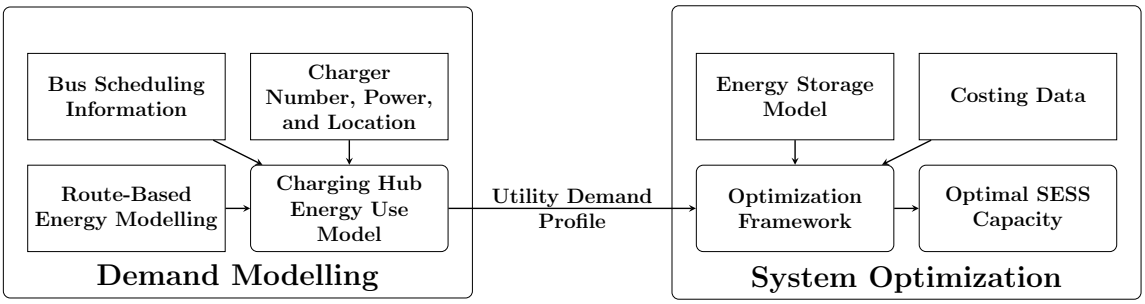

Figure 3.3: Modelling Overview

3.2.1 Modelling the Utility Demand Curve

The utility demand curve depends on the energy consumed at the charger hub, H. To calculate this, the energy consumption of the buses as well as the charging patterns of the buses must be modelled. A framework for modelling the bus energy use, locations, and schedules must be created. To start, a set of J timesteps is defined based on the arrivals and departures from the proposed charging hub. A new event is triggered when a bus arrives or leaves the charging hub. Since bus arrival and departure frequency changes throughout the day, the timestep durations, D_j, are irregular. Using event based timesteps rather than uniform minute based timesteps lowers the number of computations required, and simplifies further operations.

The route-based bus energy consumption, E_r is found using methods outlined by Wilson and Crawford for each route r [63]. Using the bus scheduling data, $E^+_{b,j}$, the energy consumption for each block at each timestep is found. While transit routes are serviced by many different buses at different times, each transit block is a unique series of routes completed by a single bus at a specific time. When block b leaves to begin route r at timestep j, then the entry for $E^+_{b,j}$ is set to E_r for the given route. At all other times, $E^+_{b,j}$ is set to 0.

This work takes the location and configuration of the charging system deployed as an input, and chooses a given terminal bus stop as the charging location. Terminal stops are frequently shared between many routes, and buses may stop for several minutes, making these stops good choices for opportunity charging systems hubs. The configuration of the chargers is defined by P, the power of the chargers in kilowatts, and N, the number of individual chargers able to operate at that power.

If more than N buses are present at H at one time, only the buses with the highest N priority ranking, $R_{b,j}$, during that timestep are assumed to be charging. The charge priority represents the net energy that a bus would have discharged up until the timestep in question. The bus priority ranking is for bus b at timestep T is calculated as:

$$R_{b,T} = \sum_{j=0}^{j=T} \left(E^+_{b,j} - E^-_{b,j}\right) \quad \forall \quad \text{eligible } b \text{ at } H \tag{3.1}$$

Where $E^-_{b,j}$ is the energy delivered to a bus at each timestep, as defined in Equation 3.2. The priority rank represents the on-board energy storage that the bus would need to complete its entire daily schedule without receiving additional charging after

timestep $T-1$.

A Boolean variable $A_{b,j}$ is used to track which buses are charging at what time. A 0 entry in $A_{b,j}$ means that bus b is not charging at timestep j, and a 1 entry means charging does occur. When fewer than N buses are present and able to accept charge at the charging hub for a timestep j, $A_{b,j}$ for each of those timesteps and buses is set to 1. When more than N buses are present, only the entries for the N highest $R_{b,j}$ are set to 1. A bus is only considered eligible to be charged if it can accept the full charging power over the current timestep duration (Ie. $\sum E^{-}_{b,j} \leq \sum E^{+}_{b,j}$ for any j).

Once $A_{b,j}$ is defined for a given timestep, the charge delivered to each bus at that timestep, $E^{-}_{b,j}$, can be calculated. $E^{+}_{b,j}$ represents the energy flowing out of the on-board battery; $E^{-}_{b,j}$ represents the energy flowing in from the charger. The charging power delivered to each bus is assumed as shown in Equation 3.2, where A $\eta_{charger}$ is the efficiency of the charging unit itself.

$$E^{-}_{b,j} = P \cdot D_j \cdot \eta_{charger} \quad \forall \quad A_{b,j} = 1 \tag{3.2}$$

$A_{b,j}$ is also used to determine the utility load L_j, shown in Figure 3.3.

$$L_j = P \cdot \sum_{b=0}^{b=B} A_{b,j} \tag{3.3}$$

While not necessary to determine the utility load, knowing the total block energy requirements, E^{req}_{b} is also of interest for transit system planning. The bus mass is assumed to be constant over time, and between each bus in the system. The buses are assumed to leave the depot in the morning with a full battery, but rather than assuming a given battery size and computing the SOC for each timestep, this work calculates the energy *requirements* for each block. This allows the work to be generally agnostic of electric bus range choices within the fleet. Once all charging events are known, the energy in and out of the bus can be cumulatively summed together, and the highest value for each block can be found. Note that the energy requirement is not necessarily the energy found at the last timestep, but rather than highest cumulative summative value for any timestep.

$$E^{req}_{b} = max\left(\sum_{j=0}^{j=T} \left(E^{+}_{b,j} - E^{-}_{b,j}\right)\right) \quad \forall \quad T \in J \tag{3.4}$$

The total procedure for calculating the utility load profile and bus block based

total energy requirements can be summarized as shown in Algorithm 1:

Algorithm 1 Utility demand profile and block energy requirements pseudocode

Assume a charging hub location and configuration, H, P, and N
Calculate route-based energy consumption, E_r
Construct event-based timesteps J, and durations D_j
Identify transit blocks B that pass through location H
for b in B **do**
    Construct block-based energy consumption $E^{+}_{b,j}$ using E_r and the transit schedule
end for
for j in J **do**
    Identify blocks, b_h present at H that can accept a charge
    for b in b_h **do**
        if size of $b_h \leq N$ **then**
            Assign $A_{b,j} = 1$ for all b_h at timestep j
        else
            Calculate charge priority ranking $R_{b,j}$ for all b_h at timestep j
            Set $A_{b,j} = 1$ for the highest N priority rankings at timestep j
        end if
        Calculate $E^{-}_{b,j}$, the energy delivered to each bus at timestep j
    end for
end for
Calculate the utility load L_j using A_j
for b in B **do**
    Calculate total energy consumption E^{tot}_{b}
end for

3.2.2 Optimizing the Utility Demand

Once the utility demand profile has been acquired, it is used as an input into the optimization framework to determine the optimal energy capacity, S_e, and power capacity, S_p, of SESS for a given charging system. A Linear Programming (LP) framework has been developed to perform the optimization. The various aspects of this optimization framework are explained in this section. While the charge scheduling and utility demand profile creation are completed using event-based timesteps, the

SESS optimization is performed minute-by-minute. To do this, the event-based utility load L_j is transformed into a time-based utility load L_k, where k represents a minute in the day.

3.2.2.1 Objective Function

The objective of the optimization is to use the SESS to reduce the overall Net Present Value (NPV) of a system deployment under the assumed interest rate i. The objective function, shown in Equation 3.5, considers the capital cost C_{cap} and the yearly operational C_{op} costs for the system over the lifetime of the system, Y.

$$\min \quad NPV = C_{cap} + \sum_{y=0}^{y=Y} \frac{1}{(1+i)^y} \cdot C_{op} \tag{3.5}$$

The capital costs can be calculated with Equation 3.6.

$$C_{cap} = \dot{C}_{bat,e} \cdot S_e + \dot{C}_{bat,p} \cdot S_p \tag{3.6}$$

$\dot{C}_{bat,e}$ and $\dot{C}_{bat,p}$ are the cost per unit of energy and power capacity. S_p and S_e are the power and energy capacity of the SESS.

The yearly operational cost C_{op} is computed with Equation 3.7, according to the fixed and variable operations and maintenance costs $\dot{C}_{O\&M,fix}$ and $\dot{C}_{O\&M,var}$, the monthly energy use E_month, and $C_{utility}$, the annual fees paid to the utility.

$$C_{op} = C_{utility} + \dot{C}_{O\&M,var} \cdot 12 \cdot E_{month} + \frac{\dot{C}_{O\&M,fix} \cdot S_p}{1000} \tag{3.7}$$

The utility costs are computed in one of two ways, depending on the utility structure being considered. A market using demand charges and a constant energy cost is considered in Equation 3.8.

$$C_{utility} = 12 \cdot \left(\dot{C}_e \cdot E_{month} + \dot{C}_p \cdot P_{max} \right) \tag{3.8}$$

$\dot{C}_e$ and E_{month} represent the fixed utility energy costs and the amount of monthly energy consumption, P_{max} is the maximum power draw over a rolling 15 minute period, and $\dot{C}_p$ represents the utility demand charge rate. A utility using TOU pricing is modelled using Equation 3.9.

$$C_{utility} = 12 \cdot \left(\dot{C}_p \cdot P_{max} + \sum_{m=0}^{m=M} \dot{C}_{e,m} \cdot E_m \right) \tag{3.9}$$

M represents the number of different electrical rates over the day, $\dot{C}_{e,m}$ and E_m represent cost and monthly amount of energy used in the timeslot associated with a given rate period m. Equation 3.9 could be used to approximate a real-time TOU market by setting $M = 1440$ and having each m represent a single minute of the day. In 3.9, $\dot{C}_p$ may be equal to 0 if no demand charges are present.

3.2.2.2 SESS Modelling

The SESS is operated such that the bus charging load at any given minute, L_k, is always met be some combination of θ_k and U_k, which are respectively the utility energy draw and the energy charged/discharged from the SESS in minute k, as shown in Equation 3.10.

$$L_k = \theta_k + U_k \tag{3.10}$$

A simple energy reservoir type model is used to model the SESS. Energy reservoir models are commonly used in this level of modelling since they are sufficiently accurate for minute-by-minute modelling, and are easily integrated into a LP framework [64]. An energy reservoir model is governed by Equation 3.11.

$$X_k = \begin{cases} X_{k-1} + \theta_{k-1} \cdot \sqrt{\eta_{RT}} & \forall \quad \theta_{k-1} \geq 0 \\ \\ X_{k-1} + \dfrac{\theta_{k-1}}{\sqrt{\eta_{RT}}} & \forall \quad \theta_{k-1} < 0 \end{cases} \tag{3.11}$$

X is the energy stored in the SESS for a given timestep, and η_{RT} is the round trip efficiency of the SESS technology. Efficiency losses are assumed to be constant, and are accounted for equally on charge and discharge from the system.

The capacity of the SESS is required to be equal at the start of the day (minute 0) and end of the day (minute 1440) to ensure that all charging costs are properly accounted for, as shown in Figure 3.12.

$$X_0 = \begin{cases} X_{1440} + \theta_{1440} \cdot \sqrt{\eta_{RT}} & \forall \quad \theta_{1440} \geq 0 \\ X_{1440} + \dfrac{\theta_{1440}}{\sqrt{\eta_{RT}}} & \forall \quad \theta_{1440} < 0 \end{cases} \tag{3.12}$$

The SESS is also constrained to not operate at charge or discharge rates higher than its maximum power rating.

$$|\theta_k| \cdot 60 \leq S_p \tag{3.13}$$

Some additional constraints to apply one or more types of SESS technology. For LIB, since the power and energy are coupled, it was assumed that the system could not discharge at more than 4 times its energy capacity, as shown in Figure 3.14.

$$S_e \cdot 4 = S_p \quad \text{For LIB} \tag{3.14}$$

Although the power and energy rating of an FESS is also decoupled, there are also practical limits on the energy to power ratio of current FESS technology. Generally, commercially available FESS are limited to a power to energy ratio of 4 [58, 65]. Based on this assumption, an additional constraint on the FESS is imposed.

$$S_e \leq S_p \cdot 4 \quad \text{For FESS} \tag{3.15}$$

Since both the SESS capacity and the SESS operational control are decided by the optimizer, S_e, S_p, X_k, θ_k, P_{max}, and U_k are variables optimized/output by the LP optimizer while all other values are defined as input parameters to the model.

3.2.2.3 Accounting for System Lifetime

The real system lifetime, Y_{real}, is calculated using a simple linear degradation model as shown in Equation 3.16, similar to models used in other literature [66].

$$Y_{real} = \frac{N_{cycles} \cdot 2 \cdot S_e}{365 \cdot \sum_{k=0}^{k=1440} |\theta_k|} \tag{3.16}$$

N_{cycles} is the rated number of cycles until end of life is reached for that technology. The denominator of Equation 3.16 represents the total energy throughput of the system in one year, and the numerator represents the total energy throughput that

the technology is rated for at the given Depth of Discharge (DoD).

While Equation 3.16 is a linear degradation model, it is not linear in regards to the decision variables from the linear programming optimization framework because two decision variables (S_e and θ_k) are divided by one another. For this reason, an iterative approach was applied to the degradation modelling, rather than directly incorporating it into the linear programming framework. The overview of this iterative approach is shown in Figure 3.4.

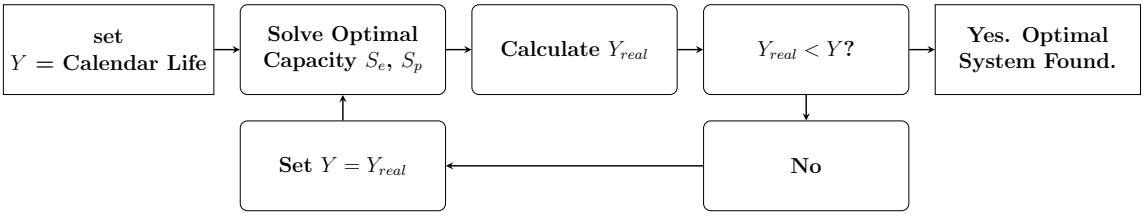

Figure 3.4: Iterate Overview

First, the optimal SESS deployment for an assumed system lifetime Y is found. Next, the real lifetime, Y_{real} of the optimal SESS deployment is calculated using Equation 3.16, outside of the optimization framework. If the assumed system lifetime is larger than the real system lifetime, then Y is set to be Y_{real} and a new optimal SESS capacity is found. This process is repeated until Y does not exceed Y_{real}. Y_{real} is calculated using a linear model based on the amount of energy passing through the SESS over its lifetime, as shown in Equation 3.16 .

Table 3.1: Degradation and operating characteristics for each technology

	DoD (%)	Cycles at DoD	Shelf Life (Years)	RT Eff. (%)
LIB	80	6,297	13	0.86
RFB	80	8,272	13	0.73
FESS	90	22,500	18	0.86

The assumed DoD for the electrochemical systems (LIB and RFB) was 80%, while the DoD for the flywheel system was taken to be 90% since degradation rates are an order of magnitude lower. The initial lifetime assumed for each technology is taken to be the nominal calendar lifetime of the technology. Table 3.1 shows the degradation characteristics used for each technology, along with the round trip (RT) efficiency [3].

3.2.2.4 Costing Data and Comparison of Technologies

This work applies a costing model based on both power and energy capacity. Energy storage capacity, PCS, and Balance of Plant (BoP) costs are all incorporated to best represent the real world cost of building and commissioning an energy storage system. Table 3.2 shows the costing data used in this work.

Table 3.2: SESS Technology Costs and Characteristics

Tech.	Year	Energy Cost ($/kWh)	Power Cost ($/kW)	Fixed O&M ($/kW-year)	Var. O&M ($/MWh)
LIB	2020	442.0	156.0	10	3
RFB	2015	439.6	1372.6	12	1
FESS	2015	8247.3	693.1	7	2

The LIB data was collected from Mongird et al. [62] which reported the cost of LIB energy storage including the cost of the storage system, PCS, and BoP costs. The RFB energy and power costs were collected from Viswanathan et al. [67], which present only the decoupled cost of the electrochemical storage system. PCS and BoP costs for a RFB were retrieved from Mongird et al. [62] and added to the electrochemical storage system costs. The FESS costs were obtained by regressing the cost of various FESS projects presented by Mongird et al. [65] before adding the cost of the PCS and BoP. The future costs of each SESS technology was projected using learning rates obtained from Schmidt et al. [3] which is shown in Table 3.3.

Since the three technologies modelled in this work may have unequal lifetimes, a method to compare them financially is required. Once the SESS capacity has been identified for each technology, Equation 3.17 is used to calculate the Equivalent Annual Annuity (EAA) for each system.

$$EAA = \frac{i \cdot NPV}{(1 - (1 + r)^{-Y})} \tag{3.17}$$

Table 3.3: SESS Technology Learning Rates

Tech.	2015	2020	2025	2030	2035	2040	2045	2050
LIB	1.0	0.55	0.34	0.23	0.18	0.16	0.15	0.14
RFB	1.0	0.49	0.34	0.26	0.21	0.19	0.18	0.17
FESS	1.0	0.84	0.66	0.53	0.44	0.39	0.36	0.33

Table 3.4: Case Study Input Parameters

Energy Cost	0.0482 $/kWh
Demand Charge	9.808 $/kW
$\eta_{charger}$	0.95

The EAA transforms the NPV into the annual cost to purchase, operate, and maintain the SESS asset, thereby accounting for the differences in lifetimes for each technology. The optimal technology for a given charging hub can be selected by choosing the technology with the lowest EAA.

3.3 Results

3.3.1 Case Study Scenario

For this work, a case study of the Victoria Regional Transit System (VRTS) was used. The location with the transit exchange with the highest number of daily transit blocks passing through it, the Legislature Terminal, is used for this case study.

Results are presented in two sections. In Section 3.3.2 the number and power of charging units was varied to investigate what the benefits of different deployments are on the required on-board bus energy requirements. Second, in Section 3.3.3, using a chosen deployment scenario from Section 3.3.2, the feasibility of the different SESS technologies at different projected costs is investigated. For all work, the bus schedule and energy consumption of the buses was unchanged.

The standard[1] utility pricing[2] for the local utility is listed in Table 3.4 [68] along with the assumed charging infrastructure efficiency. The SESS costing data and learning rates from Tables 3.2 and 3.3 were used to determine SESS cost for various years.

[1] Although a special Demand Transition Rate is currently offered by BC Hydro for electric fleet operators, this rate is temporary and not considered in this work. Instead, the "Large Service Business Rate" for customers using more than 550,000 kWh per year is used.

[2] A conversion of 1.25 $ CAD to $ USD was used to convert the local utility prices to match the currency used elsewhere in this work.

3.3.2 Charge Scheduling and Utility Load Modelling Results

Figure 3.5 shows the number of buses present at the Legislature Terminal over a single day. The terminal experiences a short traffic peak in the morning, and a more sustained peak in the afternoon.

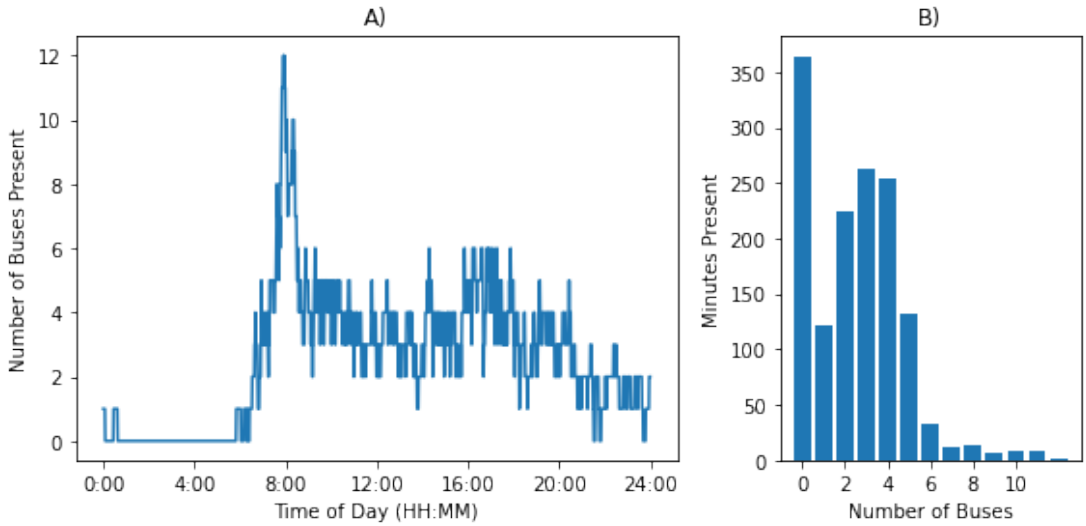

Figure 3.5: Buses Present at the Legislature Terminal A) by time of day, and B) by total minutes

While up to 12 buses are present in the morning, most of these buses are recently departed from the depot and unable to receive a charge. To evaluate the benefit of various charging deployments, two metrics are used. First, the reduction in median block energy requirements is calculated. A reduction in median block energy requirements may translate to extended on-board battery lifetime due to lower average DoD, or to capital savings in terms of reduction of on-board traction battery capacity. Second, the 95th block energy requirement is calculated. The 95th percentile is intended to represent the amount of on-board energy required for a fleet of electric buses that could services most blocks passing through the charging hub. The 95th percentile rather than the maximum energy requirement is used to lessen the importance of a single high energy route (which may be addressed with altered scheduling rather than on-route charging) influencing the results.

No economic factors are directly considered while investigating the benefits of the different charging system deployments because it is assumed that technical constraints on bus range capabilities, and reliability, are the main driver of these choices. It is also important to note that the block energy requirements are reported here, not

the actual capacity of the buses. As mentioned above a reduction in block energy requirements may allow for smaller capacity buses to be purchased and operated, but outside factors such as fleet flexibility constraints or future operational goals may lead to different results.

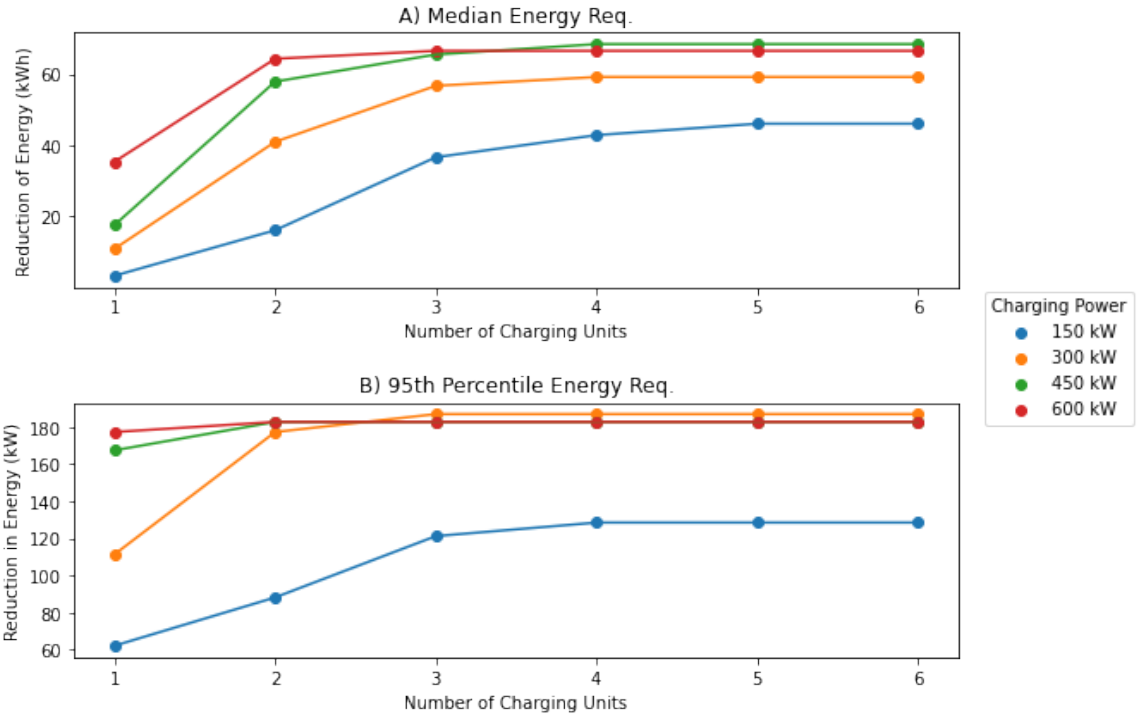

Figure 3.6: The reduction in A) median block energy requirement and B) 95th percentile block energy requirement for various number and power of chargers

Table 3.6 shows the resulting reduction in energy requirements for various power and charger number configurations. Without any charging taking place, the median energy requirement is 184.8 kWh , and the 95th percentile energy requirement is 509.6 kWh.

It can be seen that generally adding more units and increasing the power results in a higher reduction in required energy, but there are some exceptions to this. Since only buses that are able to receive the full charging power over the charging event are considered able to be charged, increasing the power sometimes disqualifies buses from being charged and results in a smaller reduction in energy requirements, as is seen in Figure 3.6A when more than 3 chargers are deployed with 450 kW and 600 kW. While this model assumes that a bus can only receive charge at the nominal capacity of the charger, real charging systems could operate at lower powers, or for more granular

time periods, meaning that this difference in results for increasing powers would not be reflected in real operations.

Figure 3.6A also shows a diminishing return in the number of chargers added. Although more than 4 buses frequently overlap at the charging location many of these buses are early in their daily missions and are unable to make use of the additional charging units. No benefit is observed when adding a 6^{th} charging unit, and benefit is only observed with a 5^{th} charging unit for the 150 kW power scenario.

The trends in Figure 3.6A are also seen in Figure 3.6B, but to a greater extent. This is because routes with high energy requirements receive the highest priority rank $R_{b,T}$, which will result in them charging any time they are able to even if only one or two charging units has been deployed. Because of this, the results in Figure 3.6A are of more relevance to differentiating the technical advantages provided by different charging scenarios.

An additional metric to observe is the charger utilization rate, calculated as shown in Equation 3.18 where the numerator represents the daily energy used to charge buses, and the denominator represents the maximum energy able to be provided by the chargers in one day.

$$utilization = \frac{\sum_{j=0}^{j=1440} \frac{L_j}{60}}{P \cdot N \cdot 24} \tag{3.18}$$

As shown in Figure 3.7, for this location the utilization ranges from 0.19 to 0.72. In agreement with the information in Figure 3.6, adding additional chargers results in diminishing returns in utilization rate.

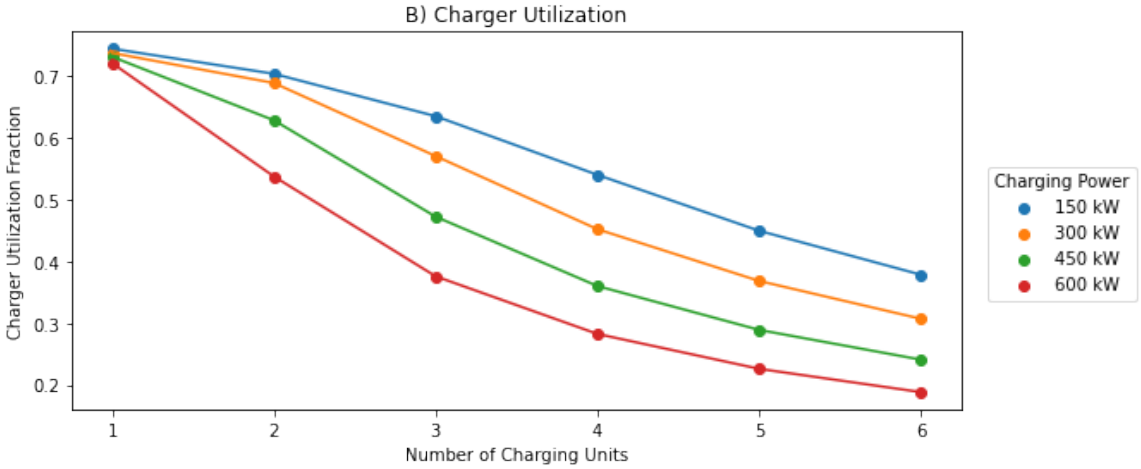

Figure 3.7: The utilization for each charging deployment

It is desirable to have a high utilization rate as it helps to reduce the demand charges as a portion of the total cost, as seen in Figure 3.8A. Given that the charging load (and therefore the energy costs) are constant in this scenario, an increasing portion of demand charges (without an SESS) results in an increase in total price, as seen in 3.8B.

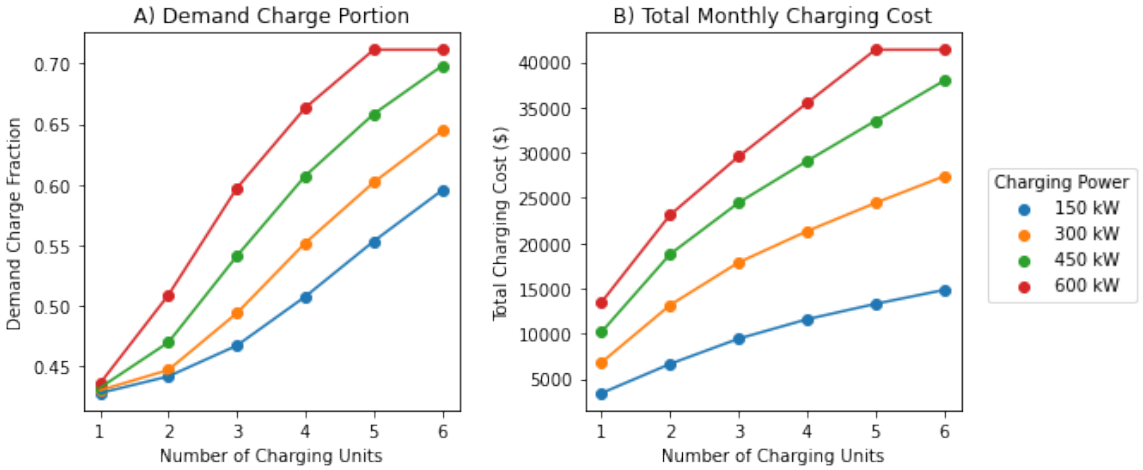

Figure 3.8: A) the portion of all fueling costs paid as demand charges B) The combined energy and power costs with no SESS

Although the interpretation of Figures 3.6 and 3.7 somewhat depends on the goals of the transit agency and its choice in bus fleet, some conclusions can be made and used for further analysis in this report. As mentioned, adding higher power charging above 450 kW or adding additional charging units above 4 has little benefit, but still increases the demand charges paid. Because of this, a deployment of four 450 kWh chargers represents a reasonable compromise between technical benefits and increasing costs, and will be used for the remainder of this case study. The block energy requirements with and without this particular charging deployment are shown in Figure 3.9.

The utility demand created by this charging configuration can be seen in Figure 3.10. The instantaneous power is shown in blue, as well as the 15 minute averaged power used to determine the utility demand charges in orange. As mentioned, although more buses are present in the morning, most of these buses are unable to receive a charging event, so the peak 15 minute power demand of 1800 kW takes place in the afternoon when all four chargers are active for 18 minutes from 16:49 to 17:07. Over the entire day, the utilization rate for all four chargers is 45.7%. The

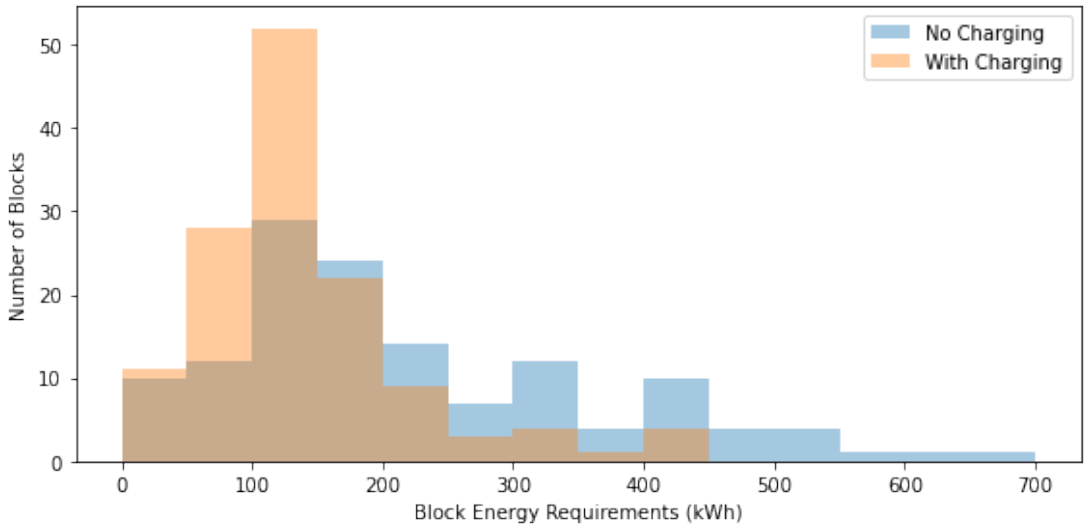

Figure 3.9: Histogram showing the impact of four 450 kWh on block energy requirements

monthly base energy and power costs for this scenario are $17,654 and $22,815, meaning that demand charges make up 43.6% of fees paid to the utility for this demand profile.

3.3.3 SESS Optimization Results

As mentioned, all scenarios considered in this section relate to a charging deployment consisting of four 450 kW charging units. The optimized utility demand profile for each technology under this charging scenario, as well as the energy stored in the SESS over a day, is shown in Figure 3.11. When viewing Figure 3.2.2, note that the demand profile displayed is the 15 minute averaged demand profile, not the absolute demand. The optimal energy and power capacity, the reduction in P_{max}, the system lifetime, and resulting EAA for the 2025 scenarios are shown in Table 3.5.

Both RFB and LIB are economical in this scenario in the year 2025. The optimal FESS system capacity for this year is 0, meaning that FESS is not feasible in this scenario. The LIB and RFB systems perform very similarly, resulting in a peak grid power draw P_{max} of 1560 and 1515 kW respectively. The demand profile and resulting EAA for the FESS is equivalent to the case where no SESS is installed, while the LIB and RFB systems result in an equivalent yearly savings of $11,334 and $8,907 respectively, when considering operating costs as well as the capital costs of the SESS.

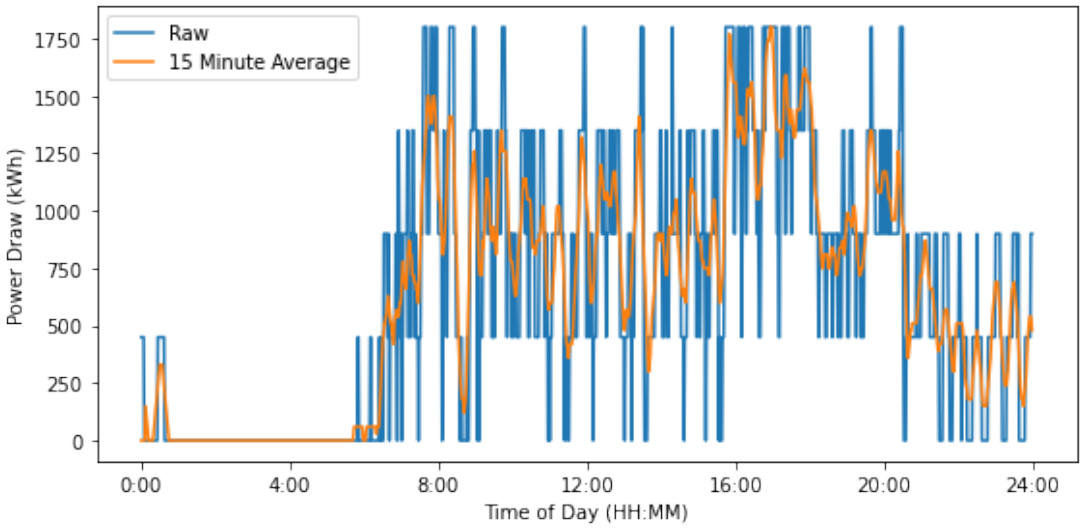

Figure 3.10: Charging Hub Demand at the Legislature Terminal

Table 3.5: Optimization Results for SESS Technologies in 2025

	SESS Energy (kWh)	SESS Power (kW)	P_{max} (kW)	EAA ($)	Lifetime (Years)
LIB	85	340	1,560	222,764	9
RFB	131	333	1,515	225,191	12
FESS	0	0	1,800	234,097	18
No SESS	0	0	1,800	234,097	N/A

To investigate the impacts of changing SESS technology costs, scenarios for the years 2020, 2025, 2030, 2040, and 2050 are considered. The SESS costing data and learning rates from Tables 3.2 and 3.3 were used to determine SESS cost for each year, and the results are presented in Figures 3.12, 3.13, and 3.14.

As SESS prices are reduced, it becomes economical to address more of the intermediate utility power peaks and P_{max} is reduced. This trend can be seen in Figure 3.12. The RFB and LIB systems have economical deployments for the entire range of scenarios considered, but the FESS only becomes feasible in the year 2050.

The optimal energy and power capacity for each technology and yearly price projection is shown in Figure 3.13. To achieve the increased power reduction in further years, both the LIB and FESS system powers are increased at a similar rate. However, the energy capacity of the RFB system increases from 131 kWh to 421 kWh, as compared to 85 kWh to 109 kWh for the LIB system.

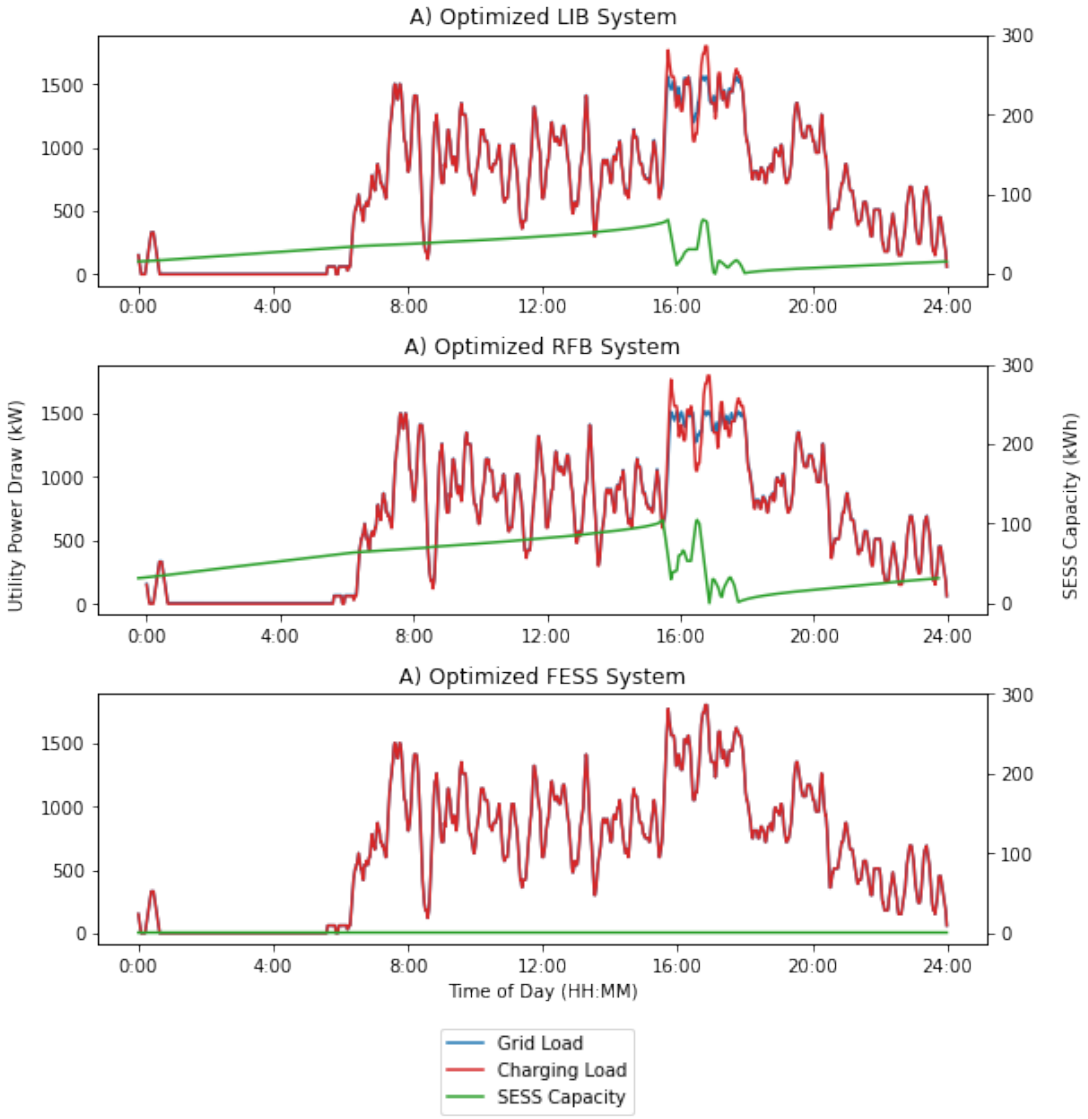

Figure 3.11: Optimized SESS deployments for the year 2025

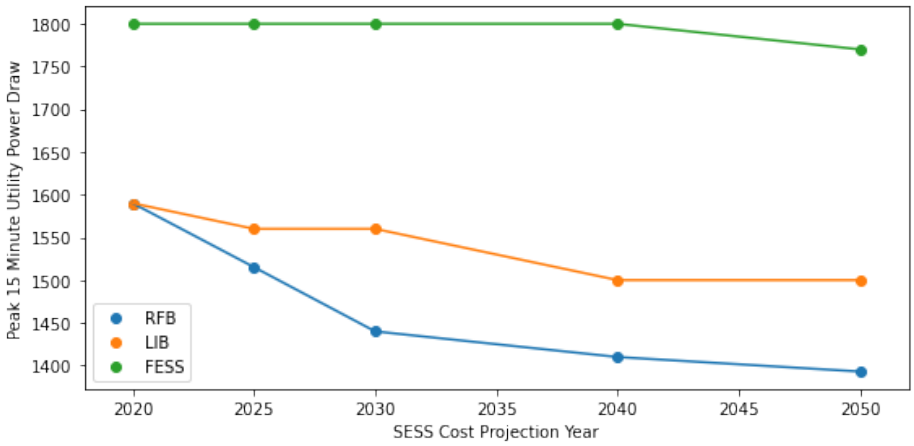

Figure 3.12: Peak 15 minute power consumption by SESS technology and price projection year

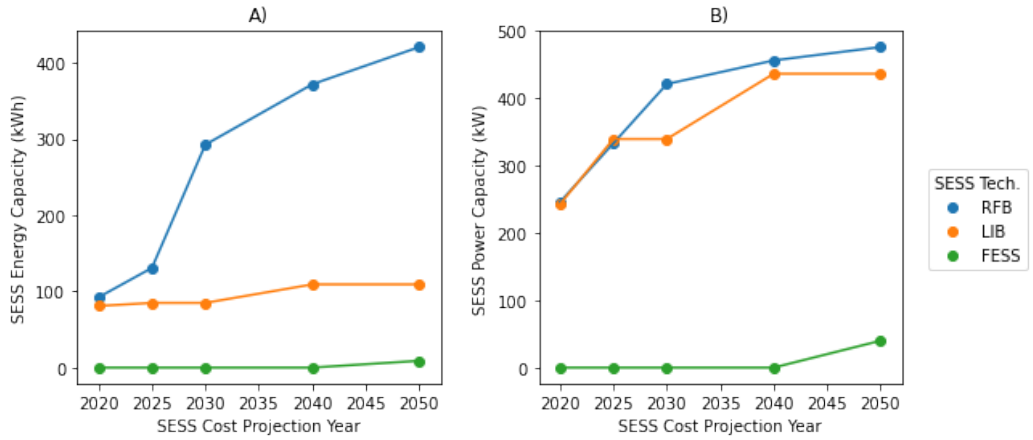

Figure 3.13: Optimal SESS A) energy capacity, and B) power capacity for different yearly prices projections

The difference in energy capacity is in part due to the affordability of RFB energy capacity, but as seen in Figure 3.14B, the lifetime of the system is also a factor. Since the RFB system lasts 5 years longer past 2030, higher investment into the LIB system is not as advantageous.

Figure 3.14A shows the EAA for each option. While the LIB is initially the most economical option, due to the more favorable cycle life of the RFB system and the increasing affordability of energy capacity, the RFB eventually becomes the optimal system, for this charging deployment. The FESS becomes feasible (but not optimal) by 2050. It is noted the scenario analysed in this case study is a high traffic, high utilization charging location. As previously noted, the FESS is better suited to less

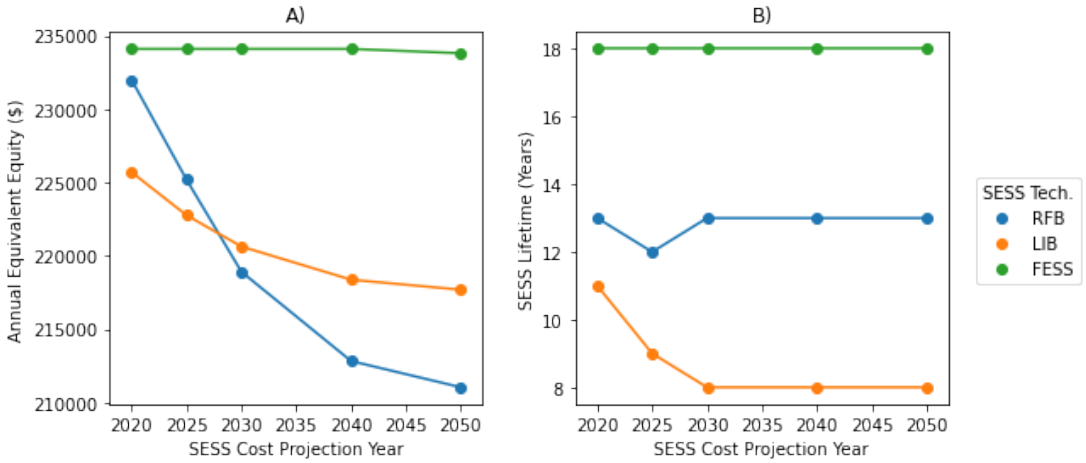

Figure 3.14: Optimal SESS A) EAA, and B) lifetime for different yearly prices projections

frequent charging locations. Although it is more expensive, there may be technical reasons that a transit agency would want to place a charger in a lower utilization location. For example, a transit agency may want to place a charging unit at the end of a long distance transit route that was only visited once or twice an hour to ensure that the route can be reliably completed. In such an instance, the value of the charging unit in terms of reliability or redundancy may outweigh the cost of operating and maintaining a low utilization charger. In such a situation, a FESS system could provide a cost competitive solution.

3.3.4 Parametric Sweep Results

As noted, the choice of charging system deployment influences the shape of the utility profile and therefore the optimal SESS deployment. To further explore this relationship, a parametric sweep was performed with the parameters listed in Table 3.6. The goal of this analysis was to investigate whether the frequency that each technology would be chosen as the most economical system.

Table 3.6: Parametric Sweep Parameter Range

Parameter	Start	End	Step Size	Notes
Charging Power (kW)	150	600	150	
Number of Chargers	1	6	1	
Cost Projection Year	2020	2050	10	Also 2025

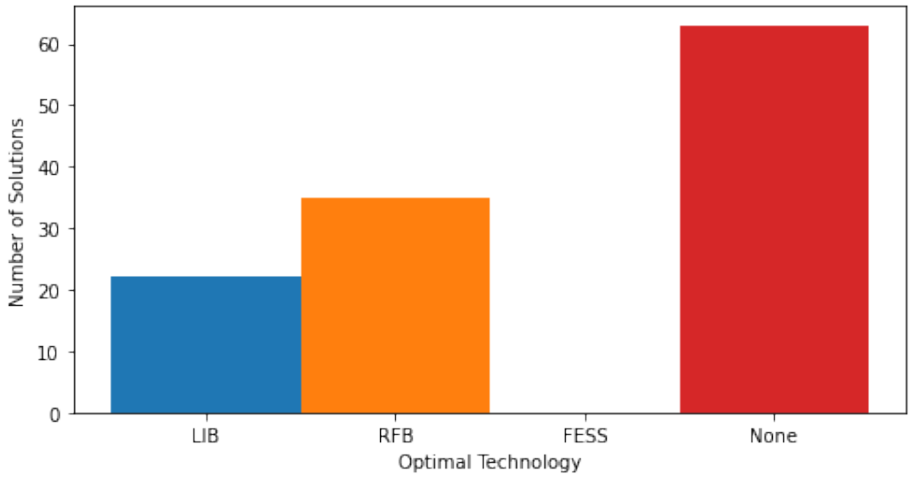

Figure 3.15: Parametric sweep results by most economical technology

The results of this parametric sweep are shown in Figure 3.15. 18% of the optimal solutions use LIB, 29% use RFB, 0 use FESS, and the remaining have no economical SESS deployment. While the range of charging deployments considered in the parametric sweep contains some extreme examples, the results shown here suggests that RFB and LIB are both feasible technologies with advantages. Figure 3.16 shows the optimal solutions for different years and charger configurations.

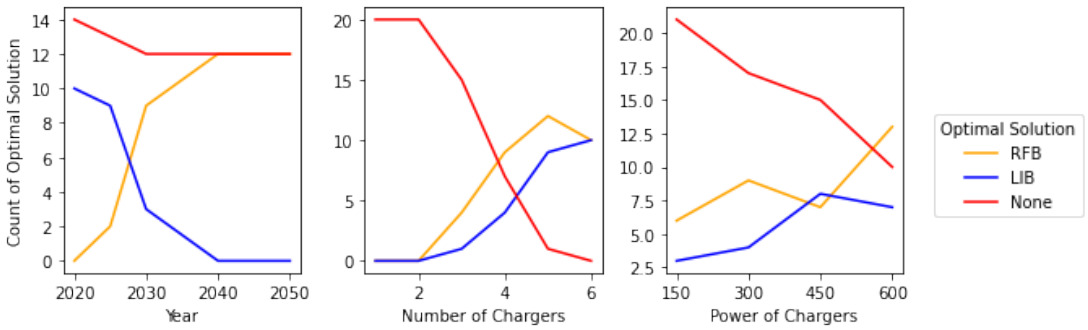

Figure 3.16: Impact of individual variables on optimal solution

Figure 3.16 shows that the year has a strong impact on whether the RFB or LIB system are optimal, suggesting that the results are sensitive to the price projections used. It is also shown that more chargers, and higher powered systems more frequently benefit from an SESS in general. No optimal solution exists when fewer than 2 chargers are deployed. This is expected, because as seen previously, systems with fewer chargers have a higher utilization rate for the chargers.

Table 3.7: Optimization Results for TOU scenario in 2025

	Energy (kWh)	Power (kW)	P_{max} (kW)	EAA ($)	Lifetime (Years)
LIB	85	340	1,560	237,358	9
RFB	148	350	1,502	239,793	12
FESS	0	0	1,800	248,761	18

3.3.5 TOU Utility Pricing

To investigate the impact of altering the utility pricing structure, another scenario was run using TOU prices and the same charging system as described in Section 3.3.3. Data from the Alberta Electric System Operators was collected from March 2021 to March 2022 and used to create a median hourly TOU profile [69]. Figure 3.17 shows the hourly TOU pricing for this market. The same demand charge used in the previous analysis, 9.808 $/kWh was used to allow for easier comparison of the results.

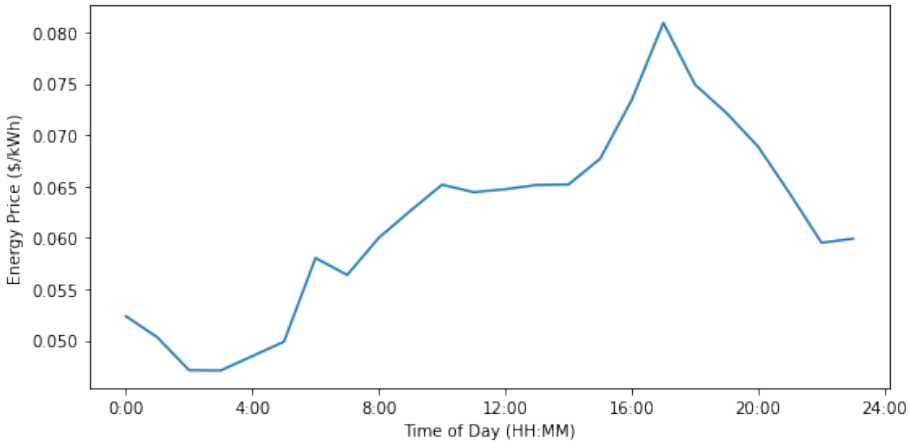

Figure 3.17: TOU energy pricing profile

While the introduction of a TOU pricing structure introduces the potential for the SESS to load shift, the demand charge pricing is overall lower, and the difference in price over the day is small. The resulting optimal SESS technologies for 2025 under the new utility pricing structure are shown in Table 3.7.

The resulting EAA for these scenarios is higher, but primarily because the energy rate in this market is higher on average. The FESS remains uneconomical, and the optimal LIB and RFB systems capacities are very similar to those found in Table 3.5.

The RFB system, which offers the most affordable energy storage, does increase in energy capacity from 131 kWh to 148 kWh when TOU pricing is present, but despite this it is still not the most economical solution in this system. Figure 3.18 shows the state of charge for the RFB system in 2025, with the TOU and fixed energy pricing.

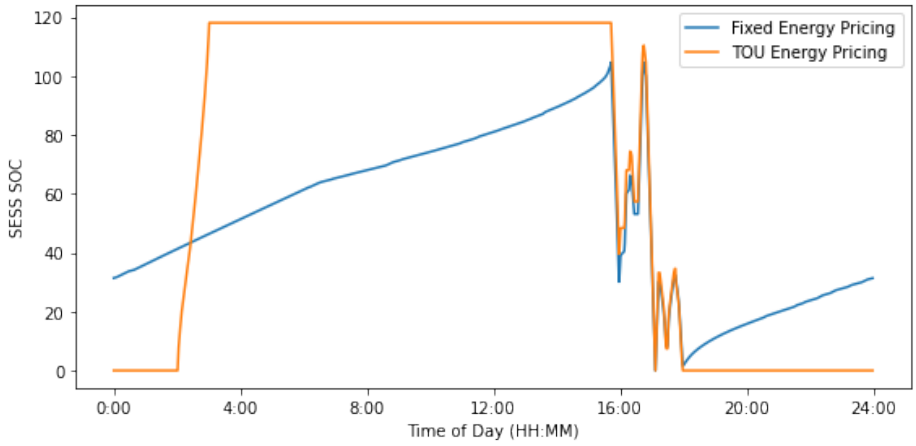

Figure 3.18: LIB State of Charge with fixed and TOU energy pricing

The system charges during low cost hours overnight, and stores slightly more energy overall, but despite this the RFB system is still not the optimal technology for this charging system. These results suggest that energy pricing and potential for load shifting does not have a substantial impact on the economics of an SESS for this application. This analysis does not consider the impacts of a sudden unexpected real-time price increase, which could be potentially mitigated with an SESS.

3.4 Conclusion

This work presented methods for investigating the techno-economic benefits provided by integrating energy storage into an electric bus charging hubs, and demonstrated these methods with a case study in Victoria, BC. The case study first analyzed different charging deployment scenarios to investigate their impacts on on-board energy storage requirements for the electric buses. Next, a charging hub demand profile was modelled for a variety of charging deployments and utility pricing structure and the optimal SESS integration was found for each.

It was found that increasing charging power and number generally resulted in reduced on-board energy requirements, but at the expense of increased demand charges.

SESS integration was found to be economical for approximately half the scenarios considered, with the most economical technologies being RFB and LIB. The year was found to have a large influence on whether the RFB or LIB system was most economical, with the LIB performing best in the short term, and the RFB in the long term. This shows that the results are sensitive to the price projections used in this work. Charger deployments with more chargers and higher power were also found to benefit more from an SESS integration due to their lower utilization rate, and higher demand charge portion.

Under the scenarios considered, the FESS system was not found to be the most economic technology, but it was noted that this technology could still offer some advantages in niche charger deployments. Finally, the impacts of a different utility pricing structure were considered and it was found to have only a small impact on the technoeconomics involved in this application.

Generally, this research shows that an SESS can assist in reducing the operating costs of an electric bus deployment. The benefit provided by the SESS depends mainly on the SESS cost projections, the bus charging system/strategy, and the demand charges present in the local utility market pricing structure.

Following the results of this paper, several opportunities for future work remain. Some system level components could be modelled in greater detail. For example, the chargers considered in this work were assumed to provide a constant charge whereas the charging power received by a real bus may vary depending on the length of charging event and the current charge level in the bus. Future work could also be performed to investigate the impacts of uncertainty in bus scheduling. While this work considered the bus schedule fixed, real bus may arrive early or late to a charging hub, which may impact the ability for a bus to receive charge at a critical moment.

Funding

This project was funded by Mitacs and the Canadian Urban Transit Research and Innovation Consortium (CUTRIC).

Chapter 4

Conclusion

4.1 Conclusion

Understanding the systems aspect of an electric bus deployment is vital to ensure economical and reliable operations. The bus, charging system/strategy, and energy provider all impose their own constraints on the other aspects of the system, and must be understood both individually and together. This work has presented methods that can be used to help guide transit agencies plan their systems accordingly, specifically regarding the energy consumption and energy management of electric bus systems.

Chapter 2 presented a method for leveraging existing transit data for energy consumption calculations, reaching a compromise between time and effort intensive ad hoc data collection and entirely theoretical simulated methods. Furthermore, this method was validated using 1 Hz GPS data collected from operating transit buses. The drivecycle estimation methods presented and validated here are a novel contribution to the field, and allow researchers and transit planners to quickly and accurately model the driving patterns of a fleet of transit buses. While the drivecycle estimation methods were presented in the context of energy consumption estimation, they may also have further applications in other fields such as transit system planning and analysis.

Chapter 3 presented modelling and analysis of an electric bus charging hub. Using the methods presented in Chapter 2, the electricity demand profile for a high-power electric bus charging hub is modelled for various locations and charging systems. The technical benefits that each charging system would provide in terms of reduction of required on-board electric bus energy capacity were explored. Next, using the modelled

demand profile, the feasibility of integrating three different SESS technologies with the charging hub was investigated. The SESS was found to provide benefit in approximately half of the scenarios considered, with both RFB and LIB systems becoming most economical, depending on the scenario. More complex charger deployments (i.e. higher power and more charger units) benefiting more from the SESS integration.

Overall, the work presented here reinforces the need for system level thinking when planning electric bus deployments. Route planning and driving characteristics influence the energy consumption of the buses. The optimal SESS deployment depend greatly on the shape of the utility demand curve, which is influenced by the charging system choices, and the demand charges present in the local utility pricing structure. The choice in charging system is also linked to the on-board energy storage requirements. This reinforces the requirement for system thinking during electric bus deployments, and shows how choices cannot be made without considering the cascading impact through the system.

4.2 Future Work

The results from Chapter 2 highlight some remaining challenges with electric bus energy consumption modelling. Uncertainties relating to vehicle mass, auxiliary power consumption, and regenerative breaking modelling are the primary concern, and may present avenues for future work as additional data becomes available (e.g. Automatic Passenger Counting data, in-situ regenerative braking data). Introducing different classes of transit buses (e.g. light, medium, and heavy duty) would also allow for a more precise estimate of vehicle mass and aerodynamics and thereby energy consumption. Methods presented here also only consider a "typical" day of transit operations, while the range of operating conditions was not explored. The variance of operating conditions and it's impact on energy consumption could be further explored. Additionally, with more information about bus operations, the non-revenue distances travelled by each bus could be integrated into the modelling from Chapter 2. All of these improvements would help system operators to further understand and plan their electric bus deployments.

Improvements could also be made to Chapter 3. Several of the system level components could be modelled in greater detail. For the energy storage modelling (of both the SESS and the on-board traction batteries) the charging power was assumed to be constant, while the real power that a battery can accept may vary depending

on the charging profile, and the current state of charge of the battery. Addressing uncertainty and flexibility in transit operations could also be useful. For the work presented here, the transit schedule was considered fixed. Buses were assumed to be able to begin charging as soon as they arrive at the charging hub. Under real operating conditions, buses may arrive late and leave early, impacting how the buses would charge.

Given that the benefits of an SESS are greatly impacted by the demand charge rates present in the local utility pricing structure, there is also potential future work involving utility rates and policies. Current incentives such as the BCHydro Demand Transition Rate provide a temporarily lower demand charge rate to electric fleet owners. Temporary incentives can help to encourage early adopters, but research into how utility market structure impact long term electrification efforts should be continued to ensure that the outcomes are desirable.

Bibliography

[1] E. a. C. C. Canada, "Greenhouse gas emissions," https://www.canada.ca/en/environment-climate-change/services/environmental-indicators/greenhouse-gas-emissions.html, 2021.

[2] "Our Fleet," https://www.bctransit.com/about/fleet, Oct. 2021.

[3] O. Schmidt, S. Melchior, A. Hawkes, and I. Staffell, "Projecting the Future Levelized Cost of Electricity Storage Technologies," *Joule*, vol. 3, no. 1, pp. 81–100, Jan. 2019.

[4] V. Masson-Delmotte, H.-O. Pörtner, J. Skea, P. Zhai, D. Roberts, P. R. Shukla, A. Pirani, R. Pidcock, Y. Chen, E. Lonnoy, W. Moufouma-Okia, C. Péan, S. Connors, J. B. R. Matthews, X. Zhou, M. I. Gomis, T. Maycock, M. Tignor, and T. Waterfield, "An IPCC Special Report on the impacts of global warming of 1.5°C above pre-industrial levels and related global greenhouse gas emission pathways, in the context of strengthening the global response to the threat of climate change, sustainable development, and efforts to eradicate poverty," p. 630, 2018.

[5] Service Canada, "A healthy environment and a healthy economy," https://www.canada.ca/en/services/environment/weather/climatechange/climate-plan/climate-plan-overview/healthy-environment-healthy-economy.html, Feb. 2021.

[6] E. Abotalebi, D. M. Scott, and M. R. Ferguson, "Can Canadian households benefit economically from purchasing battery electric vehicles?" *Transportation Research Part D: Transport and Environment*, vol. 77, pp. 292–302, Dec. 2019.

[7] N. Jakobsson, T. Gnann, P. Plötz, F. Sprei, and S. Karlsson, "Are multi-car households better suited for battery electric vehicles? – Driving patterns and

economics in Sweden and Germany," *Transportation Research Part C: Emerging Technologies*, vol. 65, pp. 1–15, Apr. 2016.

[8] N. Berkeley, D. Jarvis, and A. Jones, "Analysing the take up of battery electric vehicles: An investigation of barriers amongst drivers in the UK," *Transportation Research Part D: Transport and Environment*, vol. 63, pp. 466–481, Aug. 2018.

[9] D. A. Hensher, "Electric cars – they may in time increase car use without effective road pricing reform and risk lifecycle carbon emission increases," *Transport Reviews*, vol. 40, no. 3, pp. 265–266, May 2020.

[10] N. R. C. Government of Canada, "Comprehensive Energy Use Database - Transportation Sector - Canada," https://oee.nrcan.gc.ca/corporate/statistics/neud/dpa/menus/trends/comprehensive/trends_tran_ca.cfm, Apr. 2005.

[11] L. D. Frank, E. H. Fox, J. M. Ulmer, J. E. Chapman, and L. M. Braun, "Quantifying the health benefits of transit-oriented development: Creation and application of the San Diego Public Health Assessment Model (SD-PHAM)," *Transport Policy*, vol. 115, pp. 14–26, Jan. 2022.

[12] R. Nunno, "Fact Sheet — Battery Electric Buses: Benefits Outweigh Costs," https://www.eesi.org/papers/view/fact-sheet-electric-buses-benefits-outweigh-costs, Oct. 2018.

[13] Proterra, "ZX5 Electric Bus," https://www.proterra.com/vehicles/zx5-electric-bus/, Sep. 2020.

[14] J.-B. Gallo, Ted Bloch-Rubin, and Jasna Tomic, "Peak Demand Charges and Electric Transit Buses," U.S. Department of Transportation Federal Transit Administration, Whitepaper, 2014.

[15] D. Warren, "Charging Infrastructure for Battery-Electric Buses," *NEMA*, pp. 12–15, May 2020.

[16] John Aguilar, "RTD's electric 16th Street Mall buses cost nearly 60% more to operate than diesel coaches," *The Denver Post*, May 2019.

[17] N. Qin, A. Gusrialdi, R. Paul Brooker, and A. T-Raissi, "Numerical analysis of electric bus fast charging strategies for demand charge reduction," *Transportation Research Part A: Policy and Practice*, vol. 94, pp. 386–396, Dec. 2016.

[18] M. Andersson, *Energy Storage Solutions for Electric Bus Fast Charging Stations : Cost Optimization of Grid Connection and Grid Reinforcements*, 2017.

[19] A. Lajunen, "Lifecycle costs and charging requirements of electric buses with different charging methods," *Journal of Cleaner Production*, vol. 172, pp. 56–67, Jan. 2018.

[20] B. Zhou, Y. Wu, B. Zhou, R. Wang, W. Ke, S. Zhang, and J. Hao, "Real-world performance of battery electric buses and their life-cycle benefits with respect to energy consumption and carbon dioxide emissions," *Energy*, vol. 96, pp. 603–613, Feb. 2016.

[21] Z. Gao, Z. Lin, T. J. LaClair, C. Liu, J.-M. Li, A. K. Birky, and J. Ward, "Battery capacity and recharging needs for electric buses in city transit service," *Energy*, vol. 122, pp. 588–600, Mar. 2017.

[22] R. Prohaska, A. Duran, A. Ragatz, and K. Kelly, "Statistical Characterization of Medium-Duty Electric Vehicle Drive Cycles," Seoul, Korea: Korean Society of Automotive Engineers, Tech. Rep. NREL/CP-5400-66403, May 2015.

[23] A. Lajunen and T. Lipman, "Lifecycle cost assessment and carbon dioxide emissions of diesel, natural gas, hybrid electric, fuel cell hybrid and electric transit buses," *Energy*, vol. 106, pp. 329–342, Jul. 2016.

[24] G. De Filippo, V. Marano, and R. Sioshansi, "Simulation of an electric transportation system at The Ohio State University," *Applied Energy*, vol. 113, pp. 1686–1691, Jan. 2014.

[25] P. Sinhuber, W. Rohlfs, and D. U. Sauer, "Study on power and energy demand for sizing the energy storage systems for electrified local public transport buses," in *2012 IEEE Vehicle Power and Propulsion Conference*, Oct. 2012, pp. 315–320.

[26] M. Rogge, S. Wollny, and D. U. Sauer, "Fast Charging Battery Buses for the Electrification of Urban Public Transport—A Feasibility Study Focusing on Charging Infrastructure and Energy Storage Requirements," *Energies*, vol. 8, no. 5, pp. 4587–4606, May 2015.

[27] M. Gallet, T. Massier, and T. Hamacher, "Estimation of the energy demand of electric buses based on real-world data for large-scale public transport networks," *Applied Energy*, vol. 230, pp. 344–356, Nov. 2018.

[28] K. Kivekäs, A. Lajunen, J. Vepsäläinen, and K. Tammi, "City Bus Powertrain Comparison: Driving Cycle Variation and Passenger Load Sensitivity Analysis," *Energies*, vol. 11, no. 7, p. 1755, Jul. 2018.

[29] "General Transit Feed Specification," https://gtfs.org/, 2021.

[30] "OpenMobilityData - Public transit feeds from around the world," https://transitfeeds.com/, 2021.

[31] "SIRI White Paper," European Committee for Standardization, Tech. Rep., 2005.

[32] L. Ge, M. Sarhani, S. Voß, and L. Xie, "Review of Transit Data Sources: Potentials, Challenges and Complementarity," *Sustainability*, vol. 13, no. 20, p. 11450, Jan. 2021.

[33] A. Addo and M. Hatzopoulou, "Harnessing the Potential of Automated Data to Simulate Emissions of an Interregional Bus Route in Toronto, Canada," *Transportation Research Record*, vol. 2627, no. 1, pp. 36–45, Jan. 2017.

[34] Y. He, Z. Song, and Z. Liu, "Fast-charging station deployment for battery electric bus systems considering electricity demand charges," *Sustainable Cities and Society*, vol. 48, p. 101530, Jul. 2019.

[35] "Open Data," https://www.bctransit.com/open-data, Oct. 2021.

[36] C. Holt, "BC Transit 2020/21 Annual Service Plan Report," BC Transit, Victoria BC, Tech. Rep., Aug. 2021.

[37] M. Véronneau and J. Huang, "The Canadian Geodetic Vertical Datum of 2013 (CGVD2013)," *G E O M A T I C A*, p. 11, 2013.

[38] Kevin Walkowicz, Adam Duran, and Evan Burton, "Fleet DNA Project Data Summary Report," National Renewable Energy Laboratory, Tech. Rep., Aug. 2014.

[39] Y. Wang, Y. Zou, K. Henrickson, Y. Wang, J. Tang, and B.-J. Park, "Google Earth elevation data extraction and accuracy assessment for transportation applications," *PLOS ONE*, vol. 12, no. 4, p. e0175756, Apr. 2017.

[40] W. H. Press and S. A. Teukolsky, "Savitzky-Golay Smoothing Filters," *Computers in Physics*, vol. 4, no. 6, p. 669, 1990.

[41] "Fleet DNA Project Data," 2021.

[42] Anaissia Franca, "Electricity Consumption and battery lifespan estimation for transit electric buses: Drivetrain and electrochemical modelling," Ph.D. dissertation, University of Victoria, 2018.

[43] X. Feng, M. Lewis, and C. Hearn, "Modeling and validation for zero emission buses," in *2017 IEEE Transportation Electrification Conference and Expo (ITEC)*, Jun. 2017, pp. 501–506.

[44] M. P. O'Keefe, A. Simpson, K. J. Kelly, and D. S. Pedersen, "Duty Cycle Characterization and Evaluation Towards Heavy Hybrid Vehicle Applications," in *SAE World Congress & Exhibition*, Apr. 2007, pp. 2007–01–0302.

[45] H. He, M. Yan, C. Sun, J. Peng, M. Li, and H. Jia, "Predictive air-conditioner control for electric buses with passenger amount variation forecast," *Applied Energy*, vol. 227, pp. 249–261, Oct. 2018.

[46] D. Nicolaides, A. K. Madhusudhanan, X. Na, J. Miles, and D. Cebon, "Technoeconomic Analysis of Charging and Heating Options for an Electric Bus Service in London," *IEEE Transactions on Transportation Electrification*, vol. 5, no. 3, pp. 769–781, Sep. 2019.

[47] C. R. Jadhav and R. P. Chorage, "Modification in commercial bus model to overcome aerodynamic drag effect by using CFD analysis," *Results in Engineering*, vol. 6, p. 100091, Jun. 2020.

[48] G. Wilson, "General Transit Feed Specification Dataset for Victoria, Canada," vol. 1, Dec. 2021.

[49] "Translink low carbon fleet strategy," https://www.translink.ca/news/2020/february/translink%20low%20carbon%20fleet%20strategy, Feb. 2022.

[50] C. Johnson, E. Nobler, L. Eudy, and M. Jeffers, "Financial Analysis of Battery Electric Transit Buses," National Renewable Energy Laboratory, Tech. Rep. NREL/TP–5400-74832, 1659784, MainId:7002, Jun. 2020.

[51] J. McLaren, P. Gagnon, D. Zimny-Schmitt, M. DeMinco, and E. Wilson, "Maximum demand charge rates for commercial and industrial electricity tariffs in the United States," p. 1 files, 2017.

[52] Y. Yan, J. Jiang, W. Zhang, M. Huang, Q. Chen, and H. Wang, "Research on Power Demand Suppression Based on Charging Optimization and BESS Configuration for Fast-Charging Stations in Beijing," *Applied Sciences*, vol. 8, no. 8, p. 1212, Aug. 2018.

[53] C. Jin, J. Tang, and P. Ghosh, "Optimizing Electric Vehicle Charging With Energy Storage in the Electricity Market," *IEEE Transactions on Smart Grid*, vol. 4, no. 1, pp. 311–320, Mar. 2013.

[54] H. Ding, Z. Hu, and Y. Song, "Value of the energy storage system in an electric bus fast charging station," *Applied Energy*, vol. 157, pp. 630–639, Nov. 2015.

[55] J. A. Domínguez-Navarro, R. Dufo-Lopez, J. M. Yusta-Loyo, J. S. Artal-Sevil, and J. L. Bernal-Agustin, "Design of an electric vehicle fast-charging station with integration of renewable energy and storage systems," *International Journal of Electrical Power & Energy Systems*, 2019.

[56] Y. He, Z. Song, and Z. Liu, "Fast-charging station deployment for battery electric bus systems considering electricity demand charges," *Sustainable Cities and Society*, vol. 48, p. 101530, Jul. 2019.

[57] E. Sánchez-Díez, E. Ventosa, M. Guarnieri, A. Trovò, C. Flox, R. Marcilla, F. Soavi, P. Mazur, E. Aranzabe, and R. Ferret, "Redox flow batteries: Status and perspective towards sustainable stationary energy storage," *Journal of Power Sources*, vol. 481, p. 228804, Jan. 2021.

[58] X. Li and A. Palazzolo, "A review of flywheel energy storage systems: State of the art and opportunities," *Journal of Energy Storage*, vol. 46, Jan. 2022.

[59] L. Magallanes Ibarra, "Thermoelectrochemical model for RFB with an application at a grid level for peak shaving to reduce cost of the total electricity," Thesis, University of Victoria, 2020.

[60] Á. Cunha, F. Brito, J. Martins, N. Rodrigues, V. Monteiro, J. L. Afonso, and P. Ferreira, "Assessment of the use of vanadium redox flow batteries for energy

storage and fast charging of electric vehicles in gas stations," *Energy*, vol. 115, pp. 1478–1494, Nov. 2016.

[61] H. A. Gabbar, O. Elma, and I. Adham, "ANALYSIS AND DESIGN of FAST CHARGING SYSTEM with FLYWHEEL ENERGY STORAGE PLATFORM," p. 10.

[62] K. Mongird, V. Viswanathan, J. Alam, C. Vartanian, V. Sprenkle, and R. Baxter, "2020 Grid Energy Storage Technology Cost and Performance Assessment," p. 117, 2020.

[63] Graham Wilson and Curran Crawford, "Fleet-wide bus drivecycle modelling and energy estimation using real-time transit feed data."

[64] D. M. Rosewater, D. A. Copp, T. A. Nguyen, R. H. Byrne, and S. Santoso, "Battery Energy Storage Models for Optimal Control," *IEEE Access*, vol. 7, pp. 178 357–178 391, 2019.

[65] K. Mongird, V. V. Viswanathan, P. J. Balducci, M. J. E. Alam, V. Fotedar, V. S. Koritarov, and B. Hadjerioua, "Energy Storage Technology and Cost Characterization Report," Pacific Northwest National Laboratory, Tech. Rep. PNNL-28866, 1573487, Jul. 2019.

[66] F. Trocker, O. Teichert, M. Gallet, A. Ongel, and M. Lienkamp, "City-scale assessment of stationary energy storage supporting end-station fast charging for different bus-fleet electrification levels," *Journal of Energy Storage*, vol. 32, p. 101794, Dec. 2020.

[67] V. Viswanathan, A. Crawford, D. Stephenson, S. Kim, W. Wang, B. Li, G. Coffey, E. Thomsen, G. Graff, P. Balducci, M. Kintner-Meyer, and V. Sprenkle, "Cost and performance model for redox flow batteries," *Journal of Power Sources*, vol. 247, pp. 1040–1051, Feb. 2014.

[68] BCHydro, "Electricity rates," https://www.bchydro.com/accounts-billing/rates-energy-use/electricity-rates.html, 2022.

[69] AESO, "Alberta electric system operator historic prices," https://www.aeso.ca/market/market-and-system-reporting/, Feb. 2022.

Appendix A - Additional Optimized SESS Deployments Under Various Conditions

This appendix presents the results of a complete parametric sweep of the parameters investigated in Chapter 3. For this parametric study, Table A1 shows the entire range of parameters studied. For this appendix, only the standard BC Hydro electric rates were considered.

Table A1: Full Parametric Sweep Parameter Range

Parameter	Start	End	Step Size	Notes
Charging Power	150	600	150	
Number of Chargers	1	6	1	
Cost Projection Year	2020	2050	10	Also 2025

For this additional analysis, three additional charging locations were also considered.

1. The University of Victoria Bus Loop,
2. The Colwood Exchange at the Westshore Rec Center,
3. The Langford Bus Exchange.

For the legislature terminal location, only the results of the parametric sweep are presented. For the remaining 3 locations, the number of buses present, and the reduction in mean and 95^{th} percentile block energy requirements are plotted as to give context to the rest of the results presented.

A.1 Legislature Terminal

A.1.1 Full Parametric Results

Table A2: Optimization Results for SESS Technologies in Legislature Terminal

Year	Charge Config.		Peak Power	RFB SESS					LIB SESS					FESS SESS				
	Power	# Units	(No SESS)	Energy	Power	P_{max}	AEE	Years	Energy	Power	P_{max}	AEE	Years	Energy	Power	P_{max}	AEE	Years
	(kW)		(kW)	(kWh)	(kW)	(kW)	($)		(kWh)	(kW)	(kW)	($)		(kWh)	(kW)	(kW)	($)	
2020	150	1	150.0	0.0	0.0	150.0	20355.4	13	0.0	0.0	150.0	20355.4	13	0.0	0.0	150.0	20355.4	18
2020	300	1	300.0	0.0	0.0	300.0	40680.2	13	0.0	0.0	300.0	40680.2	13	0.0	0.0	300.0	40680.2	18
2020	450	1	450.0	0.0	0.0	450.0	60979.0	13	0.0	0.0	450.0	60979.0	13	0.0	0.0	450.0	60979.0	18
2020	600	1	600.0	0.0	0.0	600.0	81213.4	13	0.0	0.0	600.0	81213.4	13	0.0	0.0	600.0	81213.4	18
2020	150	2	300.0	0.0	0.0	300.0	40531.7	13	0.0	0.0	300.0	40531.7	13	0.0	0.0	300.0	40531.7	18
2020	300	2	600.0	0.0	0.0	600.0	80931.6	13	0.0	0.0	600.0	80931.6	13	0.0	0.0	600.0	80931.6	18
2020	450	2	900.0	0.0	0.0	900.0	120598.0	13	0.0	0.0	900.0	120598.0	13	0.0	0.0	900.0	120598.0	18
2020	600	2	1200.0	0.0	0.0	1200.0	159192.3	13	0.0	0.0	1200.0	159192.3	13	0.0	0.0	1200.0	159192.3	14
2020	150	3	450.0	0.0	0.0	450.0	60343.4	13	0.0	0.0	450.0	60343.4	13	0.0	0.0	450.0	60343.4	18
2020	300	3	900.0	0.0	0.0	900.0	119832.2	13	0.0	0.0	900.0	119832.2	13	0.0	0.0	900.0	119832.2	18
2020	450	3	1350.0	0.0	0.0	1350.0	177800.3	13	0.0	0.0	1350.0	177800.3	13	0.0	0.0	1350.0	177800.3	15
2020	600	3	1800.0	0.0	0.0	1800.0	234512.5	13	22.5	43.1	1760.0	234091.2	11	0.0	0.0	1800.0	234512.5	15
2020	150	4	600.0	0.0	0.0	600.0	79620.6	13	0.0	0.0	600.0	79620.6	13	0.0	0.0	600.0	79620.6	16
2020	300	4	1200.0	0.0	0.0	1200.0	157688.4	13	0.0	0.0	1200.0	157688.4	10	0.0	0.0	1200.0	157688.4	13
2020	450	4	1800.0	92.2	245.8	1590.0	231981.8	13	80.9	242.6	1590.0	225692.0	11	0.0	0.0	1800.0	234097.5	18
2020	600	4	2120.0	146.3	351.1	1820.0	271656.2	13	164.4	388.2	1760.0	261385.4	12	0.0	0.0	2120.0	274459.5	18
2020	150	5	750.0	0.0	0.0	750.0	98527.3	13	0.0	0.0	750.0	98527.3	13	0.0	0.0	750.0	98527.3	18
2020	300	5	1460.0	29.5	93.6	1380.0	189084.5	13	38.8	107.8	1360.0	185610.7	12	0.0	0.0	1460.0	190272.4	18
2020	450	5	1950.0	117.6	376.2	1628.6	248534.0	13	127.4	388.2	1590.0	238249.9	10	0.0	0.0	1950.0	252843.3	18
2020	600	5	2120.0	146.3	351.1	1820.0	271656.2	13	164.4	388.2	1760.0	261385.4	12	0.0	0.0	2120.0	274459.5	18
2020	150	6	900.0	64.4	140.4	780.0	115901.6	13	64.3	140.2	770.0	111089.0	13	0.0	0.0	900.0	117291.5	18
2020	300	6	1460.0	37.4	93.6	1380.0	189451.5	13	30.8	92.4	1380.0	186645.8	12	0.0	0.0	1460.0	190275.5	18
2020	450	6	1950.0	117.6	376.2	1628.6	248739.4	13	127.4	388.2	1590.0	238813.8	10	0.0	0.0	1950.0	252843.3	18
2020	600	6	2120.0	146.3	351.1	1820.0	271656.2	13	164.4	388.2	1760.0	261385.4	12	0.0	0.0	2120.0	274459.5	18
2025	150	1	150.0	0.0	0.0	150.0	20355.4	13	0.0	0.0	150.0	20355.4	13	0.0	0.0	150.0	20355.4	18
2025	300	1	300.0	0.0	0.0	300.0	40680.2	13	0.0	0.0	300.0	40680.2	13	0.0	0.0	300.0	40680.2	18
2025	450	1	450.0	0.0	0.0	450.0	60979.0	13	0.0	0.0	450.0	60979.0	13	0.0	0.0	450.0	60979.0	18
2025	600	1	600.0	0.0	0.0	600.0	81213.4	13	0.0	0.0	600.0	81213.4	13	0.0	0.0	600.0	81213.4	18
2025	150	2	300.0	0.0	0.0	300.0	40531.7	13	0.0	0.0	300.0	40531.7	13	0.0	0.0	300.0	40531.7	18
2025	300	2	600.0	0.0	0.0	600.0	80931.6	13	0.0	0.0	600.0	80931.6	13	0.0	0.0	600.0	80931.6	18
2025	450	2	900.0	0.0	0.0	900.0	120598.0	13	0.0	0.0	900.0	120598.0	13	0.0	0.0	900.0	120598.0	18
2025	600	2	1200.0	0.0	0.0	1200.0	159192.3	13	0.0	0.0	1200.0	159192.3	13	0.0	0.0	1200.0	159192.3	18
2025	150	3	450.0	0.0	0.0	450.0	60343.4	13	0.0	0.0	450.0	60343.4	13	0.0	0.0	450.0	60343.4	18
2025	300	3	900.0	0.0	0.0	900.0	119832.2	13	0.0	0.0	900.0	119832.2	13	0.0	0.0	900.0	119832.2	18
2025	450	3	1350.0	0.0	0.0	1350.0	177800.3	13	0.0	0.0	1350.0	177800.3	13	0.0	0.0	1350.0	177800.3	17
2025	600	3	1800.0	73.6	121.0	1696.6	232845.3	12	19.0	76.1	1760.0	233804.1	7	0.0	0.0	1800.0	234512.5	18
2025	150	4	600.0	0.0	0.0	600.0	79620.6	13	0.0	0.0	600.0	79620.6	13	0.0	0.0	600.0	79620.6	17
2025	300	4	1200.0	0.0	0.0	1200.0	157688.4	13	0.0	0.0	1200.0	157688.4	9	0.0	0.0	1200.0	157688.4	14
2025	450	4	1800.0	130.8	333.3	1515.2	225190.7	12	84.9	339.7	1560.0	222763.7	9	0.0	0.0	1800.0	234097.5	18
2025	600	4	2120.0	254.0	586.0	1619.3	259819.2	12	175.2	647.0	1680.0	256840.5	9	0.0	0.0	2120.0	274459.5	18

2025	150	5	750.0	46.8	46.8	710.0	98252.6	13	12.1	16.2	738.0	98483.3	13	0.0	0.0	750.0	98527.3	18
2025	300	5	1460.0	79.0	173.7	1311.6	185402.0	13	49.7	134.8	1340.0	183938.0	11	0.0	0.0	1460.0	190272.4	18
2025	450	5	1950.0	175.9	503.4	1519.9	238096.4	12	131.4	485.2	1560.0	232707.6	9	0.0	0.0	1950.0	252843.3	18
2025	600	5	2120.0	254.0	586.0	1619.3	259819.2	12	175.2	647.0	1680.0	256840.5	9	0.0	0.0	2120.0	274459.5	18
2025	150	6	900.0	124.4	234.1	700.0	111212.6	13	57.5	229.9	760.0	108627.0	13	0.0	0.0	900.0	117291.5	18
2025	300	6	1460.0	89.3	173.5	1311.7	186727.4	12	44.3	115.5	1360.0	185258.8	11	0.0	0.0	1460.0	190275.5	18
2025	450	6	1950.0	169.6	489.7	1531.6	238380.3	12	131.4	485.2	1560.0	233271.6	9	0.0	0.0	1950.0	252843.3	18
2025	600	6	2120.0	254.0	586.0	1619.3	259819.2	12	175.2	647.0	1680.0	256840.5	9	0.0	0.0	2120.0	274459.5	18
2030	150	1	150.0	0.0	0.0	150.0	20355.4	13	0.0	0.0	150.0	20355.4	13	0.0	0.0	150.0	20355.4	18
2030	300	1	300.0	0.0	0.0	300.0	40680.2	13	0.0	0.0	300.0	40680.2	13	0.0	0.0	300.0	40680.2	18
2030	450	1	450.0	0.0	0.0	450.0	60979.0	13	0.0	0.0	450.0	60979.0	13	0.0	0.0	450.0	60979.0	18
2030	600	1	600.0	0.0	0.0	600.0	81213.4	13	0.0	0.0	600.0	81213.4	13	0.0	0.0	600.0	81213.4	18
2030	150	2	300.0	0.0	0.0	300.0	40531.7	13	0.0	0.0	300.0	40531.7	13	0.0	0.0	300.0	40531.7	18
2030	300	2	600.0	0.0	0.0	600.0	80931.6	13	0.0	0.0	600.0	80931.6	13	0.0	0.0	600.0	80931.6	18
2030	450	2	900.0	0.0	0.0	900.0	120598.0	13	0.0	0.0	900.0	120598.0	13	0.0	0.0	900.0	120598.0	18
2030	600	2	1200.0	0.0	0.0	1200.0	159192.3	13	0.0	0.0	1200.0	159192.3	13	0.0	0.0	1200.0	159192.3	18
2030	150	3	450.0	0.0	0.0	450.0	60343.4	13	0.0	0.0	450.0	60343.4	13	0.0	0.0	450.0	60343.4	18
2030	300	3	900.0	0.0	0.0	900.0	119832.2	13	0.0	0.0	900.0	119832.2	13	0.0	0.0	900.0	119832.2	18
2030	450	3	1350.0	0.0	0.0	1350.0	177800.3	13	0.0	0.0	1350.0	177800.3	13	0.0	0.0	1350.0	177800.3	18
2030	600	3	1800.0	255.5	254.5	1582.6	229304.1	13	19.0	76.1	1760.0	233077.3	7	0.0	0.0	1800.0	234512.5	18
2030	150	4	600.0	0.0	0.0	600.0	79620.6	11	0.0	0.0	600.0	79620.6	13	0.0	0.0	600.0	79620.6	18
2030	300	4	1200.0	70.2	46.8	1160.0	157647.8	13	0.0	0.0	1200.0	157688.4	9	0.0	0.0	1200.0	157688.4	16
2030	450	4	1800.0	292.6	421.3	1440.0	218912.4	13	84.9	339.7	1560.0	220632.4	8	0.0	0.0	1800.0	234097.5	18
2030	600	4	2120.0	340.1	643.7	1570.0	249045.8	13	170.3	681.0	1680.0	251510.3	9	0.0	0.0	2120.0	274459.5	18
2030	150	5	750.0	87.8	87.8	675.0	97131.2	13	20.2	27.0	730.0	98282.5	13	0.0	0.0	750.0	98527.3	18
2030	300	5	1460.0	152.9	223.4	1269.1	182657.8	13	49.7	134.8	1340.0	182847.2	11	0.0	0.0	1460.0	190272.4	18
2030	450	5	1950.0	220.0	526.7	1500.0	229411.4	13	131.4	485.2	1560.0	228773.7	9	0.0	0.0	1950.0	252843.3	18
2030	600	5	2120.0	340.1	643.7	1570.0	249045.8	13	170.3	681.0	1680.0	251510.3	9	0.0	0.0	2120.0	274459.5	18
2030	150	6	900.0	159.9	275.9	664.3	107600.6	13	60.7	242.6	752.5	107210.4	13	0.0	0.0	900.0	117291.5	18
2030	300	6	1460.0	173.1	223.4	1269.1	183419.4	13	44.3	115.5	1360.0	184305.6	11	0.0	0.0	1460.0	190275.5	18
2030	450	6	1950.0	231.0	526.7	1500.0	229758.6	13	131.4	485.2	1560.0	229337.6	9	0.0	0.0	1950.0	252843.3	18
2030	600	6	2120.0	340.1	643.7	1570.0	249045.8	13	170.3	681.0	1680.0	251510.3	9	0.0	0.0	2120.0	274459.5	18
2040	150	1	150.0	0.0	0.0	150.0	20355.4	13	0.0	0.0	150.0	20355.4	13	0.0	0.0	150.0	20355.4	18
2040	300	1	300.0	0.0	0.0	300.0	40680.2	13	0.0	0.0	300.0	40680.2	13	0.0	0.0	300.0	40680.2	18
2040	450	1	450.0	0.0	0.0	450.0	60979.0	13	0.0	0.0	450.0	60979.0	13	0.0	0.0	450.0	60979.0	18
2040	600	1	600.0	0.0	0.0	600.0	81213.4	13	0.0	0.0	600.0	81213.4	13	0.0	0.0	600.0	81213.4	18
2040	150	2	300.0	0.0	0.0	300.0	40531.7	13	0.0	0.0	300.0	40531.7	13	0.0	0.0	300.0	40531.7	18
2040	300	2	600.0	0.0	0.0	600.0	80931.6	13	0.0	0.0	600.0	80931.6	13	0.0	0.0	600.0	80931.6	18
2040	450	2	900.0	0.0	0.0	900.0	120598.0	13	0.0	0.0	900.0	120598.0	13	0.0	0.0	900.0	120598.0	18
2040	600	2	1200.0	0.0	0.0	1200.0	159192.3	13	0.0	0.0	1200.0	159192.3	13	0.0	0.0	1200.0	159192.3	18
2040	150	3	450.0	0.0	0.0	450.0	60343.4	13	0.0	0.0	450.0	60343.4	13	0.0	0.0	450.0	60343.4	18
2040	300	3	900.0	0.0	0.0	900.0	119832.2	13	0.0	0.0	900.0	119832.2	13	0.0	0.0	900.0	119832.2	18
2040	450	3	1350.0	0.0	0.0	1350.0	177800.3	13	0.0	0.0	1350.0	177800.3	13	0.0	0.0	1350.0	177800.3	17
2040	600	3	1800.0	499.8	374.5	1480.0	224426.0	13	107.8	431.3	1640.0	230576.6	11	0.0	0.0	1800.0	234512.5	18
2040	150	4	600.0	0.0	0.0	600.0	79620.6	9	0.0	0.0	600.0	79620.6	13	0.0	0.0	600.0	79620.6	18
2040	300	4	1200.0	76.3	50.2	1157.1	156888.0	13	0.0	0.0	1200.0	157688.4	8	0.0	0.0	1200.0	157688.4	17
2040	450	4	1800.0	371.9	456.5	1410.0	212827.8	13	109.2	436.7	1500.0	218369.6	8	0.0	0.0	1800.0	234097.5	18
2040	600	4	2120.0	470.5	702.2	1520.0	240356.7	13	187.3	749.2	1640.0	247858.5	9	0.0	0.0	2120.0	274459.5	18
2040	150	5	750.0	138.9	132.4	636.9	95801.7	12	20.2	27.0	730.0	98093.5	13	0.0	0.0	750.0	98527.3	18

2040	300	5	1460.0	398.7	351.1	1160.0	178188.1	13	49.7	134.8	1340.0	182153.2	11	0.0	0.0	1460.0	190272.4	18
2040	450	5	1950.0	471.7	632.0	1410.0	221743.1	13	138.6	554.6	1538.6	226813.3	8	0.0	0.0	1950.0	252843.3	18
2040	600	5	2120.0	470.5	702.2	1520.0	240356.7	13	187.3	749.2	1640.0	247858.5	9	0.0	0.0	2120.0	274459.5	18
2040	150	6	900.0	186.9	302.1	641.9	104306.1	12	68.0	272.1	740.0	106351.8	12	0.0	0.0	900.0	117291.5	18
2040	300	6	1460.0	374.7	327.7	1180.0	179149.0	13	44.3	115.5	1360.0	183699.1	11	0.0	0.0	1460.0	190275.5	18
2040	450	6	1950.0	484.3	632.0	1410.0	222067.2	13	138.6	554.6	1538.6	227377.3	8	0.0	0.0	1950.0	252843.3	18
2040	600	6	2120.0	470.5	702.2	1520.0	240356.7	13	187.3	749.2	1640.0	247858.5	9	0.0	0.0	2120.0	274459.5	18
2050	150	1	150.0	0.0	0.0	150.0	20355.4	13	0.0	0.0	150.0	20355.4	13	0.0	0.0	150.0	20355.4	18
2050	300	1	300.0	0.0	0.0	300.0	40680.2	13	0.0	0.0	300.0	40680.2	13	0.0	0.0	300.0	40680.2	18
2050	450	1	450.0	0.0	0.0	450.0	60979.0	13	0.0	0.0	450.0	60979.0	13	0.0	0.0	450.0	60979.0	18
2050	600	1	600.0	0.0	0.0	600.0	81213.4	13	0.0	0.0	600.0	81213.4	13	0.0	0.0	600.0	81213.4	18
2050	150	2	300.0	0.0	0.0	300.0	40531.7	13	0.0	0.0	300.0	40531.7	13	0.0	0.0	300.0	40531.7	18
2050	300	2	600.0	0.0	0.0	600.0	80931.6	13	0.0	0.0	600.0	80931.6	13	0.0	0.0	600.0	80931.6	18
2050	450	2	900.0	0.0	0.0	900.0	120598.0	13	0.0	0.0	900.0	120598.0	13	0.0	0.0	900.0	120598.0	18
2050	600	2	1200.0	0.0	0.0	1200.0	159192.3	13	0.0	0.0	1200.0	159192.3	13	0.0	0.0	1200.0	159192.3	18
2050	150	3	450.0	0.0	0.0	450.0	60343.4	13	0.0	0.0	450.0	60343.4	13	0.0	0.0	450.0	60343.4	18
2050	300	3	900.0	0.0	0.0	900.0	119832.2	13	0.0	0.0	900.0	119832.2	13	0.0	0.0	900.0	119832.2	18
2050	450	3	1350.0	0.0	0.0	1350.0	177800.3	13	0.0	0.0	1350.0	177800.3	13	0.0	0.0	1350.0	177800.3	18
2050	600	3	1800.0	499.8	374.5	1480.0	222768.2	13	107.8	431.3	1640.0	230046.6	11	0.0	0.0	1800.0	234512.5	18
2050	150	4	600.0	0.0	0.0	600.0	79620.6	9	0.0	0.0	600.0	79620.6	13	0.0	0.0	600.0	79620.6	18
2050	300	4	1200.0	242.3	130.8	1088.3	156465.9	13	0.0	0.0	1200.0	157688.4	8	0.0	0.0	1200.0	157688.4	18
2050	450	4	1800.0	420.8	476.3	1393.0	211039.6	13	109.2	436.7	1500.0	217688.1	8	8.9	40.0	1770.0	233804.2	18
2050	600	4	2120.0	558.7	742.5	1485.6	237644.8	13	187.3	749.2	1640.0	246791.1	9	23.7	127.9	2040.0	274127.9	18
2050	150	5	750.0	153.5	140.4	630.0	95204.7	12	20.2	27.0	730.0	98039.6	13	0.0	0.0	750.0	98527.3	18
2050	300	5	1460.0	469.6	380.4	1135.0	176677.7	13	49.7	134.8	1340.0	181954.8	11	23.7	94.8	1380.0	189983.7	18
2050	450	5	1950.0	471.7	632.0	1410.0	219314.7	13	142.7	570.9	1530.0	225928.9	8	62.2	248.7	1740.0	251248.8	18
2050	600	5	2120.0	558.7	742.5	1485.6	237644.8	13	187.3	749.2	1640.0	246791.1	9	23.7	127.9	2040.0	274127.9	18
2050	150	6	900.0	212.7	316.0	630.0	103068.8	12	68.0	272.1	740.0	106037.2	12	0.0	0.0	900.0	117291.5	18
2050	300	6	1460.0	433.3	351.1	1160.0	177683.3	13	44.3	115.5	1360.0	183525.8	11	0.0	0.0	1460.0	190275.5	18
2050	450	6	1950.0	484.3	632.0	1410.0	219626.3	13	142.7	570.9	1530.0	226492.9	8	62.2	248.7	1740.0	251620.6	18
2050	600	6	2120.0	558.7	742.5	1485.6	237644.8	13	187.3	749.2	1640.0	246791.1	9	23.7	127.9	2040.0	274127.9	18

A.2 University of Victoria Bus Loop

A.2.1 Charge Scheduling and Energy Reduction Results

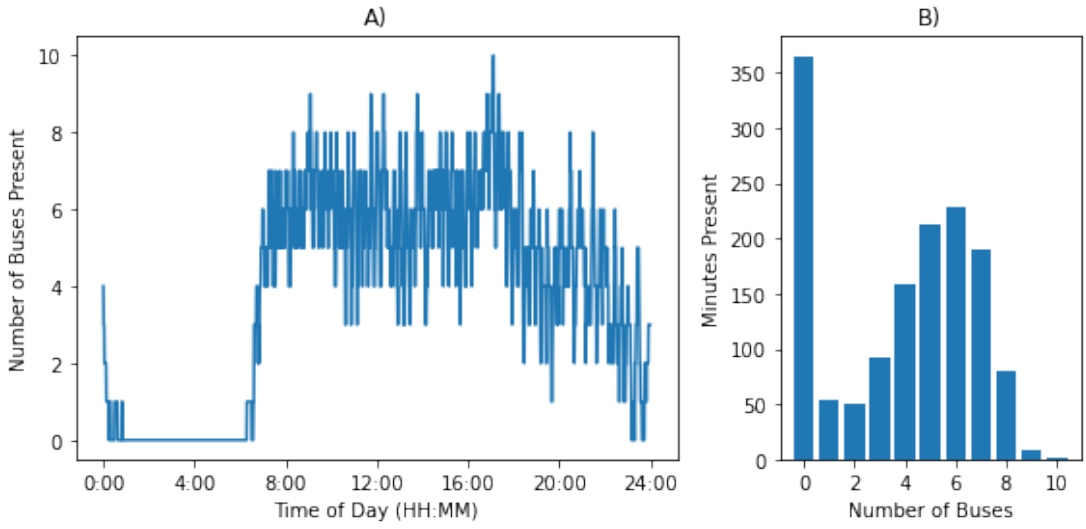

Figure A1: Buses present at UVic

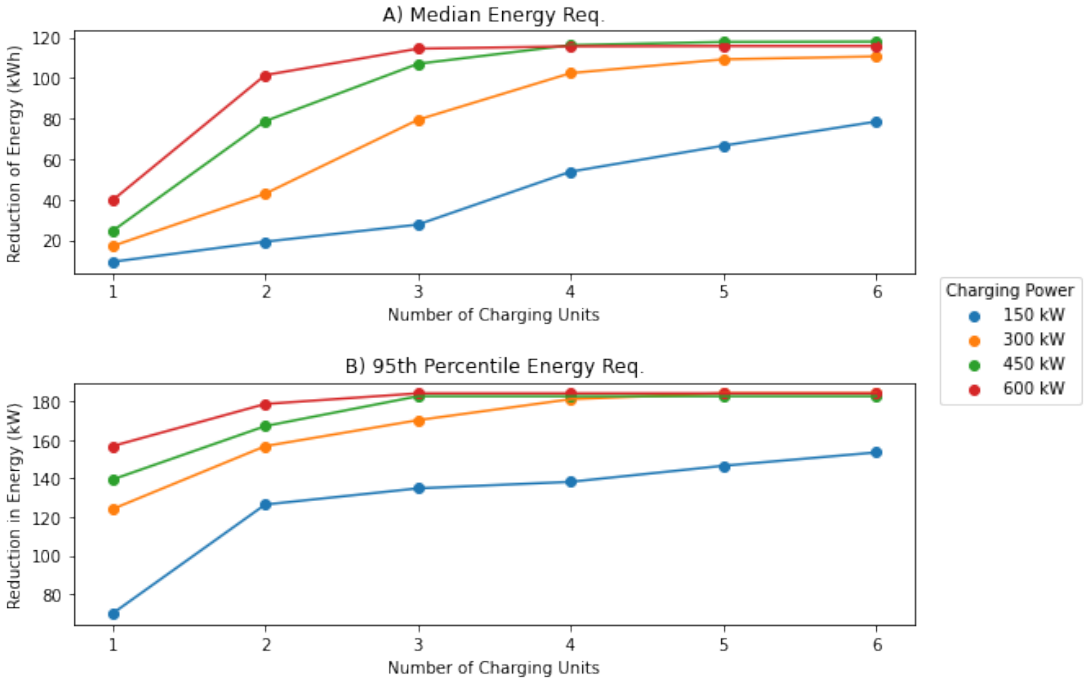

Figure A2: Reduction in mean and 95th percentile energy requirements for Uvic

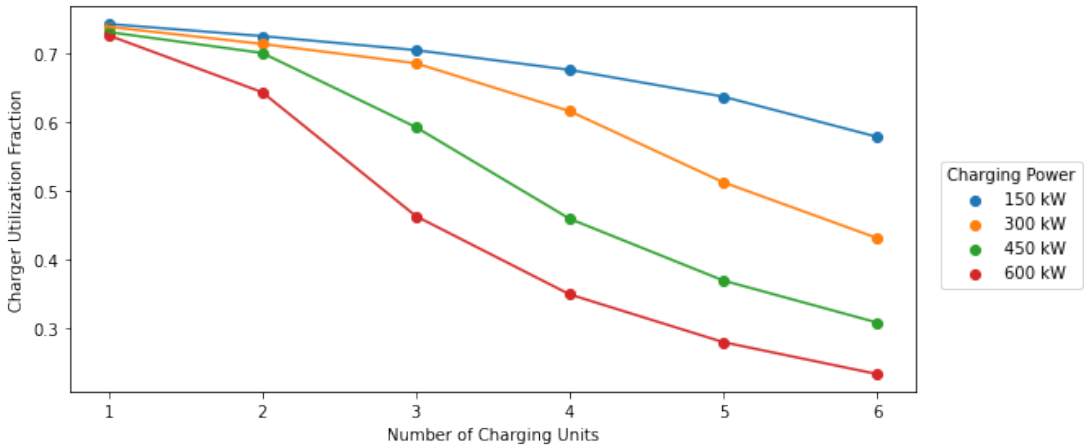

Figure A3: Charger Utilization for UVic

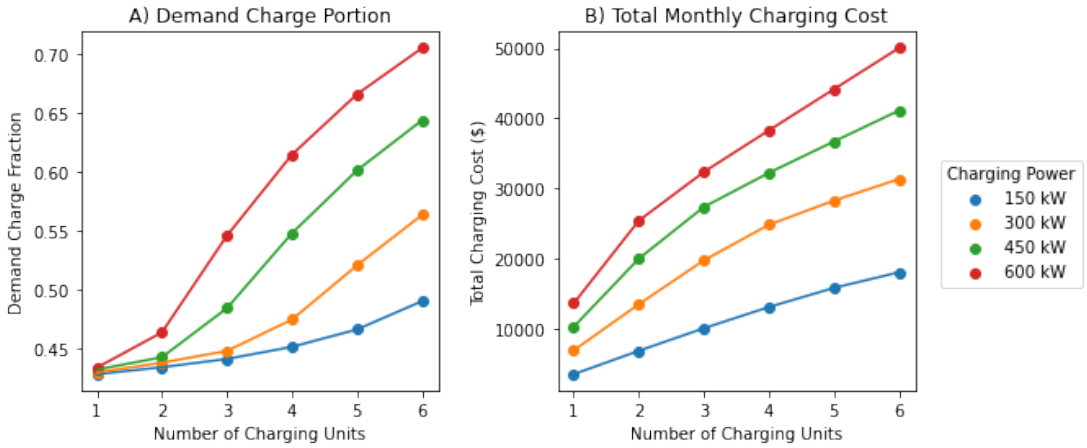

Figure A4: Demand Charge Portion and Total Cost for UVic

A.2.2 Full Parametric Results

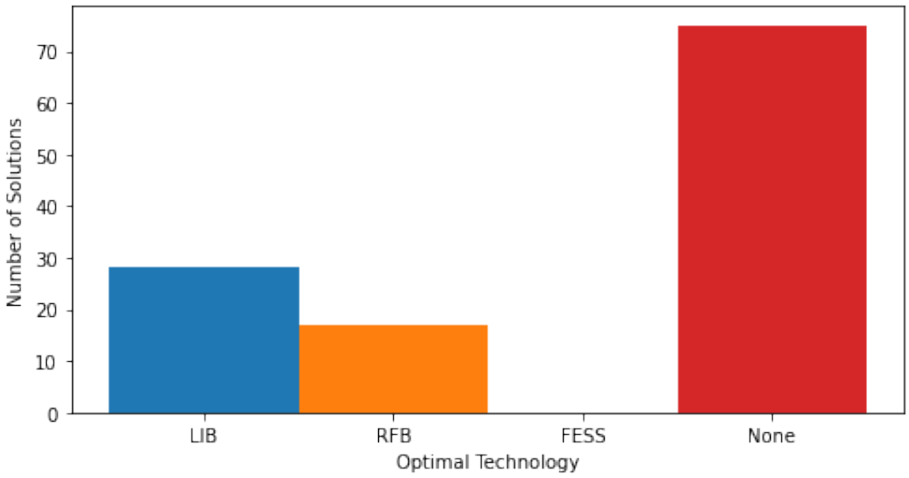

Figure A5: Optimal deployment by technology type for UVic

Table A3: Optimization Results for SESS Technologies in UVIC

Year	Charge Config.		Peak Power	RFB SESS					LIB SESS					FESS SESS				
	Power	# Units	(No SESS)	Energy	Power	P_{max}	AEE	Years	Energy	Power	P_{max}	AEE	Years	Energy	Power	P_{max}	AEE	Years
	(kW)		(kW)	(kWh)	(kW)	(kW)	($)		(kWh)	(kW)	(kW)	($)		(kWh)	(kW)	(kW)	($)	
2020	150	1	150.0	0.0	0.0	150.0	20353.9	13	0.0	0.0	150.0	20353.9	13	0.0	0.0	150.0	20353.9	18
2020	300	1	300.0	0.0	0.0	300.0	40689.4	13	0.0	0.0	300.0	40689.4	13	0.0	0.0	300.0	40689.4	18
2020	450	1	450.0	0.0	0.0	450.0	60983.6	13	0.0	0.0	450.0	60983.6	13	0.0	0.0	450.0	60983.6	18
2020	600	1	600.0	0.0	0.0	600.0	81268.5	13	0.0	0.0	600.0	81268.5	13	0.0	0.0	600.0	81268.5	18
2020	150	2	300.0	0.0	0.0	300.0	40629.7	13	0.0	0.0	300.0	40629.7	13	0.0	0.0	300.0	40629.7	18
2020	300	2	600.0	0.0	0.0	600.0	81158.3	13	0.0	0.0	600.0	81158.3	13	0.0	0.0	600.0	81158.3	18
2020	450	2	900.0	0.0	0.0	900.0	121562.8	13	0.0	0.0	900.0	121562.8	13	0.0	0.0	900.0	121562.8	18
2020	600	2	1200.0	0.0	0.0	1200.0	161073.0	13	0.0	0.0	1200.0	161073.0	13	0.0	0.0	1200.0	161073.0	18
2020	150	3	450.0	0.0	0.0	450.0	60809.0	13	0.0	0.0	450.0	60809.0	13	0.0	0.0	450.0	60809.0	18
2020	300	3	900.0	0.0	0.0	900.0	121363.7	13	0.0	0.0	900.0	121363.7	13	0.0	0.0	900.0	121363.7	18
2020	450	3	1350.0	0.0	0.0	1350.0	180194.0	13	0.0	0.0	1350.0	180194.0	13	0.0	0.0	1350.0	180194.0	17
2020	600	3	1800.0	0.0	0.0	1800.0	236822.0	8	0.0	0.0	1800.0	236822.0	6	0.0	0.0	1800.0	236822.0	9
2020	150	4	600.0	0.0	0.0	600.0	80824.4	13	0.0	0.0	600.0	80824.4	13	0.0	0.0	600.0	80824.4	18
2020	300	4	1200.0	0.0	0.0	1200.0	160585.9	13	0.0	0.0	1200.0	160585.9	13	0.0	0.0	1200.0	160585.9	15
2020	450	4	1800.0	0.0	0.0	1800.0	236720.9	10	10.5	42.2	1770.0	236709.5	7	0.0	0.0	1800.0	236720.9	15
2020	600	4	2320.0	117.0	374.5	2000.0	296423.6	13	134.8	431.3	1920.0	284128.9	10	0.0	0.0	2320.0	301751.2	18
2020	150	5	750.0	0.0	0.0	750.0	100599.4	13	0.0	0.0	750.0	100599.4	13	0.0	0.0	750.0	100599.4	18
2020	300	5	1500.0	0.0	0.0	1500.0	198442.1	10	0.0	0.0	1500.0	198442.1	8	0.0	0.0	1500.0	198442.1	16
2020	450	5	2100.0	98.8	316.0	1830.0	270427.4	13	91.0	291.1	1830.0	260967.2	11	0.0	0.0	2100.0	274203.4	18
2020	600	5	2560.0	218.5	655.4	2000.0	322683.7	13	202.2	693.2	1960.0	297203.4	13	0.0	0.0	2560.0	331693.0	18
2020	150	6	900.0	0.0	0.0	900.0	119944.0	13	0.0	0.0	900.0	119944.0	11	0.0	0.0	900.0	119944.0	18
2020	300	6	1780.0	36.6	117.0	1680.0	232706.1	12	60.7	215.7	1600.0	230128.4	7	0.0	0.0	1780.0	233481.5	18
2020	450	6	2220.0	131.7	421.3	1860.0	283600.9	13	131.4	420.5	1830.0	269751.3	11	0.0	0.0	2220.0	289183.5	18
2020	600	6	2560.0	218.5	655.4	2000.0	322683.7	13	202.2	693.2	1960.0	297203.4	13	0.0	0.0	2560.0	331693.0	18
2025	150	1	150.0	0.0	0.0	150.0	20353.9	13	0.0	0.0	150.0	20353.9	13	0.0	0.0	150.0	20353.9	18
2025	300	1	300.0	0.0	0.0	300.0	40689.4	13	0.0	0.0	300.0	40689.4	13	0.0	0.0	300.0	40689.4	18
2025	450	1	450.0	0.0	0.0	450.0	60983.6	13	0.0	0.0	450.0	60983.6	13	0.0	0.0	450.0	60983.6	18
2025	600	1	600.0	0.0	0.0	600.0	81268.5	13	0.0	0.0	600.0	81268.5	13	0.0	0.0	600.0	81268.5	18
2025	150	2	300.0	0.0	0.0	300.0	40629.7	13	0.0	0.0	300.0	40629.7	13	0.0	0.0	300.0	40629.7	18
2025	300	2	600.0	0.0	0.0	600.0	81158.3	13	0.0	0.0	600.0	81158.3	13	0.0	0.0	600.0	81158.3	18
2025	450	2	900.0	0.0	0.0	900.0	121562.8	13	0.0	0.0	900.0	121562.8	13	0.0	0.0	900.0	121562.8	18
2025	600	2	1200.0	0.0	0.0	1200.0	161073.0	13	0.0	0.0	1200.0	161073.0	13	0.0	0.0	1200.0	161073.0	18
2025	150	3	450.0	0.0	0.0	450.0	60809.0	13	0.0	0.0	450.0	60809.0	13	0.0	0.0	450.0	60809.0	18
2025	300	3	900.0	0.0	0.0	900.0	121363.7	13	0.0	0.0	900.0	121363.7	13	0.0	0.0	900.0	121363.7	18
2025	450	3	1350.0	0.0	0.0	1350.0	180194.0	13	0.0	0.0	1350.0	180194.0	13	0.0	0.0	1350.0	180194.0	18
2025	600	3	1800.0	0.0	0.0	1800.0	236822.0	7	0.0	0.0	1800.0	236822.0	6	0.0	0.0	1800.0	236822.0	12
2025	150	4	600.0	0.0	0.0	600.0	80824.4	13	0.0	0.0	600.0	80824.4	13	0.0	0.0	600.0	80824.4	18
2025	300	4	1200.0	0.0	0.0	1200.0	160585.9	13	0.0	0.0	1200.0	160585.9	13	0.0	0.0	1200.0	160585.9	18
2025	450	4	1800.0	70.2	105.3	1710.0	235527.3	12	10.5	42.2	1770.0	236345.3	5	0.0	0.0	1800.0	236720.9	18
2025	600	4	2320.0	175.6	561.8	1840.0	289554.8	10	148.3	474.5	1880.0	278345.3	9	0.0	0.0	2320.0	301751.2	18

2025	150	5	750.0	0.0	0.0	750.0	100599.4	13	0.0	0.0	750.0	100599.4	13	0.0	0.0	750.0	100599.4	18
2025	300	5	1500.0	48.3	70.2	1440.0	197809.4	12	9.5	38.1	1480.0	198306.1	8	0.0	0.0	1500.0	198442.1	17
2025	450	5	2100.0	98.8	316.0	1830.0	270141.9	8	91.0	291.1	1830.0	258634.3	8	0.0	0.0	2100.0	274203.4	18
2025	600	5	2560.0	268.3	795.9	1880.0	303253.9	13	215.7	739.4	1920.0	290175.8	11	0.0	0.0	2560.0	331693.0	18
2025	150	6	900.0	0.0	0.0	900.0	119944.0	13	0.0	0.0	900.0	119944.0	11	0.0	0.0	900.0	119944.0	18
2025	300	6	1780.0	124.4	351.1	1480.0	229595.0	9	94.4	359.4	1500.0	225172.1	7	0.0	0.0	1780.0	233481.5	18
2025	450	6	2220.0	153.6	491.6	1800.0	279854.1	9	141.5	452.9	1800.0	264333.6	10	0.0	0.0	2220.0	289183.5	18
2025	600	6	2560.0	267.5	802.6	1874.2	305774.7	12	215.7	739.4	1920.0	290175.8	11	0.0	0.0	2560.0	331693.0	18
2030	150	1	150.0	0.0	0.0	150.0	20353.9	13	0.0	0.0	150.0	20353.9	13	0.0	0.0	150.0	20353.9	18
2030	300	1	300.0	0.0	0.0	300.0	40689.4	13	0.0	0.0	300.0	40689.4	13	0.0	0.0	300.0	40689.4	18
2030	450	1	450.0	0.0	0.0	450.0	60983.6	13	0.0	0.0	450.0	60983.6	13	0.0	0.0	450.0	60983.6	18
2030	600	1	600.0	0.0	0.0	600.0	81268.5	13	0.0	0.0	600.0	81268.5	13	0.0	0.0	600.0	81268.5	18
2030	150	2	300.0	0.0	0.0	300.0	40629.7	13	0.0	0.0	300.0	40629.7	13	0.0	0.0	300.0	40629.7	18
2030	300	2	600.0	0.0	0.0	600.0	81158.3	13	0.0	0.0	600.0	81158.3	13	0.0	0.0	600.0	81158.3	18
2030	450	2	900.0	0.0	0.0	900.0	121562.8	13	0.0	0.0	900.0	121562.8	13	0.0	0.0	900.0	121562.8	18
2030	600	2	1200.0	0.0	0.0	1200.0	161073.0	13	0.0	0.0	1200.0	161073.0	13	0.0	0.0	1200.0	161073.0	18
2030	150	3	450.0	0.0	0.0	450.0	60809.0	13	0.0	0.0	450.0	60809.0	13	0.0	0.0	450.0	60809.0	18
2030	300	3	900.0	0.0	0.0	900.0	121363.7	13	0.0	0.0	900.0	121363.7	13	0.0	0.0	900.0	121363.7	18
2030	450	3	1350.0	0.0	0.0	1350.0	180194.0	13	0.0	0.0	1350.0	180194.0	13	0.0	0.0	1350.0	180194.0	18
2030	600	3	1800.0	22.4	46.8	1760.0	236709.1	7	16.2	64.7	1760.0	236457.0	6	0.0	0.0	1800.0	236822.0	14
2030	150	4	600.0	0.0	0.0	600.0	80824.4	13	0.0	0.0	600.0	80824.4	13	0.0	0.0	600.0	80824.4	18
2030	300	4	1200.0	0.0	0.0	1200.0	160585.9	13	0.0	0.0	1200.0	160585.9	13	0.0	0.0	1200.0	160585.9	18
2030	450	4	1800.0	173.4	210.7	1620.0	233077.7	12	10.5	42.2	1770.0	235651.4	6	0.0	0.0	1800.0	236720.9	18
2030	600	4	2320.0	207.8	608.6	1800.0	282720.7	9	148.3	474.5	1880.0	274241.9	9	0.0	0.0	2320.0	301751.2	18
2030	150	5	750.0	0.0	0.0	750.0	100599.4	13	0.0	0.0	750.0	100599.4	13	0.0	0.0	750.0	100599.4	18
2030	300	5	1500.0	120.0	140.4	1380.0	196264.9	12	34.1	136.2	1440.0	197681.9	9	0.0	0.0	1500.0	198442.1	18
2030	450	5	2100.0	153.6	491.6	1680.0	262546.7	8	111.2	355.8	1770.0	255312.7	8	0.0	0.0	2100.0	274203.4	18
2030	600	5	2560.0	340.2	889.5	1800.0	295839.9	11	215.7	739.4	1920.0	284833.4	11	0.0	0.0	2560.0	331693.0	18
2030	150	6	900.0	16.3	11.7	890.0	119872.5	13	0.0	0.0	900.0	119944.0	11	0.0	0.0	900.0	119944.0	18
2030	300	6	1780.0	155.6	397.9	1440.0	222881.6	9	106.3	359.4	1482.2	221518.8	7	0.0	0.0	1780.0	233481.5	18
2030	450	6	2220.0	175.6	561.8	1740.0	277241.0	7	141.5	452.9	1800.0	260713.9	10	0.0	0.0	2220.0	289183.5	18
2030	600	6	2560.0	326.7	889.5	1800.0	295643.9	11	215.7	739.4	1920.0	284833.4	11	0.0	0.0	2560.0	331693.0	18
2040	150	1	150.0	0.0	0.0	150.0	20353.9	13	0.0	0.0	150.0	20353.9	13	0.0	0.0	150.0	20353.9	18
2040	300	1	300.0	0.0	0.0	300.0	40689.4	13	0.0	0.0	300.0	40689.4	13	0.0	0.0	300.0	40689.4	18
2040	450	1	450.0	0.0	0.0	450.0	60983.6	13	0.0	0.0	450.0	60983.6	13	0.0	0.0	450.0	60983.6	18
2040	600	1	600.0	0.0	0.0	600.0	81268.5	13	0.0	0.0	600.0	81268.5	13	0.0	0.0	600.0	81268.5	18
2040	150	2	300.0	0.0	0.0	300.0	40629.7	13	0.0	0.0	300.0	40629.7	13	0.0	0.0	300.0	40629.7	18
2040	300	2	600.0	0.0	0.0	600.0	81158.3	13	0.0	0.0	600.0	81158.3	13	0.0	0.0	600.0	81158.3	18
2040	450	2	900.0	0.0	0.0	900.0	121562.8	13	0.0	0.0	900.0	121562.8	13	0.0	0.0	900.0	121562.8	18
2040	600	2	1200.0	0.0	0.0	1200.0	161073.0	13	0.0	0.0	1200.0	161073.0	13	0.0	0.0	1200.0	161073.0	18
2040	150	3	450.0	0.0	0.0	450.0	60809.0	13	0.0	0.0	450.0	60809.0	13	0.0	0.0	450.0	60809.0	18
2040	300	3	900.0	0.0	0.0	900.0	121363.7	13	0.0	0.0	900.0	121363.7	13	0.0	0.0	900.0	121363.7	18
2040	450	3	1350.0	0.0	0.0	1350.0	180194.0	13	0.0	0.0	1350.0	180194.0	13	0.0	0.0	1350.0	180194.0	18
2040	600	3	1800.0	78.1	108.0	1707.7	234771.6	9	16.2	64.7	1760.0	236010.7	6	0.0	0.0	1800.0	236822.0	16
2040	150	4	600.0	0.0	0.0	600.0	80824.4	13	0.0	0.0	600.0	80824.4	13	0.0	0.0	600.0	80824.4	18
2040	300	4	1200.0	0.0	0.0	1200.0	160585.9	13	0.0	0.0	1200.0	160585.9	13	0.0	0.0	1200.0	160585.9	18
2040	450	4	1800.0	226.4	263.3	1575.0	230930.8	10	49.6	132.3	1710.0	234820.6	8	0.0	0.0	1800.0	236720.9	18
2040	600	4	2320.0	279.1	702.2	1720.0	275494.5	8	148.3	474.5	1880.0	272199.5	8	0.0	0.0	2320.0	301751.2	18
2040	150	5	750.0	0.0	0.0	750.0	100599.4	13	0.0	0.0	750.0	100599.4	13	0.0	0.0	750.0	100599.4	18

2040	300	5	1500.0	120.0	140.4	1380.0	194988.9	10	34.7	138.6	1440.0	197147.1	8	0.0	0.0	1500.0	198442.1	18
2040	450	5	2100.0	216.6	561.8	1620.0	253778.8	8	111.2	355.8	1770.0	253718.7	7	0.0	0.0	2100.0	274203.4	18
2040	600	5	2560.0	513.6	1115.4	1607.0	284694.3	10	215.7	739.4	1920.0	281989.9	10	0.0	0.0	2560.0	331693.0	18
2040	150	6	900.0	20.4	14.6	887.5	119676.2	13	0.0	0.0	900.0	119944.0	11	0.0	0.0	900.0	119944.0	18
2040	300	6	1780.0	248.3	482.8	1367.5	214483.7	10	107.1	363.9	1480.0	219154.9	7	0.0	0.0	1780.0	233481.5	18
2040	450	6	2220.0	220.1	704.3	1618.2	265422.8	7	141.5	452.9	1800.0	259385.7	8	0.0	0.0	2220.0	289183.5	18
2040	600	6	2560.0	496.8	1115.6	1606.8	288209.1	9	215.7	739.4	1920.0	281989.9	10	0.0	0.0	2560.0	331693.0	18
2050	150	1	150.0	0.0	0.0	150.0	20353.9	13	0.0	0.0	150.0	20353.9	13	0.0	0.0	150.0	20353.9	18
2050	300	1	300.0	0.0	0.0	300.0	40689.4	13	0.0	0.0	300.0	40689.4	13	0.0	0.0	300.0	40689.4	18
2050	450	1	450.0	0.0	0.0	450.0	60983.6	13	0.0	0.0	450.0	60983.6	13	0.0	0.0	450.0	60983.6	18
2050	600	1	600.0	0.0	0.0	600.0	81268.5	13	0.0	0.0	600.0	81268.5	13	0.0	0.0	600.0	81268.5	18
2050	150	2	300.0	0.0	0.0	300.0	40629.7	13	0.0	0.0	300.0	40629.7	13	0.0	0.0	300.0	40629.7	18
2050	300	2	600.0	0.0	0.0	600.0	81158.3	13	0.0	0.0	600.0	81158.3	13	0.0	0.0	600.0	81158.3	18
2050	450	2	900.0	0.0	0.0	900.0	121562.8	13	0.0	0.0	900.0	121562.8	13	0.0	0.0	900.0	121562.8	18
2050	600	2	1200.0	0.0	0.0	1200.0	161073.0	13	0.0	0.0	1200.0	161073.0	13	0.0	0.0	1200.0	161073.0	18
2050	150	3	450.0	0.0	0.0	450.0	60809.0	13	0.0	0.0	450.0	60809.0	13	0.0	0.0	450.0	60809.0	18
2050	300	3	900.0	0.0	0.0	900.0	121363.7	13	0.0	0.0	900.0	121363.7	13	0.0	0.0	900.0	121363.7	18
2050	450	3	1350.0	0.0	0.0	1350.0	180194.0	13	0.0	0.0	1350.0	180194.0	13	0.0	0.0	1350.0	180194.0	18
2050	600	3	1800.0	114.1	140.4	1680.0	234171.4	9	16.2	64.7	1760.0	235883.2	6	0.0	0.0	1800.0	236822.0	16
2050	150	4	600.0	0.0	0.0	600.0	80824.4	13	0.0	0.0	600.0	80824.4	13	0.0	0.0	600.0	80824.4	18
2050	300	4	1200.0	0.0	0.0	1200.0	160585.9	13	0.0	0.0	1200.0	160585.9	13	0.0	0.0	1200.0	160585.9	18
2050	450	4	1800.0	282.1	316.0	1530.0	229566.7	10	49.6	132.3	1710.0	234571.2	8	0.0	0.0	1800.0	236720.9	18
2050	600	4	2320.0	377.1	830.8	1610.1	271825.5	8	148.3	474.5	1880.0	271382.3	8	82.9	331.6	2040.0	299129.4	18
2050	150	5	750.0	0.0	0.0	750.0	100599.4	13	0.0	0.0	750.0	100599.4	13	0.0	0.0	750.0	100599.4	18
2050	300	5	1500.0	120.0	140.4	1380.0	194321.8	10	40.4	161.7	1430.0	196929.5	8	0.0	0.0	1500.0	198442.1	18
2050	450	5	2100.0	219.2	564.3	1617.9	250979.6	8	111.2	355.8	1770.0	253036.9	7	53.3	213.2	1920.0	272624.2	18
2050	600	5	2560.0	513.6	1115.4	1607.0	279920.5	10	229.1	785.6	1880.0	280926.4	10	130.3	521.2	2120.0	326015.0	18
2050	150	6	900.0	22.6	16.0	886.4	119607.9	13	0.0	0.0	900.0	119944.0	11	0.0	0.0	900.0	119944.0	18
2050	300	6	1780.0	265.0	498.1	1354.4	212341.8	10	132.6	444.8	1440.0	218336.5	7	23.7	94.8	1700.0	233192.7	18
2050	450	6	2220.0	220.1	704.3	1618.2	261612.7	7	141.5	452.9	1800.0	258605.7	8	80.0	319.8	1950.0	286442.9	18
2050	600	6	2560.0	496.8	1115.6	1606.8	283064.3	9	229.1	785.6	1880.0	280926.4	10	130.3	521.2	2120.0	326015.0	18

A.3 Colwood Exchange

A.3.1 Charge Scheduling and Energy Reduction Results

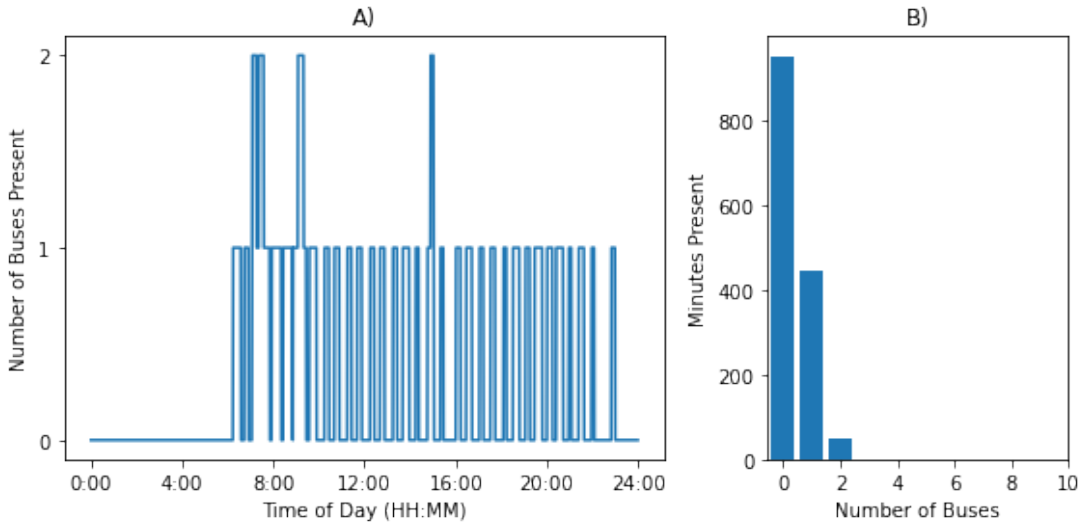

Figure A6: Buses present at Colwood

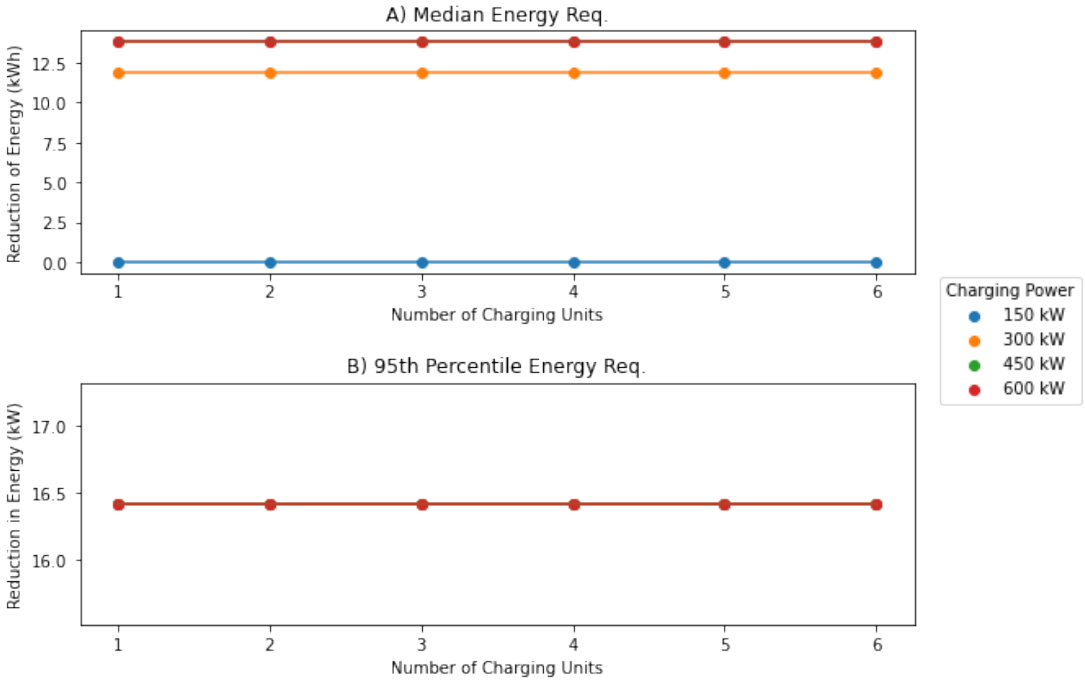

Figure A7: Reduction in mean and 95th percentile energy requirements for Colwood

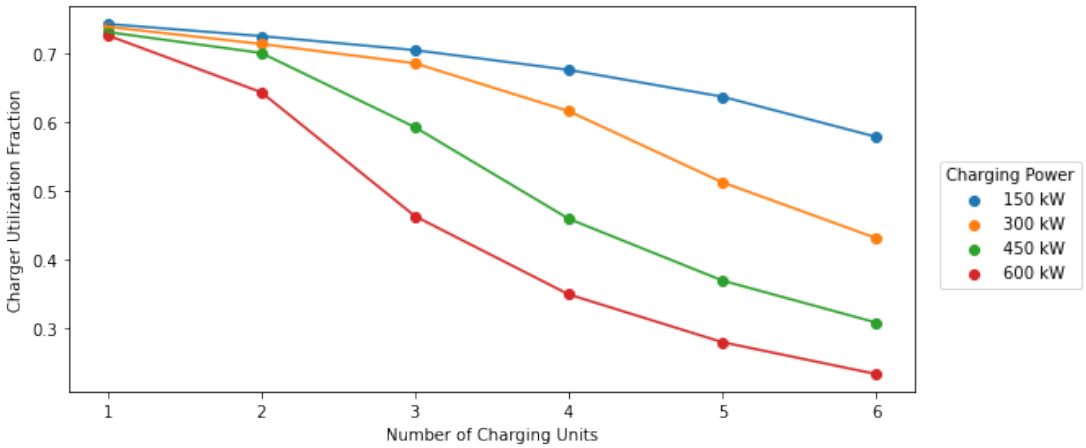

Figure A8: Charger Utilization for Colwood

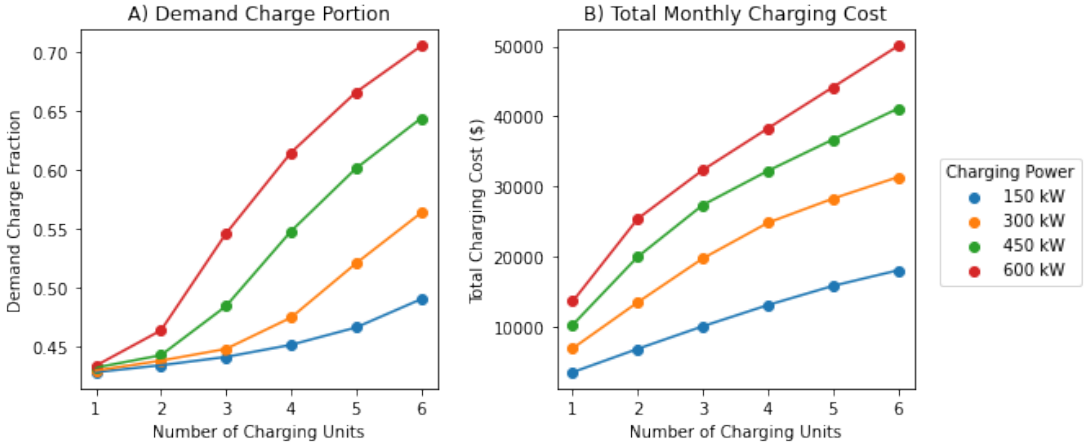

Figure A9: Demand Charge Portion and Total Cost for Colwood

A.3.2 Full Parametric Results

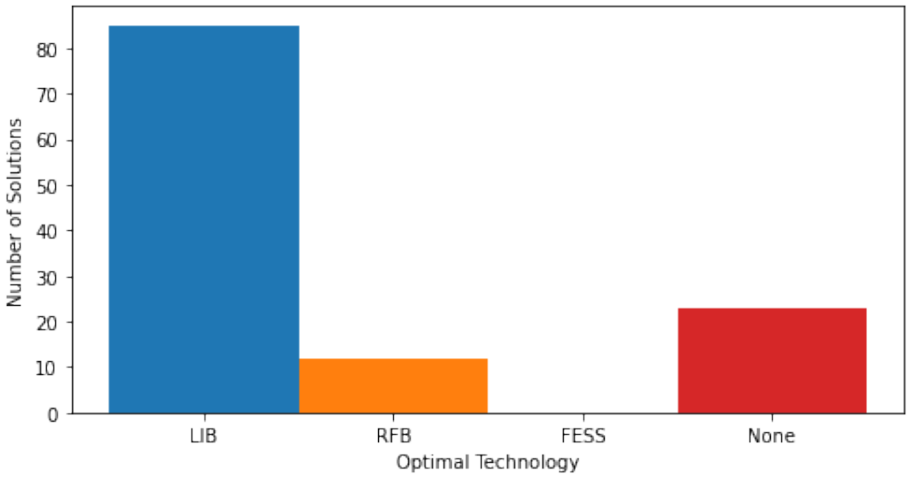

Figure A10: Optimal deployment by technology type for Colwood

Table A4: Optimization Results for SESS Technologies in Colwood Exchange

Year	Charge Config.		Peak Power	RFB SESS					LIB SESS					FESS SESS				
	Power	# Units	(No SESS)	Energy	Power	P_{max}	AEE	Years	Energy	Power	P_{max}	AEE	Years	Energy	Power	P_{max}	AEE	Years
	(kW)		(kW)	(kWh)	(kW)	(kW)	($)		(kWh)	(kW)	(kW)	($)		(kWh)	(kW)	(kW)	($)	
2020	150	1	150.0	0.0	0.0	150.0	19409.0	13	0.0	0.0	150.0	19409.0	13	0.0	0.0	150.0	19409.0	4
2020	300	1	300.0	0.0	0.0	300.0	38585.1	6	0.0	0.0	300.0	38585.1	4	0.0	0.0	300.0	38585.1	4
2020	450	1	390.0	11.0	40.5	360.0	49741.1	13	30.3	112.0	300.0	45208.2	12	0.0	0.0	390.0	49932.8	18
2020	600	1	520.0	58.5	216.1	360.0	65131.8	13	80.9	298.6	280.0	52283.4	13	0.0	0.0	520.0	66154.4	18
2020	150	2	170.0	7.3	27.0	150.0	21780.9	13	6.7	24.9	150.0	20564.8	13	0.0	0.0	170.0	21908.7	18
2020	300	2	300.0	0.0	0.0	300.0	38585.1	6	0.0	0.0	300.0	38585.1	4	0.0	0.0	300.0	38585.1	4
2020	450	2	390.0	11.0	40.5	360.0	49741.1	13	30.3	112.0	300.0	45208.2	12	0.0	0.0	390.0	49932.8	18
2020	600	2	520.0	58.5	216.1	360.0	65131.8	13	80.9	298.6	280.0	52283.4	13	0.0	0.0	520.0	66154.4	18
2020	150	3	170.0	7.3	27.0	150.0	21780.9	13	6.7	24.9	150.0	20564.8	13	0.0	0.0	170.0	21908.7	18
2020	300	3	300.0	0.0	0.0	300.0	38585.1	6	0.0	0.0	300.0	38585.1	4	0.0	0.0	300.0	38585.1	4
2020	450	3	390.0	11.0	40.5	360.0	49741.1	13	30.3	112.0	300.0	45208.2	12	0.0	0.0	390.0	49932.8	18
2020	600	3	520.0	58.5	216.1	360.0	65131.8	13	80.9	298.6	280.0	52283.4	13	0.0	0.0	520.0	66154.4	18
2020	150	4	170.0	7.3	27.0	150.0	21780.9	13	6.7	24.9	150.0	20564.8	13	0.0	0.0	170.0	21908.7	18
2020	300	4	300.0	0.0	0.0	300.0	38585.1	6	0.0	0.0	300.0	38585.1	4	0.0	0.0	300.0	38585.1	4
2020	450	4	390.0	11.0	40.5	360.0	49741.1	13	30.3	112.0	300.0	45208.2	12	0.0	0.0	390.0	49932.8	18
2020	600	4	520.0	58.5	216.1	360.0	65131.8	13	80.9	298.6	280.0	52283.4	13	0.0	0.0	520.0	66154.4	18
2020	150	5	170.0	7.3	27.0	150.0	21780.9	13	6.7	24.9	150.0	20564.8	13	0.0	0.0	170.0	21908.7	18
2020	300	5	300.0	0.0	0.0	300.0	38585.1	6	0.0	0.0	300.0	38585.1	4	0.0	0.0	300.0	38585.1	4
2020	450	5	390.0	11.0	40.5	360.0	49741.1	13	30.3	112.0	300.0	45208.2	12	0.0	0.0	390.0	49932.8	18
2020	600	5	520.0	58.5	216.1	360.0	65131.8	13	80.9	298.6	280.0	52283.4	13	0.0	0.0	520.0	66154.4	18
2020	150	6	170.0	7.3	27.0	150.0	21780.9	13	6.7	24.9	150.0	20564.8	13	0.0	0.0	170.0	21908.7	18
2020	300	6	300.0	0.0	0.0	300.0	38585.1	6	0.0	0.0	300.0	38585.1	4	0.0	0.0	300.0	38585.1	4
2020	450	6	390.0	11.0	40.5	360.0	49741.1	13	30.3	112.0	300.0	45208.2	12	0.0	0.0	390.0	49932.8	18
2020	600	6	520.0	58.5	216.1	360.0	65131.8	13	80.9	298.6	280.0	52283.4	13	0.0	0.0	520.0	66154.4	18
2025	150	1	150.0	0.0	0.0	150.0	19409.0	11	0.0	0.0	150.0	19409.0	13	0.0	0.0	150.0	19409.0	4
2025	300	1	300.0	0.0	0.0	300.0	38585.1	6	0.0	0.0	300.0	38585.1	4	0.0	0.0	300.0	38585.1	7
2025	450	1	390.0	32.9	121.5	300.0	46696.6	13	30.3	112.0	300.0	43802.1	12	0.0	0.0	390.0	49932.8	18
2025	600	1	520.0	87.8	324.1	280.0	57250.6	13	80.9	298.6	280.0	48732.5	13	0.0	0.0	520.0	66154.4	18
2025	150	2	170.0	7.3	27.0	150.0	21098.2	13	6.7	24.9	150.0	20268.9	13	0.0	0.0	170.0	21908.7	18
2025	300	2	300.0	0.0	0.0	300.0	38585.1	6	0.0	0.0	300.0	38585.1	4	0.0	0.0	300.0	38585.1	6
2025	450	2	390.0	32.9	121.5	300.0	46696.6	13	30.3	112.0	300.0	43802.1	12	0.0	0.0	390.0	49932.8	18
2025	600	2	520.0	87.8	324.1	280.0	57250.6	13	80.9	298.6	280.0	48732.5	13	0.0	0.0	520.0	66154.4	18
2025	150	3	170.0	7.3	27.0	150.0	21098.2	13	6.7	24.9	150.0	20268.9	13	0.0	0.0	170.0	21908.7	18
2025	300	3	300.0	0.0	0.0	300.0	38585.1	6	0.0	0.0	300.0	38585.1	4	0.0	0.0	300.0	38585.1	6
2025	450	3	390.0	32.9	121.5	300.0	46696.6	13	30.3	112.0	300.0	43802.1	12	0.0	0.0	390.0	49932.8	18
2025	600	3	520.0	87.8	324.1	280.0	57250.6	13	80.9	298.6	280.0	48732.5	13	0.0	0.0	520.0	66154.4	18
2025	150	4	170.0	7.3	27.0	150.0	21098.2	13	6.7	24.9	150.0	20268.9	13	0.0	0.0	170.0	21908.7	18
2025	300	4	300.0	0.0	0.0	300.0	38585.1	6	0.0	0.0	300.0	38585.1	4	0.0	0.0	300.0	38585.1	6
2025	450	4	390.0	32.9	121.5	300.0	46696.6	13	30.3	112.0	300.0	43802.1	12	0.0	0.0	390.0	49932.8	18
2025	600	4	520.0	87.8	324.1	280.0	57250.6	13	80.9	298.6	280.0	48732.5	13	0.0	0.0	520.0	66154.4	18
2025	150	5	170.0	7.3	27.0	150.0	21098.2	13	6.7	24.9	150.0	20268.9	13	0.0	0.0	170.0	21908.7	18

2025	300	5	300.0	0.0	0.0	300.0	38585.1	6	0.0	0.0	300.0	38585.1	4	0.0	0.0	300.0	38585.1	6
2025	450	5	390.0	32.9	121.5	300.0	46696.6	13	30.3	112.0	300.0	43802.1	12	0.0	0.0	390.0	49932.8	18
2025	600	5	520.0	87.8	324.1	280.0	57250.6	13	80.9	298.6	280.0	48732.5	13	0.0	0.0	520.0	66154.4	18
2025	150	6	170.0	7.3	27.0	150.0	21098.2	13	6.7	24.9	150.0	20268.9	13	0.0	0.0	170.0	21908.7	18
2025	300	6	300.0	0.0	0.0	300.0	38585.1	6	0.0	0.0	300.0	38585.1	4	0.0	0.0	300.0	38585.1	6
2025	450	6	390.0	32.9	121.5	300.0	46696.6	13	30.3	112.0	300.0	43802.1	12	0.0	0.0	390.0	49932.8	18
2025	600	6	520.0	87.8	324.1	280.0	57250.6	13	80.9	298.6	280.0	48732.5	13	0.0	0.0	520.0	66154.4	18
2030	150	1	150.0	0.0	0.0	150.0	19409.0	9	0.0	0.0	150.0	19409.0	13	0.0	0.0	150.0	19409.0	5
2030	300	1	300.0	0.0	0.0	300.0	38585.1	6	0.0	0.0	300.0	38585.1	4	0.0	0.0	300.0	38585.1	10
2030	450	1	390.0	32.9	121.5	300.0	47324.4	8	30.3	112.0	300.0	43065.6	12	0.0	0.0	390.0	49932.8	18
2030	600	1	520.0	87.8	324.1	280.0	52881.6	13	80.9	298.6	280.0	46872.5	13	0.0	0.0	520.0	66154.4	18
2030	150	2	170.0	7.3	27.0	150.0	20734.2	13	6.7	24.9	150.0	20113.9	13	0.0	0.0	170.0	21908.7	18
2030	300	2	300.0	0.0	0.0	300.0	38585.1	6	0.0	0.0	300.0	38585.1	4	0.0	0.0	300.0	38585.1	10
2030	450	2	390.0	32.9	121.5	300.0	47324.4	8	30.3	112.0	300.0	43065.6	12	0.0	0.0	390.0	49932.8	18
2030	600	2	520.0	87.8	324.1	280.0	52881.6	13	80.9	298.6	280.0	46872.5	13	0.0	0.0	520.0	66154.4	18
2030	150	3	170.0	7.3	27.0	150.0	20734.2	13	6.7	24.9	150.0	20113.9	13	0.0	0.0	170.0	21908.7	18
2030	300	3	300.0	0.0	0.0	300.0	38585.1	6	0.0	0.0	300.0	38585.1	4	0.0	0.0	300.0	38585.1	10
2030	450	3	390.0	32.9	121.5	300.0	47324.4	8	30.3	112.0	300.0	43065.6	12	0.0	0.0	390.0	49932.8	18
2030	600	3	520.0	87.8	324.1	280.0	52881.6	13	80.9	298.6	280.0	46872.5	13	0.0	0.0	520.0	66154.4	18
2030	150	4	170.0	7.3	27.0	150.0	20734.2	13	6.7	24.9	150.0	20113.9	13	0.0	0.0	170.0	21908.7	18
2030	300	4	300.0	0.0	0.0	300.0	38585.1	6	0.0	0.0	300.0	38585.1	4	0.0	0.0	300.0	38585.1	10
2030	450	4	390.0	32.9	121.5	300.0	47324.4	8	30.3	112.0	300.0	43065.6	12	0.0	0.0	390.0	49932.8	18
2030	600	4	520.0	87.8	324.1	280.0	52881.6	13	80.9	298.6	280.0	46872.5	13	0.0	0.0	520.0	66154.4	18
2030	150	5	170.0	7.3	27.0	150.0	20734.2	13	6.7	24.9	150.0	20113.9	13	0.0	0.0	170.0	21908.7	18
2030	300	5	300.0	0.0	0.0	300.0	38585.1	6	0.0	0.0	300.0	38585.1	4	0.0	0.0	300.0	38585.1	10
2030	450	5	390.0	32.9	121.5	300.0	47324.4	8	30.3	112.0	300.0	43065.6	12	0.0	0.0	390.0	49932.8	18
2030	600	5	520.0	87.8	324.1	280.0	52881.6	13	80.9	298.6	280.0	46872.5	13	0.0	0.0	520.0	66154.4	18
2030	150	6	170.0	7.3	27.0	150.0	20734.2	13	6.7	24.9	150.0	20113.9	13	0.0	0.0	170.0	21908.7	18
2030	300	6	300.0	0.0	0.0	300.0	38585.1	6	0.0	0.0	300.0	38585.1	4	0.0	0.0	300.0	38585.1	10
2030	450	6	390.0	32.9	121.5	300.0	47324.4	8	30.3	112.0	300.0	43065.6	12	0.0	0.0	390.0	49932.8	18
2030	600	6	520.0	87.8	324.1	280.0	52881.6	13	80.9	298.6	280.0	46872.5	13	0.0	0.0	520.0	66154.4	18
2040	150	1	150.0	0.0	0.0	150.0	19409.0	7	0.0	0.0	150.0	19409.0	13	0.0	0.0	150.0	19409.0	6
2040	300	1	300.0	9.8	23.4	280.0	38481.7	5	0.0	0.0	300.0	38585.1	4	0.0	0.0	300.0	38585.1	12
2040	450	1	390.0	43.9	162.1	270.0	45031.4	8	30.3	112.0	300.0	42596.9	12	0.0	0.0	390.0	49932.8	18
2040	600	1	520.0	87.8	324.1	280.0	49058.7	13	80.9	298.6	280.0	45688.8	13	0.0	0.0	520.0	66154.4	18
2040	150	2	170.0	7.3	27.0	150.0	20415.6	13	6.7	24.9	150.0	20015.3	13	0.0	0.0	170.0	21908.7	18
2040	300	2	300.0	9.8	23.4	280.0	38481.7	5	0.0	0.0	300.0	38585.1	4	0.0	0.0	300.0	38585.1	12
2040	450	2	390.0	43.9	162.1	270.0	45031.4	8	30.3	112.0	300.0	42596.9	12	0.0	0.0	390.0	49932.8	18
2040	600	2	520.0	87.8	324.1	280.0	49058.7	13	80.9	298.6	280.0	45688.8	13	0.0	0.0	520.0	66154.4	18
2040	150	3	170.0	7.3	27.0	150.0	20415.6	13	6.7	24.9	150.0	20015.3	13	0.0	0.0	170.0	21908.7	18
2040	300	3	300.0	9.8	23.4	280.0	38481.7	5	0.0	0.0	300.0	38585.1	4	0.0	0.0	300.0	38585.1	12
2040	450	3	390.0	43.9	162.1	270.0	45031.4	8	30.3	112.0	300.0	42596.9	12	0.0	0.0	390.0	49932.8	18
2040	600	3	520.0	87.8	324.1	280.0	49058.7	13	80.9	298.6	280.0	45688.8	13	0.0	0.0	520.0	66154.4	18
2040	150	4	170.0	7.3	27.0	150.0	20415.6	13	6.7	24.9	150.0	20015.3	13	0.0	0.0	170.0	21908.7	18
2040	300	4	300.0	9.8	23.4	280.0	38481.7	5	0.0	0.0	300.0	38585.1	4	0.0	0.0	300.0	38585.1	12
2040	450	4	390.0	43.9	162.1	270.0	45031.4	8	30.3	112.0	300.0	42596.9	12	0.0	0.0	390.0	49932.8	18
2040	600	4	520.0	87.8	324.1	280.0	49058.7	13	80.9	298.6	280.0	45688.8	13	0.0	0.0	520.0	66154.4	18
2040	150	5	170.0	7.3	27.0	150.0	20415.6	13	6.7	24.9	150.0	20015.3	13	0.0	0.0	170.0	21908.7	18
2040	300	5	300.0	9.8	23.4	280.0	38481.7	5	0.0	0.0	300.0	38585.1	4	0.0	0.0	300.0	38585.1	12

2040	450	5	390.0	43.9	162.1	270.0	45031.4	8	30.3	112.0	300.0	42596.9	12	0.0	0.0	390.0	49932.8	18
2040	600	5	520.0	87.8	324.1	280.0	49058.7	13	80.9	298.6	280.0	45688.8	13	0.0	0.0	520.0	66154.4	18
2040	150	6	170.0	7.3	27.0	150.0	20415.6	13	6.7	24.9	150.0	20015.3	13	0.0	0.0	170.0	21908.7	18
2040	300	6	300.0	9.8	23.4	280.0	38481.7	5	0.0	0.0	300.0	38585.1	4	0.0	0.0	300.0	38585.1	12
2040	450	6	390.0	43.9	162.1	270.0	45031.4	8	30.3	112.0	300.0	42596.9	12	0.0	0.0	390.0	49932.8	18
2040	600	6	520.0	87.8	324.1	280.0	49058.7	13	80.9	298.6	280.0	45688.8	13	0.0	0.0	520.0	66154.4	18
2050	150	1	150.0	0.0	0.0	150.0	19409.0	7	0.0	0.0	150.0	19409.0	13	0.0	0.0	150.0	19409.0	6
2050	300	1	300.0	16.3	39.0	266.7	38307.3	5	7.4	29.4	280.0	38580.1	4	0.0	0.0	300.0	38585.1	13
2050	450	1	390.0	43.9	162.1	270.0	44252.8	8	30.3	112.0	300.0	42463.0	12	8.9	36.9	360.0	49574.5	18
2050	600	1	520.0	87.8	324.1	280.0	47966.4	13	80.9	298.6	280.0	45350.6	13	47.4	196.8	360.0	64243.6	18
2050	150	2	170.0	7.3	27.0	150.0	20943.7	6	6.7	24.9	150.0	19987.1	13	5.9	24.6	150.0	21669.9	18
2050	300	2	300.0	16.3	39.0	266.7	38307.3	5	7.4	29.4	280.0	38580.1	4	0.0	0.0	300.0	38585.1	13
2050	450	2	390.0	43.9	162.1	270.0	44252.8	8	30.3	112.0	300.0	42463.0	12	8.9	36.9	360.0	49574.5	18
2050	600	2	520.0	87.8	324.1	280.0	47966.4	13	80.9	298.6	280.0	45350.6	13	47.4	196.8	360.0	64243.6	18
2050	150	3	170.0	7.3	27.0	150.0	20943.7	6	6.7	24.9	150.0	19987.1	13	5.9	24.6	150.0	21669.9	18
2050	300	3	300.0	16.3	39.0	266.7	38307.3	5	7.4	29.4	280.0	38580.1	4	0.0	0.0	300.0	38585.1	13
2050	450	3	390.0	43.9	162.1	270.0	44252.8	8	30.3	112.0	300.0	42463.0	12	8.9	36.9	360.0	49574.5	18
2050	600	3	520.0	87.8	324.1	280.0	47966.4	13	80.9	298.6	280.0	45350.6	13	47.4	196.8	360.0	64243.6	18
2050	150	4	170.0	7.3	27.0	150.0	20943.7	6	6.7	24.9	150.0	19987.1	13	5.9	24.6	150.0	21669.9	18
2050	300	4	300.0	16.3	39.0	266.7	38307.3	5	7.4	29.4	280.0	38580.1	4	0.0	0.0	300.0	38585.1	13
2050	450	4	390.0	43.9	162.1	270.0	44252.8	8	30.3	112.0	300.0	42463.0	12	8.9	36.9	360.0	49574.5	18
2050	600	4	520.0	87.8	324.1	280.0	47966.4	13	80.9	298.6	280.0	45350.6	13	47.4	196.8	360.0	64243.6	18
2050	150	5	170.0	7.3	27.0	150.0	20943.7	6	6.7	24.9	150.0	19987.1	13	5.9	24.6	150.0	21669.9	18
2050	300	5	300.0	16.3	39.0	266.7	38307.3	5	7.4	29.4	280.0	38580.1	4	0.0	0.0	300.0	38585.1	13
2050	450	5	390.0	43.9	162.1	270.0	44252.8	8	30.3	112.0	300.0	42463.0	12	8.9	36.9	360.0	49574.5	18
2050	600	5	520.0	87.8	324.1	280.0	47966.4	13	80.9	298.6	280.0	45350.6	13	47.4	196.8	360.0	64243.6	18
2050	150	6	170.0	7.3	27.0	150.0	20943.7	6	6.7	24.9	150.0	19987.1	13	5.9	24.6	150.0	21669.9	18
2050	300	6	300.0	16.3	39.0	266.7	38307.3	5	7.4	29.4	280.0	38580.1	4	0.0	0.0	300.0	38585.1	13
2050	450	6	390.0	43.9	162.1	270.0	44252.8	8	30.3	112.0	300.0	42463.0	12	8.9	36.9	360.0	49574.5	18
2050	600	6	520.0	87.8	324.1	280.0	47966.4	13	80.9	298.6	280.0	45350.6	13	47.4	196.8	360.0	64243.6	18

A.4 Langford Bus Exchange

A.4.1 Charge Scheduling and Energy Reduction Results

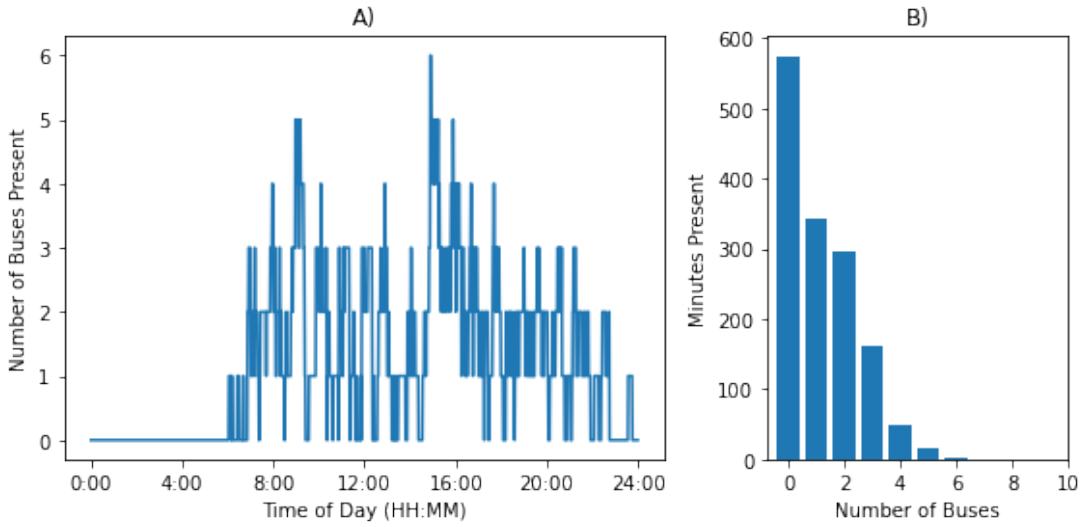

Figure A11: Buses present at Langford

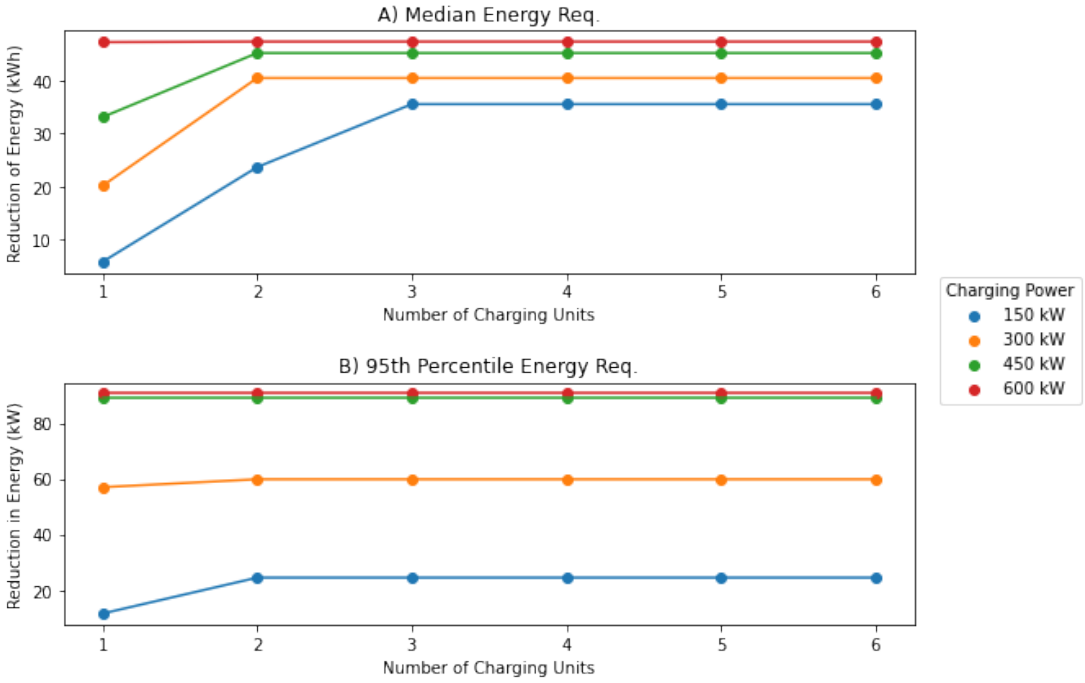

Figure A12: Reduction in mean and 95th percentile energy requirements for Langford

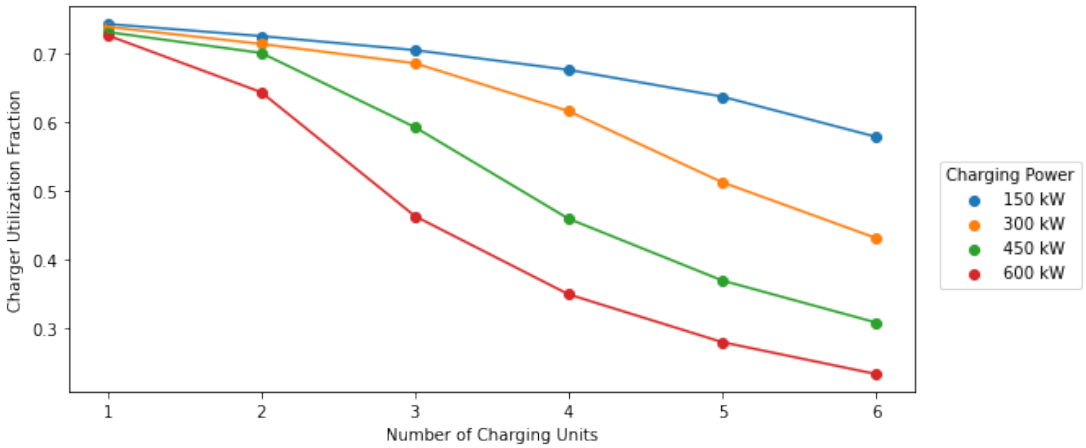

Figure A13: Charger Utilization for Langford

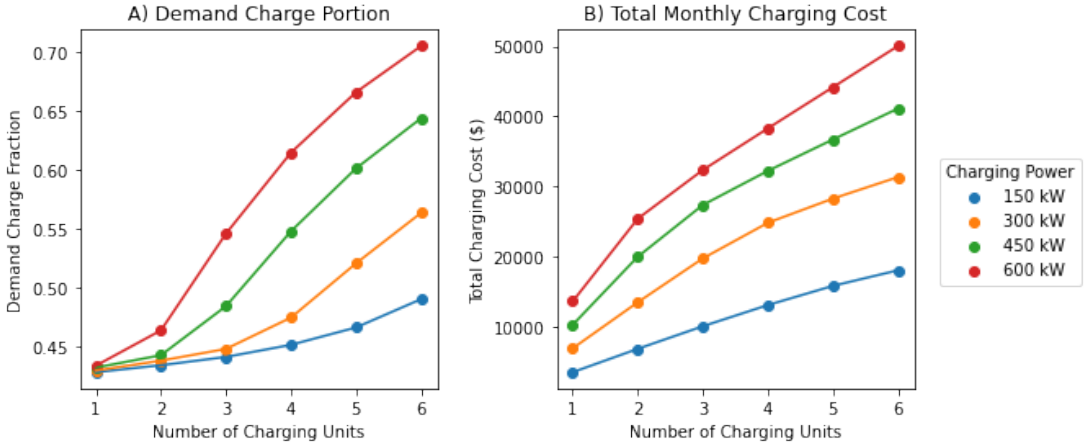

Figure A14: Demand Charge Portion and Total Cost for Langford

A.4.2 Full Parametric Results

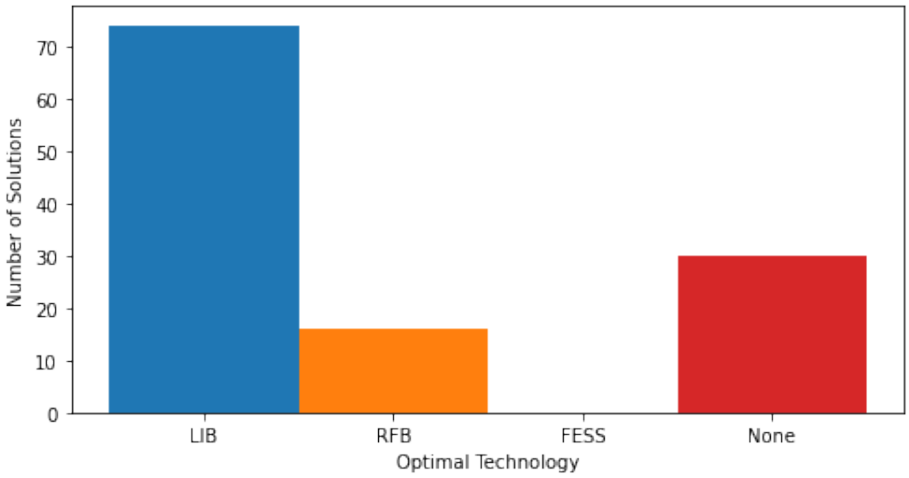

Figure A15: Optimal deployment by technology type for Langford

Table A5: Optimization Results for SESS Technologies in Langford Exchange

Year	Charge Config.		Peak Power	RFB SESS					LIB SESS					FESS SESS				
	Power	# Units	(No SESS)	Energy	Power	P_{max}	AEE	Years	Energy	Power	P_{max}	AEE	Years	Energy	Power	P_{max}	AEE	Years
	(kW)		(kW)	(kWh)	(kW)	(kW)	($)		(kWh)	(kW)	(kW)	($)		(kWh)	(kW)	(kW)	($)	
2020	150	1	150.0	0.0	0.0	150.0	20035.3	13	0.0	0.0	150.0	20035.3	13	0.0	0.0	150.0	20035.3	18
2020	300	1	300.0	0.0	0.0	300.0	40009.4	13	0.0	0.0	300.0	40009.4	13	0.0	0.0	300.0	40009.4	14
2020	450	1	450.0	0.0	0.0	450.0	59651.2	13	0.0	0.0	450.0	59651.2	13	0.0	0.0	450.0	59651.2	9
2020	600	1	600.0	0.0	0.0	600.0	78897.8	13	0.0	0.0	600.0	78897.8	13	0.0	0.0	600.0	78897.8	6
2020	150	2	300.0	0.0	0.0	300.0	39516.3	13	0.0	0.0	300.0	39516.3	13	0.0	0.0	300.0	39516.3	10
2020	300	2	600.0	0.0	0.0	600.0	78288.3	8	0.0	0.0	600.0	78288.3	13	0.0	0.0	600.0	78288.3	9
2020	450	2	840.0	17.6	52.7	795.0	108221.2	13	24.9	64.7	780.0	106583.3	11	0.0	0.0	840.0	108871.8	18
2020	600	2	960.0	35.1	93.6	880.0	123292.5	13	27.0	107.8	880.0	121031.4	10	0.0	0.0	960.0	124098.5	18
2020	150	3	450.0	7.3	23.4	430.0	58123.4	13	6.7	21.6	430.0	57401.4	11	0.0	0.0	450.0	58415.3	18
2020	300	3	760.0	41.0	93.6	680.0	97781.1	13	33.7	107.8	680.0	95733.5	11	0.0	0.0	760.0	98307.7	18
2020	450	3	930.0	23.4	70.2	870.0	118958.6	13	20.2	69.3	870.0	117281.3	7	0.0	0.0	930.0	120100.0	18
2020	600	3	1120.0	87.8	301.0	880.0	141862.6	13	80.9	277.3	880.0	131063.7	12	0.0	0.0	1120.0	144059.7	18
2020	150	4	530.0	25.1	75.2	465.7	67460.1	13	41.6	107.8	430.0	64792.7	11	0.0	0.0	530.0	68418.8	18
2020	300	4	820.0	39.0	117.0	720.0	104451.0	13	33.7	121.3	720.0	101639.9	9	0.0	0.0	820.0	105805.4	18
2020	450	4	930.0	23.4	70.2	870.0	118958.6	13	20.2	69.3	870.0	116923.8	8	0.0	0.0	930.0	120100.0	18
2020	600	4	1120.0	58.5	200.6	960.0	141870.5	13	80.9	277.3	880.0	133884.5	10	0.0	0.0	1120.0	144065.9	18
2020	150	5	540.0	28.3	81.9	470.0	68582.3	13	46.7	118.6	430.0	65289.7	12	0.0	0.0	540.0	69666.4	18
2020	300	5	820.0	39.0	117.0	720.0	104451.0	13	33.7	121.3	720.0	101639.9	9	0.0	0.0	820.0	105805.4	18
2020	450	5	930.0	23.4	70.2	870.0	118958.6	13	20.2	69.3	870.0	116923.8	8	0.0	0.0	930.0	120100.0	18
2020	600	5	1120.0	58.5	200.6	960.0	141870.5	13	80.9	277.3	880.0	133884.5	10	0.0	0.0	1120.0	144065.9	18
2020	150	6	540.0	28.3	81.9	470.0	68582.3	13	46.7	118.6	430.0	65289.7	12	0.0	0.0	540.0	69666.4	18
2020	300	6	820.0	39.0	117.0	720.0	104451.0	13	33.7	121.3	720.0	101639.9	9	0.0	0.0	820.0	105805.4	18
2020	450	6	930.0	23.4	70.2	870.0	118958.6	13	20.2	69.3	870.0	116923.8	8	0.0	0.0	930.0	120100.0	18
2020	600	6	1120.0	58.5	200.6	960.0	141870.5	13	80.9	277.3	880.0	133884.5	10	0.0	0.0	1120.0	144065.9	18
2025	150	1	150.0	0.0	0.0	150.0	20035.3	13	0.0	0.0	150.0	20035.3	13	0.0	0.0	150.0	20035.3	18
2025	300	1	300.0	0.0	0.0	300.0	40009.4	13	0.0	0.0	300.0	40009.4	13	0.0	0.0	300.0	40009.4	18
2025	450	1	450.0	0.0	0.0	450.0	59651.2	13	0.0	0.0	450.0	59651.2	13	0.0	0.0	450.0	59651.2	13
2025	600	1	600.0	0.0	0.0	600.0	78897.8	13	0.0	0.0	600.0	78897.8	13	0.0	0.0	600.0	78897.8	7
2025	150	2	300.0	0.0	0.0	300.0	39516.3	13	0.0	0.0	300.0	39516.3	13	0.0	0.0	300.0	39516.3	12
2025	300	2	600.0	0.0	0.0	600.0	78288.3	7	0.0	0.0	600.0	78288.3	13	0.0	0.0	600.0	78288.3	11
2025	450	2	840.0	27.1	70.2	780.0	107307.4	10	24.9	64.7	780.0	105561.1	11	0.0	0.0	840.0	108871.8	18
2025	600	2	960.0	35.1	93.6	880.0	122520.5	9	27.0	107.8	880.0	119987.7	8	0.0	0.0	960.0	124098.5	18
2025	150	3	450.0	7.3	23.4	430.0	58102.2	8	8.4	27.0	425.0	57213.9	8	0.0	0.0	450.0	58415.3	18
2025	300	3	760.0	51.2	117.0	660.0	95921.1	11	33.7	107.8	680.0	94198.0	11	0.0	0.0	760.0	98307.7	18
2025	450	3	930.0	23.4	70.2	870.0	119551.3	7	50.5	173.3	780.0	114832.3	7	0.0	0.0	930.0	120100.0	18
2025	600	3	1120.0	87.8	301.0	880.0	136333.5	11	80.9	277.3	880.0	127465.7	12	0.0	0.0	1120.0	144059.7	18
2025	150	4	530.0	59.1	146.3	405.0	64603.8	12	46.7	118.6	420.0	63494.3	9	0.0	0.0	530.0	68418.8	18
2025	300	4	820.0	72.0	189.1	658.5	101578.9	11	48.5	194.1	680.0	99208.8	9	0.0	0.0	820.0	105805.4	18
2025	450	4	930.0	23.4	70.2	870.0	118894.8	8	42.5	145.6	804.0	115066.0	7	0.0	0.0	930.0	120100.0	18
2025	600	4	1120.0	87.8	301.0	880.0	138281.3	10	80.9	277.3	880.0	129786.1	10	0.0	0.0	1120.0	144065.9	18

2025	150	5	540.0	66.1	160.9	402.5	65448.3	12	44.7	178.8	420.0	63824.3	10	0.0	0.0	540.0	69666.4	18
2025	300	5	820.0	72.0	189.1	658.5	101578.9	11	48.5	194.1	680.0	99208.8	9	0.0	0.0	820.0	105805.4	18
2025	450	5	930.0	23.4	70.2	870.0	118894.8	8	42.5	145.6	804.0	115066.0	7	0.0	0.0	930.0	120100.0	18
2025	600	5	1120.0	87.8	301.0	880.0	134763.2	13	80.9	277.3	880.0	129786.1	10	0.0	0.0	1120.0	144065.9	18
2025	150	6	540.0	66.1	160.9	402.5	65448.3	12	44.7	178.8	420.0	63824.3	10	0.0	0.0	540.0	69666.4	18
2025	300	6	820.0	72.0	189.1	658.5	101578.9	11	48.5	194.1	680.0	99208.8	9	0.0	0.0	820.0	105805.4	18
2025	450	6	930.0	23.4	70.2	870.0	118894.8	8	42.5	145.6	804.0	115066.0	7	0.0	0.0	930.0	120100.0	18
2025	600	6	1120.0	87.8	301.0	880.0	134763.2	13	80.9	277.3	880.0	129786.1	10	0.0	0.0	1120.0	144065.9	18
2030	150	1	150.0	0.0	0.0	150.0	20035.3	13	0.0	0.0	150.0	20035.3	13	0.0	0.0	150.0	20035.3	18
2030	300	1	300.0	0.0	0.0	300.0	40009.4	13	0.0	0.0	300.0	40009.4	13	0.0	0.0	300.0	40009.4	18
2030	450	1	450.0	0.0	0.0	450.0	59651.2	13	0.0	0.0	450.0	59651.2	13	0.0	0.0	450.0	59651.2	15
2030	600	1	600.0	0.0	0.0	600.0	78897.8	13	0.0	0.0	600.0	78897.8	13	0.0	0.0	600.0	78897.8	9
2030	150	2	300.0	0.0	0.0	300.0	39516.3	13	0.0	0.0	300.0	39516.3	13	0.0	0.0	300.0	39516.3	13
2030	300	2	600.0	0.0	0.0	600.0	78288.3	7	0.0	0.0	600.0	78288.3	13	0.0	0.0	600.0	78288.3	13
2030	450	2	840.0	65.1	140.4	720.0	106514.9	8	24.9	64.7	780.0	105025.7	11	0.0	0.0	840.0	108871.8	18
2030	600	2	960.0	52.7	140.4	840.0	120855.2	8	32.3	129.4	864.0	119218.2	7	0.0	0.0	960.0	124098.5	18
2030	150	3	450.0	15.5	40.5	415.4	57469.1	8	11.5	32.3	420.0	56932.9	8	0.0	0.0	450.0	58415.3	18
2030	300	3	760.0	51.2	117.0	660.0	95693.9	8	33.7	107.8	680.0	93393.7	11	0.0	0.0	760.0	98307.7	18
2030	450	3	930.0	70.2	210.7	750.0	116743.9	7	50.5	173.3	780.0	113563.5	6	0.0	0.0	930.0	120100.0	18
2030	600	3	1120.0	87.8	301.0	880.0	135773.3	8	80.9	277.3	880.0	125581.1	12	0.0	0.0	1120.0	144059.7	18
2030	150	4	530.0	89.0	187.3	370.0	63260.0	10	40.4	161.7	420.0	62235.2	9	0.0	0.0	530.0	68418.8	18
2030	300	4	820.0	87.8	210.7	640.0	100154.4	9	48.5	194.1	680.0	97687.8	9	0.0	0.0	820.0	105805.4	18
2030	450	4	930.0	47.9	143.6	807.3	118513.9	6	50.5	173.3	780.0	113305.0	7	0.0	0.0	930.0	120100.0	18
2030	600	4	1120.0	87.8	301.0	880.0	138452.9	7	80.9	277.3	880.0	127639.3	10	0.0	0.0	1120.0	144065.9	18
2030	150	5	540.0	93.9	199.0	370.0	63994.7	10	44.7	178.8	420.0	62529.6	10	0.0	0.0	540.0	69666.4	18
2030	300	5	820.0	87.8	210.7	640.0	100154.4	9	48.5	194.1	680.0	97687.8	9	0.0	0.0	820.0	105805.4	18
2030	450	5	930.0	47.9	143.6	807.3	118513.9	6	50.5	173.3	780.0	113305.0	7	0.0	0.0	930.0	120100.0	18
2030	600	5	1120.0	87.8	301.0	880.0	136327.4	8	80.9	277.3	880.0	127639.3	10	0.0	0.0	1120.0	144065.9	18
2030	150	6	540.0	93.9	199.0	370.0	63994.7	10	44.7	178.8	420.0	62529.6	10	0.0	0.0	540.0	69666.4	18
2030	300	6	820.0	87.8	210.7	640.0	100154.4	9	48.5	194.1	680.0	97687.8	9	0.0	0.0	820.0	105805.4	18
2030	450	6	930.0	47.9	143.6	807.3	118513.9	6	50.5	173.3	780.0	113305.0	7	0.0	0.0	930.0	120100.0	18
2030	600	6	1120.0	87.8	301.0	880.0	136327.4	8	80.9	277.3	880.0	127639.3	10	0.0	0.0	1120.0	144065.9	18
2040	150	1	150.0	0.0	0.0	150.0	20035.3	13	0.0	0.0	150.0	20035.3	13	0.0	0.0	150.0	20035.3	18
2040	300	1	300.0	0.0	0.0	300.0	40009.4	13	0.0	0.0	300.0	40009.4	13	0.0	0.0	300.0	40009.4	18
2040	450	1	450.0	0.0	0.0	450.0	59651.2	13	0.0	0.0	450.0	59651.2	13	0.0	0.0	450.0	59651.2	18
2040	600	1	600.0	0.0	0.0	600.0	78897.8	13	0.0	0.0	600.0	78897.8	13	0.0	0.0	600.0	78897.8	15
2040	150	2	300.0	0.0	0.0	300.0	39516.3	13	0.0	0.0	300.0	39516.3	13	0.0	0.0	300.0	39516.3	18
2040	300	2	600.0	0.0	0.0	600.0	78288.3	6	0.0	0.0	600.0	78288.3	13	0.0	0.0	600.0	78288.3	14
2040	450	2	840.0	84.1	175.6	690.0	104620.7	7	24.9	64.7	780.0	105006.5	7	0.0	0.0	840.0	108871.8	18
2040	600	2	960.0	98.0	210.7	780.0	117619.0	8	42.6	170.3	840.0	118380.4	7	0.0	0.0	960.0	124098.5	18
2040	150	3	450.0	47.5	93.6	370.0	56571.7	7	11.5	32.3	420.0	56725.6	8	0.0	0.0	450.0	58415.3	18
2040	300	3	760.0	95.1	187.3	600.0	93880.8	7	33.7	107.8	680.0	92881.9	11	0.0	0.0	760.0	98307.7	18
2040	450	3	930.0	79.8	239.4	725.5	114184.6	6	60.7	242.6	750.0	112186.9	6	0.0	0.0	930.0	120100.0	18
2040	600	3	1120.0	102.4	351.1	840.0	134151.1	6	80.9	277.3	880.0	124381.8	12	0.0	0.0	1120.0	144059.7	18
2040	150	4	530.0	89.0	187.3	370.0	61070.9	9	40.4	161.7	420.0	61428.6	9	0.0	0.0	530.0	68418.8	18
2040	300	4	820.0	156.1	304.3	560.0	97255.6	8	50.5	202.2	680.0	96533.9	10	0.0	0.0	820.0	105805.4	18
2040	450	4	930.0	70.2	210.7	750.0	114532.8	6	50.5	173.3	780.0	112179.2	7	0.0	0.0	930.0	120100.0	18
2040	600	4	1120.0	123.3	401.3	800.0	132254.9	7	80.9	277.3	880.0	126273.1	10	0.0	0.0	1120.0	144065.9	18
2040	150	5	540.0	102.4	210.7	360.0	61616.4	9	44.7	178.8	420.0	61705.8	10	0.0	0.0	540.0	69666.4	18

2040	300	5	820.0	156.1	304.3	560.0	97255.6	8	50.5	202.2	680.0	96533.9	10	0.0	0.0	820.0	105805.4	18
2040	450	5	930.0	70.2	210.7	750.0	114532.8	6	50.5	173.3	780.0	112179.2	7	0.0	0.0	930.0	120100.0	18
2040	600	5	1120.0	102.4	351.1	840.0	132553.3	7	80.9	277.3	880.0	126273.1	10	0.0	0.0	1120.0	144065.9	18
2040	150	6	540.0	102.4	210.7	360.0	61616.4	9	44.7	178.8	420.0	61705.8	10	0.0	0.0	540.0	69666.4	18
2040	300	6	820.0	156.1	304.3	560.0	97255.6	8	50.5	202.2	680.0	96533.9	10	0.0	0.0	820.0	105805.4	18
2040	450	6	930.0	70.2	210.7	750.0	114532.8	6	50.5	173.3	780.0	112179.2	7	0.0	0.0	930.0	120100.0	18
2040	600	6	1120.0	102.4	351.1	840.0	132553.3	7	80.9	277.3	880.0	126273.1	10	0.0	0.0	1120.0	144065.9	18
2050	150	1	150.0	0.0	0.0	150.0	20035.3	13	0.0	0.0	150.0	20035.3	13	0.0	0.0	150.0	20035.3	18
2050	300	1	300.0	0.0	0.0	300.0	40009.4	13	0.0	0.0	300.0	40009.4	13	0.0	0.0	300.0	40009.4	18
2050	450	1	450.0	0.0	0.0	450.0	59651.2	13	0.0	0.0	450.0	59651.2	13	0.0	0.0	450.0	59651.2	18
2050	600	1	600.0	0.0	0.0	600.0	78897.8	13	0.0	0.0	600.0	78897.8	13	0.0	0.0	600.0	78897.8	18
2050	150	2	300.0	0.0	0.0	300.0	39516.3	13	0.0	0.0	300.0	39516.3	13	0.0	0.0	300.0	39516.3	18
2050	300	2	600.0	0.0	0.0	600.0	78288.3	6	0.0	0.0	600.0	78288.3	13	0.0	0.0	600.0	78288.3	15
2050	450	2	840.0	84.1	175.6	690.0	104769.7	6	24.9	64.7	780.0	104868.9	7	8.9	35.5	810.0	108484.7	18
2050	600	2	960.0	98.0	210.7	780.0	117571.2	7	42.6	170.3	840.0	118084.8	7	11.8	53.3	920.0	123707.5	18
2050	150	3	450.0	47.5	93.6	370.0	56036.3	7	11.5	32.3	420.0	56713.0	7	3.8	15.2	437.1	58284.7	18
2050	300	3	760.0	124.4	234.1	560.0	92707.8	7	33.7	107.8	680.0	92735.7	11	0.0	0.0	760.0	98307.7	18
2050	450	3	930.0	70.2	210.7	750.0	114754.0	5	60.7	242.6	750.0	111708.8	6	17.8	71.1	870.0	119325.7	18
2050	600	3	1120.0	102.4	351.1	840.0	132007.7	6	80.9	277.3	880.0	124039.1	12	47.4	189.5	960.0	141995.0	18
2050	150	4	530.0	111.0	217.5	344.2	60115.1	9	40.4	161.7	420.0	61198.2	9	17.8	71.1	470.0	68016.4	18
2050	300	4	820.0	173.1	327.7	540.0	95667.6	8	50.5	202.2	680.0	96267.7	10	22.8	91.4	742.9	105270.3	18
2050	450	4	930.0	70.2	210.7	750.0	115082.8	5	50.5	173.3	780.0	111857.6	7	17.8	71.1	870.0	119325.7	18
2050	600	4	1120.0	102.4	351.1	840.0	132561.8	6	80.9	277.3	880.0	125882.8	10	47.4	189.5	960.0	142001.1	18
2050	150	5	540.0	116.3	229.8	343.7	60561.3	9	44.7	178.8	420.0	61470.4	10	18.5	73.8	477.7	69138.8	18
2050	300	5	820.0	173.1	327.7	540.0	95667.6	8	50.5	202.2	680.0	96267.7	10	22.8	91.4	742.9	105270.3	18
2050	450	5	930.0	70.2	210.7	750.0	115082.8	5	50.5	173.3	780.0	111857.6	7	17.8	71.1	870.0	119325.7	18
2050	600	5	1120.0	102.4	351.1	840.0	132835.7	6	80.9	277.3	880.0	125882.8	10	47.4	189.5	960.0	142001.1	18
2050	150	6	540.0	116.0	229.3	344.1	60593.8	9	44.7	178.8	420.0	61470.4	10	18.5	73.8	477.7	69138.8	18
2050	300	6	820.0	173.1	327.7	540.0	95667.6	8	50.5	202.2	680.0	96267.7	10	22.8	91.4	742.9	105270.3	18
2050	450	6	930.0	70.2	210.7	750.0	115082.8	5	50.5	173.3	780.0	111857.6	7	17.8	71.1	870.0	119325.7	18
2050	600	6	1120.0	102.4	351.1	840.0	132835.7	6	80.9	277.3	880.0	125882.8	10	47.4	189.5	960.0	142001.1	18